125 p.

66 p.

N64-15792
CODE-1
CR-53065

Space Programs Summary No. 37-25, Volume III

for the period November 1, 1963 to December 31, 1963

The Deep Space Instrumentation Facility

OTS PRICE

XEROX $ 6.60 ph.

MICROFILM $ 2.18 mf.

JET PROPULSION LABORATORY
CALIFORNIA INSTITUTE OF TECHNOLOGY
PASADENA, CALIFORNIA

January 31, 1964

Space Programs Summary No. 37-25, Volume III

for the period November 1, 1963 to December 31, 1963

The Deep Space Instrumentation Facility

JET PROPULSION LABORATORY
CALIFORNIA INSTITUTE OF TECHNOLOGY
PASADENA, CALIFORNIA

January 31, 1964

(NASA CR - - - ;

 OTS:

Preface

The *Space Programs Summary* is a six volume, bimonthly publication designed to report on JPL space exploration programs, and related supporting research and advanced development projects. The subtitles of all volumes of the *Space Programs Summary* are:

Vol. I. The Lunar Program (Confidential)

Vol. II. The Planetary–Interplanetary Program (Confidential)

Vol. III. The Deep Space Instrumentation Facility (Unclassified)

Vol. IV. Supporting Research and Advanced Development (Unclassified)

Vol. V. Supporting Research and Advanced Development (Confidential)

Vol. VI. Space Exploration Programs and Space Sciences (Unclassified)

The *Space Programs Summary,* Volume VI is an unclassified digest of appropriate material from Volumes I through V, plus the space science instrumentation studies of the JPL Space Sciences Division.

W. H. Pickering, *Director*
Jet Propulsion Laboratory

Space Programs Summary No. 37-25, Volume III

Copyright © 1964, Jet Propulsion Laboratory, California Institute of Technology

Prepared under Contract No. NAS 7-100, National Aeronautics & Space Administration

(NASA

Contents

I. Résumé 1
A. Tracking Station Operations 1
B. Engineering Developments 2
C. Research and Development 2
D. Advanced Antenna System 4
II. Tracking Station Operations 5
A. Goldstone 5
B. Woomera 8
Reference 11
III. Engineering Developments 12
A. Systems Engineering 12
B. Computer Programs 13
C. *Mariner C* 100-kw Transmitter 18
References 20
IV. Research and Development 21
A. Ground Antennas 21
B. Planetary Radar Project 30
C. Lunar Radar Project 38
D. Ranging and Tracking System Development 47
E. S-Band Implementation for DSIF 51
References 58
V. Advanced Antenna System 59
A. Synopsis 59

I. Résumé

15792 Author

The DSIF is a precision tracking and data acquisition network which is designed to track, command, and receive data from deep space probes. It utilizes large antennas, low-noise phase-lock receiving systems, and high-power transmitters at stations positioned approximately 120 deg around the Earth. Its policy is to continuously conduct research and development of new components and systems and to engineer them into the DSIF so as to continually maintain a state-of-the-art capability. Identification of stations is given in the following tabulation: Author

Goldstone Pioneer	DSIF 11
Goldstone Echo	DSIF 12
Goldstone Venus	DSIF 13
Goldstone Mars	DSIF 14
Woomera	DSIF 41
Canberra	DSIF 42
Johannesburg	DSIF 51
Mobile Tracking	DSIF 59
Madrid	DSIF 61
Spacecraft Monitoring	DSIF 71

A. Tracking Station Operations

1. Goldstone

In order to meet the *Ranger 6* video bandwidth requirements, unity gain 30-Mc isolation amplifiers were installed at the Echo and Pioneer Stations to feed data to the ground TV equipment and to the noise monitoring equipment. Similar modified equipment was sent to the overseas stations to feed the video recorders. A new quadripod and an equipment cage have been installed on the Goldstone Pioneer antenna.

2. Woomera

The Woomera Station successfully acquired, tracked, and received data from the *Atlas–Centaur* (AC-2) which was launched on November 27, 1963. Tracking operations lasted from 20:07 to 20:26 GMT. The AGC voltage exhibited a very predominant ripple at 0.67 cps. The Woomera Station accomplished this mission in addition to making preparations for tracking the Interplanetary Magnetic Probe (S-74) which was also launched on November 27, 1963.

B. Engineering Developments

1. S-Band Systems Engineering

Systems engineering has completed: drawings of antenna cage and equipment, control building floor layouts, S-band receiver and CDC compatibility tests, tests of commands generated in the CDC, plans for making a compatibility test with a *Surveyor* spacecraft, system performance tests with a *Ranger 6* PTM and a preliminary function description of the Ames/DSIF *Pioneer* Program.

2. Computer Programs

a. Trajectory program for on-site computers. A spacecraft trajectory program has been developed for small size digital computers which is accurate enough to generate prediction data and antenna drive tapes. Position and velocity components at injection are used, and a variable step size numerical integration is used to improve accuracy and to reduce the computation time required.

b. Method of rejecting possible blunder points. Tracking data which is used in the orbit determination computer program has a tendency to be contaminated with what are known as "blunder points." To reduce the effect of these "points" a method of using auto regression smoothing is proposed, which is accomplished by differencing the sampled time series of tracking data with a predicted time series based on the trajectory's initial conditions. Preliminary tests indicate that there is merit to the proposal.

3. Mariner C 100-kw Transmitter

The 100-kw transmitter at the Venus site will be used in *Mariner C* operations when the spacecraft is on its way to Mars in 1965. In order to accomplish this at the operations frequency range of 2110 to 2120 Mc, a complete Cassegrain cone with two klystron amplifiers (one for redundancy) and switching capabilities will be constructed. This will be done on a fixed price basis because of the availability of complete documentation.

C. Research and Development

1. Ground Antennas

a. Boresight calibrations for DSIF antennas. Several techniques for boresighting DSIF ground antennas using radio star sources have been developed. One of these methods uses an ephemeris angle drive tape to drive the antenna to the source location and angular offsets to steer the antenna exactly on course. The offsets required determine the boresight error. Using this method on the 85-ft Venus antenna, a 0.035-deg peak-to-peak cyclic error was discovered which was corrected by replacing the elevation angle encoder.

b. Antenna instrumentation. An automatic typewriter (Flexowriter) has been added to the transportable antenna instrumentation system to permit simultaneous line printing of scanned data, the punching of a paper tape, and the later verification of punched data. The system will be used to make additional measurements on the 85-ft Venus antenna and also to check the 210-ft antenna when it is erected.

c. Radio frequency interference tests. Although fluorescent lighting fixtures have several advantages, they have not been used in DSIF Stations because of the danger of potential RF interference. A new unit with RF shielding has been tested and was found not to increase the noise temperature by more than 0.02°K when illuminating an isotropic side lobe at a distance of 50 ft.

Similarly, a dc tachometer was tested and no noticeable interference was noted. It is estimated that it would cause a maximum of 0.1°K increase in noise temperature in an operational situation.

d. 30-ft antenna reflector calculations. Recent structural deflection measurements which were made on the Venus 30-ft antenna have made it posible to check the STAIR Computer Program which is being used in the design of the 210-ft antenna. When the computed deflection values were compared to the actual measurements, the results were considered to be within reasonable tolerance except for one joint. This is being investigated.

e. 85-ft antenna, reflector resurfacing. A new reflector surface has been installed on the 85-ft antenna at the Goldstone Venus site and has been measured to have 0.4-db more gain than the old surface.

An improvement installed with the new surface was the use of new panel mounting assemblies which were specially designed to minimize temperature effects, to allow adjustments from the front of the panel, and normal to the reflector surface.

2. Planetary Radar Project

a. Water rotary joint for Az–El antenna. Continued surveillance of the water rotary joint installed in the 85-ft antenna at the Goldstone Venus site indicates that the carbon seals are satisfactorily wearing in.

b. High-power transmitter. The series limiter for the 100-kw klystron at the Goldstone Venus site is a water cooled triode, operated as a diode, which uses an emission limited cathode. Limiting is controlled by varying the filament voltage. A new klystron filament supply has been designed and built. This includes a new solid-state rectifier assembly, protective diodes, and a filter choke. A lightweight, sensitive, shielded unit for measuring incidental phase modulation has been built and tested.

c. Mod IV planetary radar receiver—a note on reliability. The Mod IV planetary radar receiver has operated for more than 7400 hr without a tube failure. This is attributed to a 100-hr tube aging test made prior to use in the receiver and the reduction of plate voltage from 150 to 120 v. The receiver is also more stable and drift free.

d. Nine-channel autocorrelator. A nine-channel autocorrelator is being built which will resolve the received planetary radar signal into nine separate and adjacent geographical zones, detect the power in each zone's signal using bandwidths from 25 to 400 cps, accumulate 50 autocorrelation points for each signal and feed the data to a stored program computer for control, integration, recording, and display. The nine channels are obtained by modulating the transmitted signal with a pseudonoise (PN) code and demodulating the received signal with nine separate demodulators, which are fed with the same PN code, each displaced in phase by 1 code bit.

e. Central frequency synthesizer. A central frequency synthesizer is planned for use at the Venus site to supply all the coherent reference frequencies for the receiver–transmitter systems at both the 85- and 30-ft antennas. By consolidating all the equipment, considerable reduction is possible. Improvements will be made in some cases in that all reference frequencies will be coherent.

3. Lunar Radar Project

a. A range-gated lunar radar experiment. In a previous *SPS* (*37-23*, Vol. III), a proposed method of making radar experiments on the Moon was discussed. This system has been implemented and used with satisfactory results. A PN code modulation of the carrier (length 16,383) was used, running at a 1-Mc digit rate. Correlation of the return signal, using a fixed delay between the transmit and receive coders, provided a measurement of a range-gate increment of 150 m. System temperatures are considerably degraded at low elevation angles. Range calibrations using the collimation tower agree within the system uncertainty. Actual measurements on the Moon revealed lunar ephemeris inaccuracies which are being corrected. Data on lunar surface characteristics is now being reduced.

b. Lunar radar range measurements. Preliminary results from the lunar radar measurements indicate that the observed response curves may be a powerful means of studying the lunar topography over regions of 45-km sizes, and will require a major research effort to improve the lunar ephemeris for the purposes of calculating significant astronomical constants from radar observations.

4. Ranging and Tracking System Development

a. Monostatic radar operating parameters. Preliminary test results of the anti-sideband system coupled with the effects of target dynamics (discussed in *SPS 37-24*, Vol. III) have pointed up several areas of compromise in the selection of receiver loop bandwidth, keying rate, and predetection bandwidth. Inherent in the problem are the uncertainties of prediction of range and range rate at the time of satellite acquisition.

b. Monostatic satellite and lunar radar transmitter. The 10-kw transmitter, which will be used on the 30-ft antenna at the Venus site, will have improved directional couplers to reduce the uncertainty of back power measurements, a photodiode arc detector near the klystron window with a 5-μsec response time instead of several milliseconds, new power meters that are linear and not temperature sensitive, a waveguide switch to eliminate the necessity of manually connecting the transmitter to the antenna feed on the water load, and water flow gages. All are expected to improve reliability.

5. S-Band Implementation for DSIF

a. TWM for DSIF. The closed cycle refrigerators (CCR) for two traveling wave masers (TWM) have been received and tested. The compressor unit has been repackaged and is more compact than the old version. Two TWM units are nearly complete.

b. Acquisition aid for DSIF. The S-band acquisition aid antenna will use the basic 85-ft S-band feed horn

as an antenna and will have its own angle tracking channels in the receiver. An erectile, close-in collimation tower is being designed to provide a rapid multipath free means for phasing and collimating the acquisition antenna.

c. DSIF microwave switch control assembly. In order to rapidly and safely control the various microwave switches in the S-band system, an automatic control system has been developed. Logic circuits are used to interlock the controls so specific modes of operation may be switched without endangering equipment or personnel.

D. Advanced Antenna System

1. Synopsis

Excavations for the antenna pedestal and the instrument tower have been completed, and placement of forms and reinforcing steel for pouring of concrete is in process. The outside diameter of the pedestal is 88 ft, 8 in. and that of the tower is 26 ft. The foundation depths are 11 and 35 ft, respectively. A 5-mi road 24½ ft wide has been completed, and erection of the 315-ft-high guyed derrick is in progress. Preliminary design and engineering analysis of the antenna is nearly completed.

II. Tracking Station Operations

A. Goldstone

Preparation for the *Ranger 6* mission continues to be the primary activity at Goldstone. Station effectiveness evaluations have proved satisfactory, and the mission equipment is ready for the approaching DSIF net integration tests.

1. General Activities

The video compatibility tests conducted through September indicated a difficulty with the receiver capability to pass a 2.0-Mc bandwidth. Channel parameters of the *Ranger 6* video cameras require a minimum of 2.25 Mc for synchronization and white/black contrast stability. Two channels, one on the upper and one on the lower sidebands, will be used.

A unity gain isolation amplifier with four balanced 50-ohm outputs was installed between the preamplifier port and the video equipment, providing a balanced 50-ohm input to each of the two video preamplifiers. Maser system noise temperatures are measured from the third output; the fourth, grounded through a 50-ohm resistor, is available as a spare.

Tests made with this new configuration were satisfactory. An approximate bandwidth of 3.0 Mc is available, and video pictures have been taken and recorded at signal strength levels which are calculated for lunar distances. The *Ranger* Proof Test Model was used for these experiments.

2. Receiver Modifications

As a result of the success of the 2.0-Mc bandwidth investigation and modifications to the Echo receiver, the Pioneer receiver was modified in essentially the same way as that performed on the Echo receiver. Since only one video preamplifier is used with the Pioneer back-up video installation, the isolation amplifier has two ports available for other use, whereas Echo has only one. A block diagram of the modified Echo/Pioneer configuration is illustrated in Fig. 1.

Modifications similar to Echo/Pioneer were made to the 30-Mc preamplifiers for Woomera and Johannesburg to provide additional bandwidth. An International Telephone and Telegraph isolation amplifier, having two wide-band (5.0-Mc) output ports, feeds a Lel, Incorporated 30-Mc preamplifier from one port and a 30-Mc noise

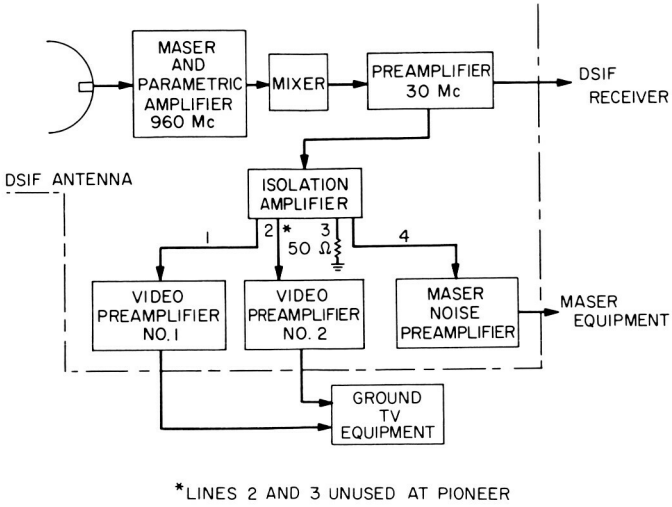

Fig. 1. Echo and Pioneer receiver configuration modification

amplifier from the other port. Two FR-800 (previously designated as FR-700-21) video tape recorders are connected to the balanced outputs of the Lel amplifier. Fig. 2 is a block diagram of the planned overseas configuration.

3. Ranger 6 *Proof Test Model*

A Proof Test Model (PTM) of the *Ranger 6* spacecraft was installed in a screen room near the Echo collimation tower. Fig. 3 illustrates the two sections of the spacecraft

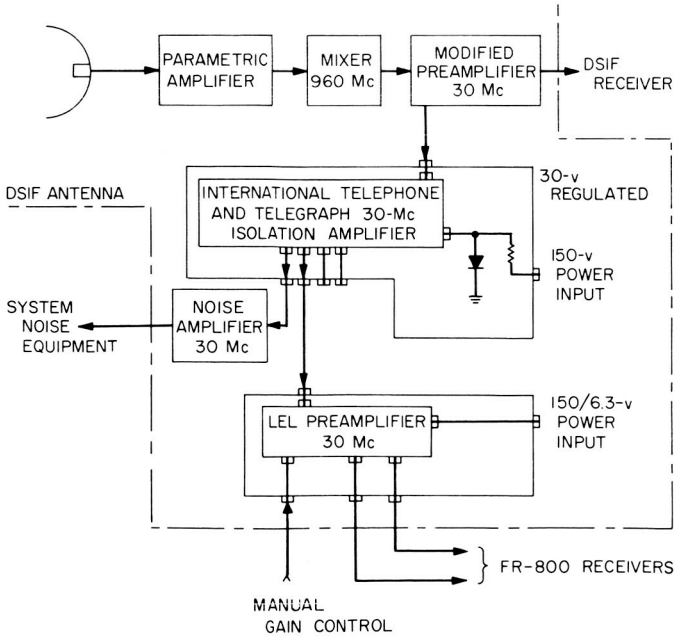

Fig. 2. Woomera and Johannesburg receiver configuration modification

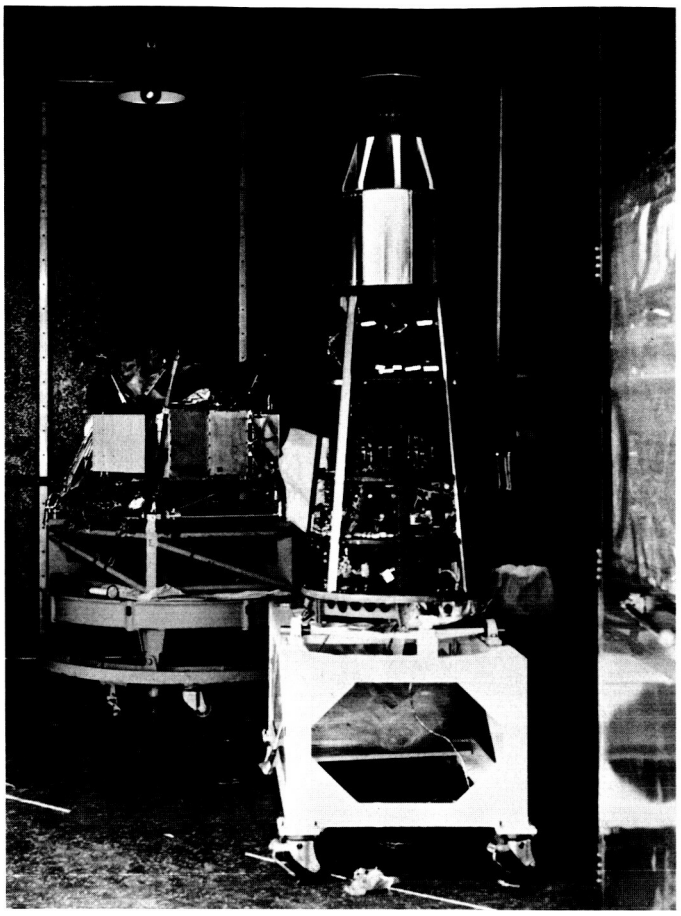

Fig. 3. *Ranger 6* PTM in screen room

as they were installed; the video camera installation is in the nose section (foreground). Tests were made for receiver operation, transmitter operation for doppler and command signals, and video reception. These tests were conducted from October 26, 1963 to November 9, 1963.

4. Atlas–Centaur 2 *Mission*

The *Atlas–Centaur 2* (AC-2) mission was integrated into the preparation for *Ranger 6*. During the period that the PTM tests were being conducted, two station preparedness tests for AC-2 were handled simultaneously with the PTM test. A final net integration test for AC-2 was conducted on November 22, 1963. The launch was rescheduled for November 27, 1963 and was performed on that day. While the launch was successful, the Goldstone Echo and Pioneer sites were unsuccessful in receiving signals from *Centaur*. Operational readiness tests, performed during the station countdown (and immediately after the first and second pass), indicated that the receiver and antenna were functioning properly.

5. Equipment Installation

a. Echo site. Final preparations for *Ranger 6* have had first priority. AC-2 served as an operational test, and mission equipment is being maintained in an operational status.

The mission-oriented command system previously installed (Ref. 1) was tested with the PTM. Start and stop commands were successfully transmitted.

An Ampex FR-800 2-in. video tape recorder (Fig. 4) is being readied for installation at Echo, Johannesburg, and Woomera. It will be used to provide back-up for special video purposes requiring the additional bandwidth of the FR-800. A 1-wk schooling period, which covered the operation and maintenance of the recorder, was conducted in November at the Echo site, and was attended by personnel from Goldstone, Johannesburg, and Woomera.

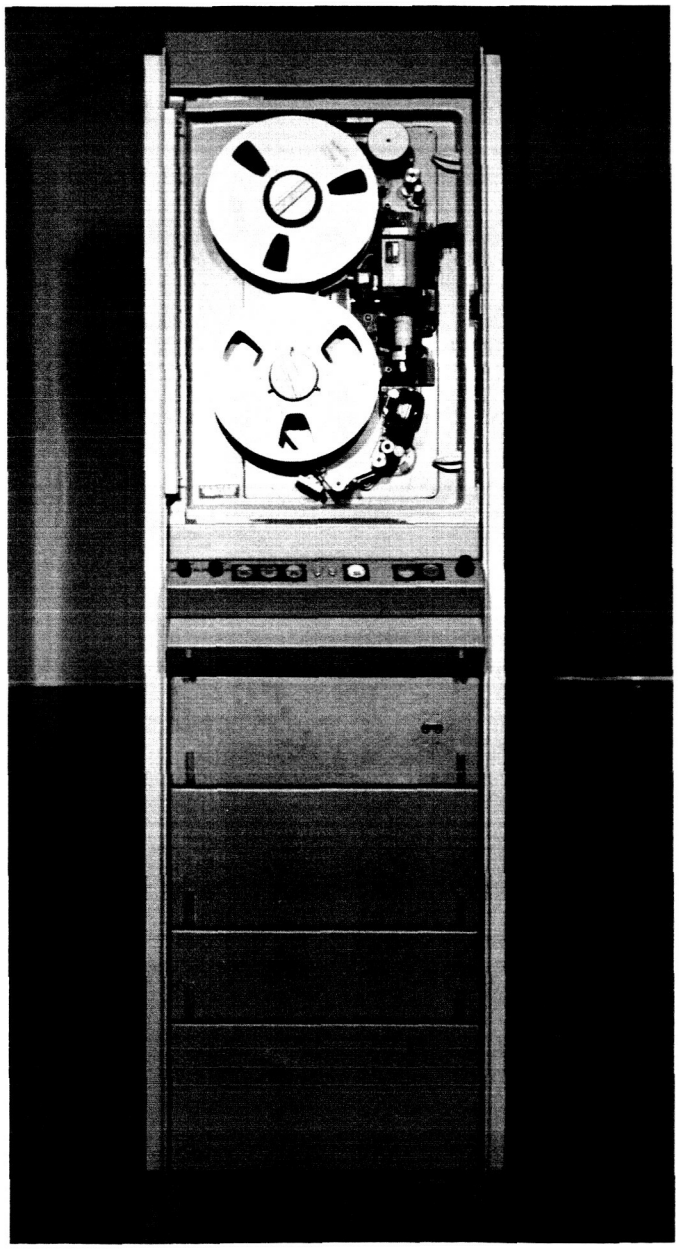

Fig. 4. Ampex FR-800 video tape recorder

The microwave link between Pasadena and Goldstone is completed except for final adjustments and testing. The Montana Mines relay station (Fig. 5), approximately 5 mi west–southwest of Goldstone, is one of two relays in the link circuit. In addition to the Pasadena–Goldstone circuit, a similar, shorter link is nearing completion between the Echo and Venus sites.

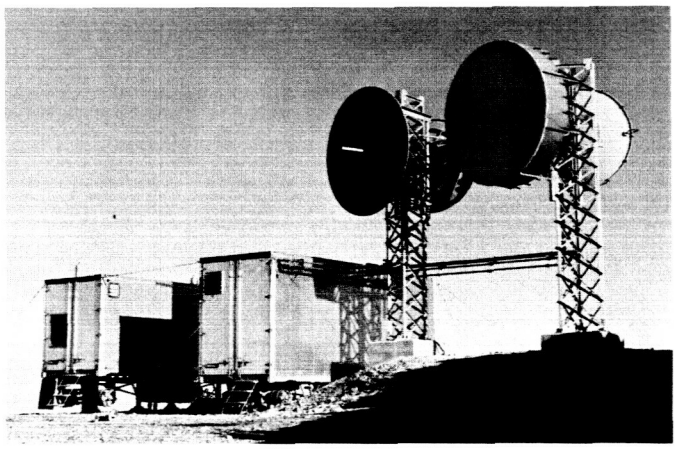

Fig. 5. Montana Mines relay station

b. Pioneer site. Installation of the S-band transmitter is progressing on schedule. The Pioneer site antenna was rebuilt with a new quadripod (Fig. 6) to support the additional apex-mounted reflector and equipment, and an equipment cage to house part of the receiver and transmitter equipment. The klystron cabinet, containing the klystron and the focusing magnets, have been installed in the cage. Interconnecting cables have been installed between the antenna-mounted cabinet and the high-voltage power supply located in the hydromechanical building. Primary electric input power cables have been installed and connected and are ready for use. The air conditioning equipment has been installed for the equipment cage and associated equipment.

A back-up video receiver (Fig. 7) for the Echo video equipment has been installed at the Pioneer site, and is capable of recording both video channels and the Channel 8 telemetry. However, it has no reproducing facilities;

Fig. 6. New quadripod on Pioneer site antenna

therefore, the video tapes must be brought to the Echo site for this purpose. The Pioneer antenna will be tracking simultaneously with the Echo antenna.

B. Woomera

1. Participation in Atlas–Centaur 2 Mission

a. Prelaunch preparation.

Training and calibrations. The DSIF Tracking Station at Woomera, Australia, had to make concurrent preparations for the Interplanetary Magnetic Probe (IMP) S-74 mission and the *Atlas–Centaur 2* (AC-2) mission, with the result that station preparations for the AC-2 were not as detailed as they might otherwise have been. Time did not permit patterns, boresight versus polarization and signal strength, and ellipticity calibrations on the wide-band feed which was installed to provide the dual 136 960-Mc capability on November 16, 1963. Sufficient

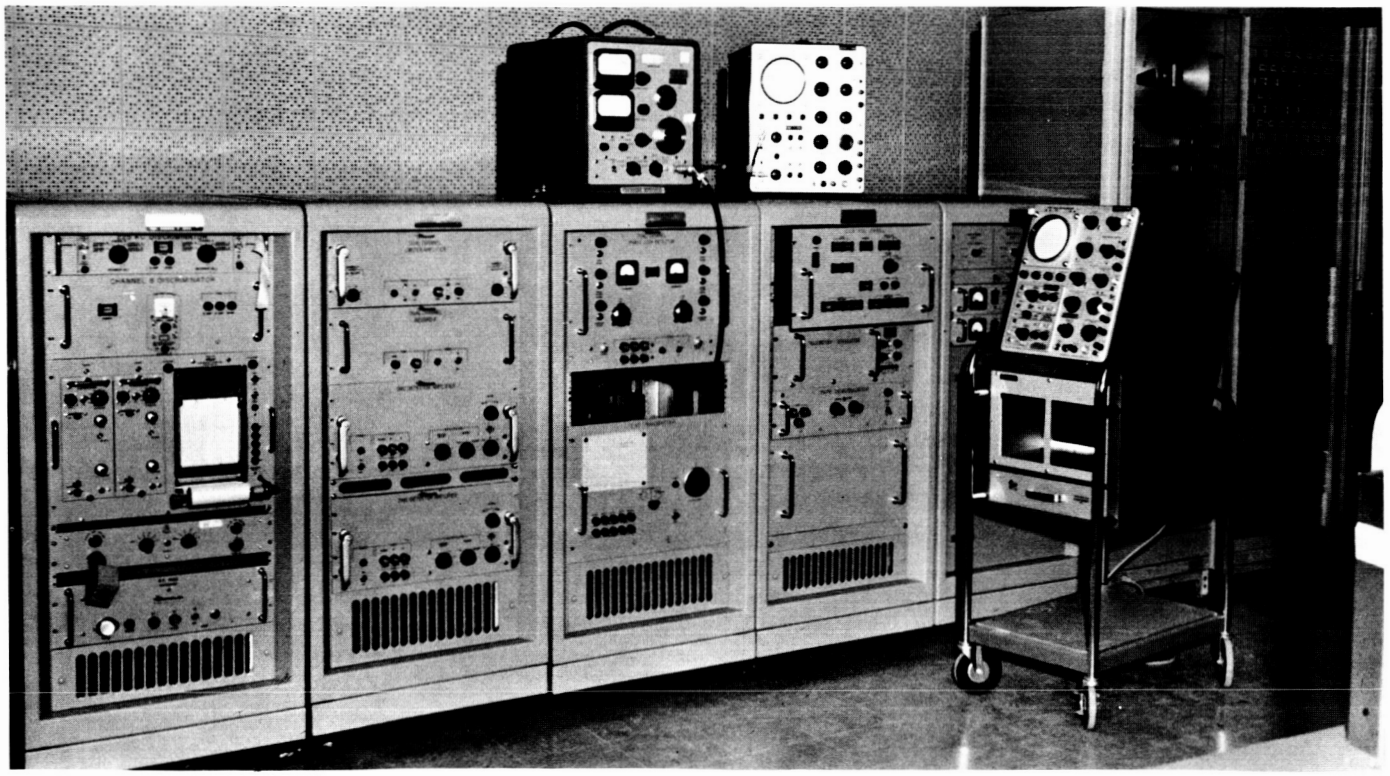

Fig. 7. Back-up video receiver at Pioneer site

checks were made to ensure correct operation of the feed and its associated acquisition aid relays.

Earlier, a star track was conducted as part of the preparations for *Ranger 6*. The data was processed on the IBM 7090 at Weapons Research Establishment (WRE), Salisbury, and found to be noisy and to show an hour angle bias of about 0.02 deg. This was attributed to normal coupler wear, and plans were made for replacement of the Thomas couplers in the angle encoding system.

Net integration tests were held on October 30 and November 1, 1963 and operational readiness tests on November 5 and 22, 1963.

Aircraft tracks were held on November 7 and 21, 1963 to provide operator training on the newly installed monitoring arrangements for use with the acquisition aid, to collimate the acquisition aid, and to demonstrate capability to carry out the mission. During checkout of the acquisition aid on the near collimation tower installed for this purpose, difficulty was experienced, due to interaction between the acquisition aid, which was then mounted at the quad tip, and defocused radiation from the dish. It was therefore moved to the dish rim where this problem would be eliminated. The aircraft track on November 21 revealed acquisition aid collimation errors of 0.7 deg in declination and 1.3 deg in hour angle which were taken out mechanically using the antenna angle readouts as reference.

b. Station operations.

Departures from normal recording. Although not specifically requested in the Operations Support Plan, it was assumed that a recording on the Consolidated Electrodynamics Corporation (CEC) oscillograph of the monitor receiver signal strength would be desirable. Just prior to acquisition, the temporary patching arrangements to provide this record became disturbed and the calibration upset. This recording was therefore missed. In the transfer to the IMP S-74 configuration immediately following the AC-2 mission, the monitor receiver line was used for 136-Mc signals, preventing a post-track calibration.

The system temperature was recorded on the CEC oscillograph Channel 29 and, as on previous occasions, gave a record of signal strength independent of the phase-locked loop. This showed the system temperature variation due to signal strength variations as the spacecraft rolled.

Only one of two magnetic tape recorders was used for AC-2; the other was set up on 1⅞ in./sec for the IMP S-74 configuration.

Countdown. The countdown started at 09:00 GMT on November 27, 1963 and was uneventful apart from an excessive residual phase error and a faulty metering circuit for system noise temperature. The excessive residual phase error was traced to 60-cps pickup from the Hewlett-Packard counter and, after rerouting the cable, no further trouble was experienced. No action was taken on the system noise temperature problem after it had been traced to the reference channel mixer because of possible bad effects on station calibrations.

Collimation tower target illumination lights were defective so that optical and TV boresights had to wait until post-track.

Tracking operations. In view of the big delay before launch, a second AGC calibration was taken just before acquisition. Acquisition aid phasing was checked and the near collimation tower lowered to the ground.

The station received predictions at the nominal time and it was evident that the spacecraft was on a near nominal trajectory. Nevertheless, as confirmed by Net Control, the station followed the full acquisition scan and acquired signals as the scan pattern converged onto the predictions. No difficulty was experienced in transferring from the acquisition aid to the dish soon after going to autotrack.

The sequence of tracking events was as follows:

20:02:33	Antenna at acquisition point 1; Receiver bandwidth, 20 cps; AGC time constant, 10 sec.
20:05:03	Antenna moves to acquisition point 2.
20:06:33	Antenna moves to acquisition point 3.
20:06:44	Signals acquired; sideband lock suspected; data transmission started; servo remains in aided track.
20:07:05	Receiver breaks lock to check carrier lock; servo moves on into prediction path.
20:08:52	Receiver in lock on carrier; good doppler data; tracking data transmission updated.
20:09:12	−135-dbm peak; receiver switched from manual to normal, giving first AGC reading indicated a ripple of 0.67 cps.

20:10:12 Autotrack; servo bandwidth, 0.2 cps both HA and Dec (high speed).

20:10:20 −100-dbm peak received signal level, transfer from acquisition aid to dish; elevation, 11 deg; telemetry Channel 4 in lock with slight noise on signal strength nulls.

20:10:40 −98-dbm peak received signal level, snap-on complete; angle data switch to *good*.

20:10:50 AGC ripple very regular and varying between −98 and −115 dbm. Signals fall to extremely low level but, at this relatively high rate (0.67 cps), there is insufficient time for receiver to lose lock on the signal level nulls.

20:18:16 Reduction in amplitude of telemetry Channel 4 signals by about 25%.

20:23:27 Dec prelimit reached; telemetry Channel 4 commutator rate possibly reduced by 50% during pass.

20:26:40 Receiver out of lock having tracked in hour angle as long as possible.

Post-track calibrations.

End of mission.

c. Equipment operation.

Receiver. The receiver system operated well for AC-2, although there were residual phase error and system temperature monitoring difficulties.

There was evidence that the declination error channel was more sensitive than the hour angle error channel, and this was traced to the wide-band feed. When time permits, antenna patterns will reveal the true extent of the variations, but it is not expected to be serious.

Prior to the mission, attempts were made to use the recently installed wave analyzer to confirm carrier lock. This was found to be operationally difficult; it is unlikely to be successful until a motorized drive is delivered so that a pen recording of the received spectrum can be taken.

An alternative method used in the mission was to display a lissajous figure of the 455-kc oscillator and signal on an oscilloscope. The pattern is quite distinctive, depending on whether sideband or carrier lock has been achieved, and is similar to the sketches in Fig. 8. Operators soon come to recognize the various patterns, and in addition to the general appearance of the dynamic phase error signal, good carrier lock confirmation is achieved.

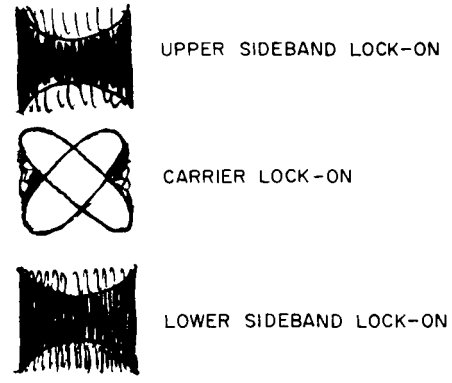

NOTES:
(1) 3-db SUPPRESSION, −110-TO-140-dbm SIGNAL STRENGTHS (APPROX)
(2) HIGHER DEPTHS OF MODULATION AND SIGNAL STRENGTHS OUTSIDE THE RANGE SHOWN MODIFY THE PATTERNS

Fig. 8. Lissajous figures

The arrangement of the acquisition aid system is shown in Fig. 9. The monitor receiver used consisted of a Collins Mixer followed by the 51J4 receiver tuned to 30 Mc. The local oscillator for the mixer was derived from the ×6 multiplier of the reference channel of the receiver. The recorder used was a locally available four-channel pen recorder.

The acquisition aid relays were located in the tracking feed drum and ⅞-in. spiraline run from the dish rim to the quad tip carrying the acquisition aid signals. Phasing of the acquisition aid was accomplished by automatically switching in 455-kc phase shifters when in the acquisition aid mode.

Performance during the aircraft tracks and the mission was excellent; no difficulty has been experienced with phasing or with transferring from the acquisition aid to the main beam.

Servo. Considerable effort was directed toward obtaining satisfactory collimation tower high-speed snap-ons in both track (far collimation tower) and acquisition (near collimation tower). These efforts were rewarded by trouble-free acquisition and tracking throughout the mission.

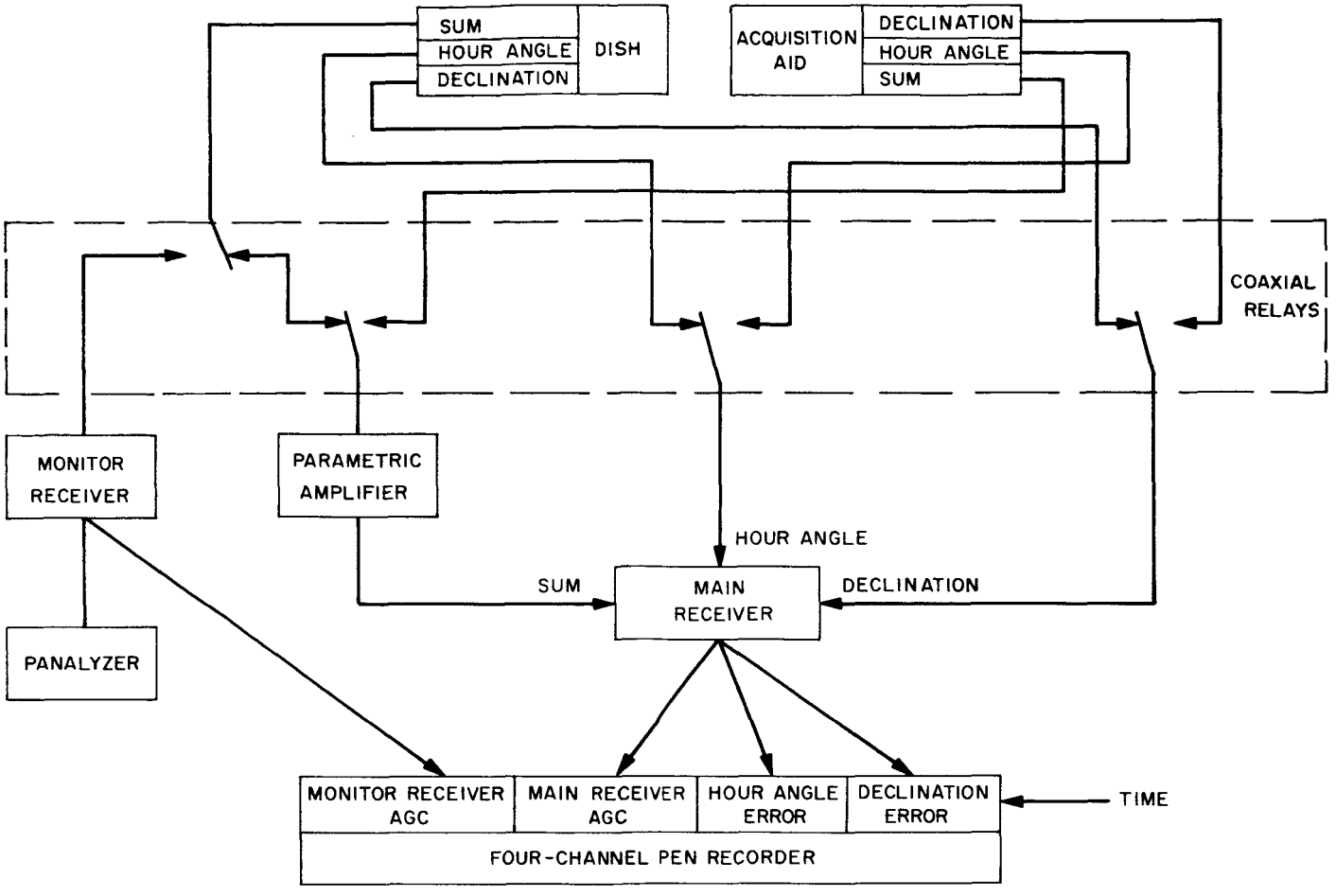

Fig. 9. Acquisition system for AC-2 mission

A major advance in operating procedure was made by calibrating the x–y plotter over a range 90 deg in hour angle and 60 deg in declination. Angle grids were marked on the chart and the horizon, and the 10- and 20-deg elevation contours drawn in. In addition, the nominal and extreme trajectories were plotted as well as acquisition scan pattern. New predictions were marked on the plotter as they arrived. It was then a simple matter to follow the acquisition scan to intercept the nominal predictions and to tell if the antenna was wandering off predictions. The elevation contours were particularly helpful in indicating how much perturbation could be expected from the ground.

Data. No difficulties were experienced in the data system.

Instrumentation. Only one tape recording was taken so that the second tape recorder could remain set up on 1⅞ in./sec to support the IMP S-74 mission.

Equipment behavior throughout the mission was satisfactory.

Reference

1. "Goldstone Operations," *Space Programs Summary No. 37-24*, Vol. III, p. 6, November 30, 1963.

III. Engineering Developments

A. Systems Engineering

1. S-Band Systems Engineering

A preliminary IBM listing of all inter-subsystem signal paths has been published and is undergoing review by the respective cognizant engineers for each subsystem.

A detail drawing has been issued of the internal cage structural members which will be used for mounting racks and equipment in the antenna cage. A second assembly drawing is being prepared showing the mounting location of the various racks and equipment in the antenna cage.

Operation and calibration procedure outlines and quarter-scale front panel drawings have been received from all subsystem cognizant engineers. The quarter-scale drawings have been made into cardboard mockups. Floor layouts of the Control Buildings for each of the DSIF Stations have been collected. It is intended to use the mockup racks in conjunction with quarter-scale floor plans of the various stations to human engineer the control room layouts.

An indentured specification list is being compiled using the Deep Space Net System Specification as the top document and will work down through the subsystem functional design and test specifications; module design and test specifications; and the DSIF standard and general specifications. The subsystem functional specification rough drafts have been completed and are now undergoing review.

2. Project Engineering

a. **Surveyor.** A series of compatibility tests between the feasibility model of the S-band receiver and the command and data console (CDC) at Hughes Aircraft has been conducted in accordance with the test plan reference in Ref. 1.

Commands generated in the CDC modulated a model of the ground transmitter and were received through a coax line by a spacecraft receiver where the received bit error rate was checked against received signal strength. Simulated telemetry and television signals from the spacecraft transmitter were received in the same way by the CDC and evaluated as a function of signal strength.

The tests revealed a need for some minor redesign of the DSIF feasibility model receiver; and a full report is being written and published by Hughes Aircraft Co.

The document controlling the *Surveyor*/DSIF/CDC interface requirements[1] has been revised and expanded to cover more technical details of the *Surveyor* spacecraft.

Approval has been obtained for a plan to carry out compatibility tests of the T-21 *Surveyor* spacecraft with the full GSDS S-band system at Goldstone. This plan proposes to mount the T-21 spacecraft in a radio transparent igloo at the Goldstone antenna range. The igloo will be 32 ft in diameter, 16 ft high at the apex, and built of fiberglass and foamed plastic laminate.

A radio path from the antenna range to the Echo site will be established via a passive reflector on the Echo collimation tower. The propagation loss of the path is expected to be about 200 db. Site measurements and procurement action are proceeding.

Material relating to the DSIF commitments for the *Surveyor* Project has been prepared for presentation to the *Surveyor* Design Review Board.

***b.* Ranger.** System performance tests were performed between the *Ranger 6* Proof Test Model spacecraft and the DSIF. Some of the more important tests conducted are:

(1) Measurement of the performance of the spacecraft television system through the DSIF system.

(2) Threshold tests of the spacecraft DSIF receiving link.

(3) Test of the data loop from the spacecraft through the DSIF to the Space Flight Operations Facility at JPL. Test results are still under evaluation.

The Operational Support Equipment document stipulating the DSIF performance numbers is in the process of revision.

***c.* Pioneer.** A preliminary functional description of the Ames DSIF *Pioneer* Program was completed for forwarding to Ames and Space Technology Laboratories (STL). This description, together with similar inputs from STL, will form the basis for an interface specification to be issued by Ames Research Center.

[1]"Surveyor Spacecraft/DSIF Interface Requirements," JPL Project Control Document No. 6.

Coordination with STL continued in the areas of telemetry, command, recording, and display. A review of STL's experience in computer processing of pulse code modulation telemetry data was held at STL with representatives from the Telecommunications Division of JPL. A familiarization tour of the Goldstone facilities was conducted for STL and Ames representatives.

3. Systems Analysis

A contract is being initiated for rewrite of the DSIF Systems Manual. Initially, the manual will contain only L-band information. At a later date it will be expanded to include the system capabilities of the S-band system. Most of the technical information will be supplied by JPL personnel.

Patterns of illumination of the Moon by an 85-ft DSIF antenna at L-band have been calculated and plotted. Effects on system signal-to-noise ratio, when the Moon is within the antenna beam, have also been calculated and plotted.

A systems specification for the AMR Spacecraft Monitoring Station is being prepared. It will include mission support objectives, system requirements, and subsystem hardware requirements.

B. Computer Programs

1. Trajectory Program for On-Site Computers

A spacecraft trajectory program has been developed for small, on-site computers (SDS 920, IBM 1620) to relieve the Central Computing Facility of the responsibility of providing predictions and/or antenna drive tapes for the DSIF Stations. Although the program will be kept as small as possible, it will be accurate enough to permit the spacecraft to be within the beamwidth of the antenna pattern. However, many effects which normally would be considered in a precision trajectory program must now be omitted. A method of minimizing the error caused by omitting certain terms will be given in the following program discussion. The program does not attempt to consider powered flight during midcourse maneuver.

The solution to the trajectory problem is obtained by a variable step size numerical integration of the equations of motion. The integration is accomplished by a second-order Runge–Kutta integration scheme, starting with the position and velocity vector components at injection epoch. At present, the program has provision for three step sizes which are used as follows:

(1) The first step size is used for adjusting time to some even value. This procedure is necessary because injection usually occurs at an odd time, i.e., decimal parts of a second.

(2) The second step size is used as a coarse integration step. That is, if the predictions were required at a 2-sec interval and the first value was required 3 hr after injection, it would be too time consuming to perform the integration for 3 hr with a 2-sec step size. In this case, the second step size could be any value greater than 2 that would not cause a loss in accuracy. The maximum value that can be used will vary with the type of mission.

(3) The third step size is equal to the desired prediction printout interval.

During that portion of the spacecraft trajectory for which the Earth is the central body, the second harmonic of the oblateness potential is used. Due to limited computer storage, no other perturbation effects are used in the program. By starting the integration with forward-mapped position and velocity vectors (together with their associated time), the effect of omitting the other perturbations should be minimized.

The integration is performed in geocentric "space-fixed" Cartesian coordinates. When the first printout time is reached, the vectors are transformed to geocentric Earth-fixed Cartesian coordinates. These, in turn, are transformed to topocentric coordinates, i.e., azimuth–elevation or hour angle and declination angle. A refraction correction is then computed and added to the coordinate values. If an antenna angle drive tape is required, these values are punched out on paper tape and the next point is computed. If a prediction listing is required, both the one-way and two-way doppler detector outputs (D1 and D2) are computed. These computations are made with the last reported spacecraft transponder frequency (prior to launch), and a nominal transmitter VCO frequency of 29.668212 Mc. The generation of a set of predictions (horizon-to-horizon listing and angle drive tape) for a given station requires 14 min on the SDS 920 computer. Only 6 min are required for the actual computation and drive tape punching; the remaining 8 min are used for the printing of the predicted values on the Flexowriter.

To date, two test trajectory computations have been made using *Ranger 4* and *Mariner 2* data. In the *Ranger 4* test, integration was started at injection epoch and carried out until lunar impact. Topocentric coordinates for both the Woomera and Johannesburg Tracking Stations were obtained on an hourly printout. These values were compared with those obtained from the IBM 7090 Space Trajectory Program. The error, defined as the difference between values obtained from this program and the 7090 program, was less than or equal to 0.2 deg in hour angle and less than or equal to 0.029 deg in declination angle throughout the entire trajectory. These values are well within the antenna beamwidth.

In the *Mariner 2* test, the program was started at injection epoch and integrated forward for 6 days. When compared with the 7090 trajectory output, the maximum error was less than 0.090 deg in hour angle, 0.040 deg in declination angle, 4.8 cps at one-way doppler detector output, and 4.8 cps at two-way doppler detector output throughout the total integration period. In both tests, the integration step size was 60 sec. By using a smaller step size, it should be possible to reduce the magnitude of the errors.

Further investigation is continuing with both *Mariner 2* and *Atlas–Centaur 2* data.

2. A Method of Rejecting Possible Blunder Points in Tracking Data

a. Introduction. The tracking data used by the Orbit Determination Program (ODP) has a tendency to be contaminated by discrete noise with large variance. This usually happens with very small probability. Because of the nature of the estimation technique used in the ODP, great importance is given to the removal of these points. These points or observations are usually called "blunder points." The optimum time for removing the blunder points is just before the tracking data is used by the ODP; this is the method discussed in this article.

If doppler tracking data is considered as an observed time series and differenced with a second time series made up of the predicted doppler values, based on the best estimate of the initial conditions of the spacecraft's trajectory, then the differenced time series acts like a stationary time series.

Let the sampled time series of the tracking data be denoted as $S(i)$ where $i = 1, \cdots, N$ and let $P(i)$ be the best estimate of $S(i)$ based on the knowledge of the trajectory's initial conditions. The ODP assumes that the sample time series $S(i)$ is the sum of two time series, one representing real-time range rate $R(i)$ and a noise time series consisting of a set of random variables that are independent of the time series $R(i)$ and having zero mean; i.e., $S(i) = R(i) + N(i)$ where $R(\ )$ and $N(\ )$ are independent, with $R(i)$ being representative of the real-time rate between the spacecraft and the tracking station and $N(i)$ is a random variable with mean zero. The differenced times series is

$$D(i) = S(i) - P(i) = [R(i) - P(i)] + N(i) \tag{1}$$

If $[R(i) - P(i)] \equiv 0$, there would be no problem with rejecting possible blunder points; but, in general, this is not the case. Usually a time series has an increasing trend to it, which must be removed before the time series can be handled as a stationary time series.

Even though the difference time series $D(i)$ generally is not just the noise, it was found through experimenting that $D(i)$ reasonably could be assumed to be a stationary time series. This suggests the use of autoregression, smoothing as given by Wold (Ref. 2) or Hannan (Ref. 3) to reject possible blunder points.

b. Analysis. Consider the time series $W(t)$, operated on by the expectation operator $E(\ )$. The mean value function $M(t)$ is defined

$$M(t) = E[W(t)] \tag{2}$$

The existence of the covariance kernel $K(t,s)$ is also assumed, where:

$$K(t,s) = E\{[W(t) - M(t)][W(s) - M(s)]\} \tag{3}$$

and if

$$K(t,s) = R(t-s) \tag{4}$$

for all t and s such that the time series $W(t)$ and $M(t)$ and $K(t,s)$ have meaning, then the time series is called stationary (Ref. 4). Wold (Ref. 2) showed that there exists, when the time series has a discrete index, a nondecreasing bounded function $F(\omega)$, defined for $-\pi \leq \omega \leq \pi$ such that

$$R(\gamma) = \int_{-\pi}^{\pi} \exp(it\omega)\, dF(\omega) \tag{5}$$

$F(\omega)$ is known as the spectral distribution function when

$$1 = F(\pi) - F(-\pi) \tag{6}$$

It is shown by Hannan (Ref. 3) that if

$$\int_{-\pi}^{\pi} \log f(\omega)\, d\omega > -\infty \tag{7}$$

where

$$f(\omega) = \frac{dF(\omega)}{d\omega}$$

then the time series $W(t)$ can be written as

$$W(t) - E[W(t)] = \sum_{j=0}^{\infty} Z_j \exp(it\lambda_j) + \sum_{j=0}^{\infty} \alpha_j \xi(t-j) \tag{8}$$

(Ref. 3) where Z's and $\xi(t-j)$ are uncorrelated random variables and α's are constants. It is also shown that if Eq. (7) holds and $F(\omega)$ is absolutely continuous then the first summation in Eq. (8) can be dropped (i.e., no pure sinusoids), and the time series $W(t)$ can be written as

$$W(t) - M(t) = \sum_{j=0}^{\infty} \alpha_j \xi(t-j) \tag{9}$$

where α's are constants and $\xi(t-j)$ are uncorrelated random variables with mean zero. In practice, it is unknown how to estimate the constants α_j and characteristics of the random variables $\xi(t-j)$, without some *a priori* knowledge of how the time series is generated. Instead, a transformation of Eq. (9) is made to

$$\sum_{j=0}^{\infty} \beta_i [W(t-j) - E[W(t-j)] = \xi(t-c) \qquad \beta_c = 1 \tag{10}$$

which is almost the same problem as above except that, under the condition of Eqs. (3) and (4), it is possible to estimate the constants β_j. A procedure that uses Eq. (10) is usually called autoregressive filtering.

In order to use autoregression, a check must be made on the stationarity of the time series of interest, and a test must be made to determine whether the spectrum distribution function $F(\omega)$ is absolutely continuous or not. In using autoregression, the transition from an infinite series to something finite is made in terms of limits; i.e.,

$$\sum_{j=0}^{m} \beta_i [W(t-j)] - E[W(t-j)] = \xi(t-c) \qquad \beta_c = 1 \tag{11}$$

and let $m \to \infty$. If Eq. (11) is used for estimating $W(t)$ then the variance of $[\widehat{W}(t) - W(t)]$ is monotonically decreasing in m. Therefore, it is only necessary to select a value of m large enough. It was found that $m = 2$ was sufficient for tracking data editing (Ref. 3). Let

$$Y(t) = W(t) - E[W(t)] \tag{12}$$

then in terms of $Y(t)$ and for a fixed m the solution for the $\beta_0, \cdots, \beta_m$ where $\beta_c = 1$ is found by:

$$\sum_{j=0}^{m} \beta_j Y(t-j) = \delta(t-c) \tag{13a}$$

$$Y(t-i) \sum_{j=0}^{m} \beta_j Y(t-i) = Y(t-i)\,\delta(t-c) \tag{13b}$$

$$E\left[Y(t-i) \sum_{j=0}^{m} \beta_i Y(t-j)\right] = E[Y(t-i)\,\delta(t-c)] \tag{13c}$$

$$= E[Y(t-i)]\,E[\delta(t-c)] = 0$$

Therefore,

$$\sum_{j=0}^{m} \beta_i E[Y(t-i)\,Y(t-j)] = \sum_{j=0}^{m} \beta_i R(j-i) = 0 \tag{13d}$$

Let

$$\bar{\Lambda} = \begin{bmatrix} \rho(0) \cdots \rho(m-1-c) & \rho(m+1-c) \cdots \rho(m) \\ \vdots & \\ \rho(m-1-c) & \rho(m+1-c) \\ \rho(m+1-c) & \rho(m-1-c) \\ \vdots & \\ \rho(m) \cdots \rho(m+1-c) & \rho(m-1-c) \cdots \rho(0) \end{bmatrix} \tag{14}$$

where

$$\rho(\gamma) = \frac{R(\gamma)}{R(0)}$$

$$\bar{\beta} = \begin{bmatrix} \beta_0 \\ \vdots \\ \beta_{c-1} \\ \beta_{c+1} \\ \vdots \\ \beta_m \end{bmatrix}$$

and

$$\bar{\Gamma} = \begin{bmatrix} \rho(-c) \\ \vdots \\ \rho(-1) \\ \rho(+1) \\ \vdots \\ \rho(m-c) \end{bmatrix} \tag{15}$$

In terms of matrixes, the equation for the β's is

$$\bar{\Lambda}\bar{\beta} = \bar{\Gamma} \tag{16}$$

There is always a unique solution of Eq. (16) since if $c = 0$, $\bar{\Lambda}$ is a positive definite matrix which implies that $\bar{\Lambda}$ is positive for any c, and in general there is an easy solution of a matrix equation like Eq. (16). (See Wilkinson, Ref. 5.) The solution of Eq. (16) gives an estimate $\widehat{X}(t-c)$ of $X(t-c)$ in terms of m other values of the time series. Depending on c, this can be either a prediction or smoothing.

In practice, for a small period of time the mean value is taken to be a constant, M, and is estimated by

$$\widehat{M}(t) = \frac{1}{N} \sum_{t=1}^{N} W(t) \tag{17}$$

and

$$\widehat{R}(\gamma) = \frac{1}{N} \sum_{t=1}^{N} W(t)\,W(t+\gamma) - [M(t)]^2 \tag{18}$$

It is clear that $\widehat{R}(\gamma)$ is a consistent estimate of $R(\gamma)$ and is positive definite. This means that there always exists an inverse to $\bar{\Lambda}$ in Eq. (16).

With $2N + 1$ observations denoted as $D(-N), \cdots, D(0), \cdots, D(N)$ it is possible to estimate $M(0)$, and $R(\gamma)$ for $\gamma = 0, 1, 2$ then make a test of $D(0)$. If $D(0)$ is rejected when it is greater than 2 cps different from predicted, less than one-fourth of the data would be rejected based on simulating the method below. This checking could be done on a computer by keeping three auxiliary series c_1, c_2, and c_3, defined as follows:

$$c_1(j) = D^2(j) \tag{19a}$$

$$c_2(j) = D(j)\,D(j-1) \tag{19b}$$

$$c_3(j) = D(j)\,D(j-2) \tag{19c}$$

for $j = -N, \cdots, 0, \cdots, N$. The estimate for the mean value $M(0)$ is

$$\hat{M}(0) = \frac{1}{2N+1} \sum_{j=-N}^{N} D(j) \tag{20a}$$

and for $R(\gamma)$,

$$\hat{R}(0) = \frac{1}{2N+1} \sum_{j=-N}^{N} c_1(j) - \hat{M}^2(0) \tag{20b}$$

$$\hat{R}(1) = \frac{1}{2N+1} \sum_{j=-N}^{N} c_2(j) - \hat{M}^2(0) \tag{20c}$$

$$\hat{R}(2) = \frac{1}{2N+1} \sum_{j=-N}^{N} c_3(j) - \hat{M}^2(0) \tag{20d}$$

for $\gamma = 0$, 1, and 2, respectively.

With the solution of the two following equations [derived from Eq. (16)] for $c = 0$ and $+1$

$$\begin{bmatrix} \hat{R}(0) & \hat{R}(1) \\ \hat{R}(1) & \hat{R}(0) \end{bmatrix} \begin{bmatrix} \hat{\beta}_1 \\ \hat{\beta}_2 \end{bmatrix} = \begin{bmatrix} \hat{R}(1) \\ \hat{R}(2) \end{bmatrix} \tag{21a}$$

$$\begin{bmatrix} \hat{R}(0) & \hat{R}(2) \\ \hat{R}(2) & \hat{R}(0) \end{bmatrix} \begin{bmatrix} \hat{\delta}_1 \\ \hat{\delta}_1 \end{bmatrix} = \begin{bmatrix} \hat{R}(1) \\ \hat{R}(1) \end{bmatrix} \tag{21b}$$

Three checks of $D(0)$ can be made using two other points. These are:

$$D(0) = \hat{M}(0)(1 - \hat{\beta}_1 - \hat{\beta}_2) + \hat{\beta}_1 D(-1) + \hat{\beta}_2 D(-2) \tag{22a}$$

$$D(0) = \hat{M}(0)(1 - \hat{\beta}_1 - \hat{\beta}_2) + \hat{\beta}_1 D(1) + \hat{\beta}_2 D(2) \tag{22b}$$

$$D(0) = \hat{M}(0) + \hat{\delta}_1 [D(-1) - D(1)] \tag{22c}$$

for the three main tests using two points.

The rejection criterion would be in terms of what the ODP could tolerate as a possible error. When points of $D(j)$ are missing to compute $\hat{M}(0)$, $\hat{R}(0)$, $\hat{R}(1)$, and $\hat{R}(2)$, it is possible to assume the missing points were zero and average in Eq. (20) by the number of points observed, or in the case of $\hat{R}(0)$, $\hat{R}(1)$, and $\hat{R}(2)$ it is possible to use *a priori* estimates of $\rho(1)$ and $\rho(2)$. This approach also needs points surrounding $D(0)$ to make a test; but if there are none due to bad transmission conditions, it is probably best to reject $D(0)$ also.

c. Description of experiment to test stationarity and continuity of spectrum. The basic idea of the test of stationarity was to take simulated tracking data that might be observed and difference this data with what could have been the available predictions. This was accomplished by perturbing the initial conditions of a set of predictions to get simulated tracking data. The amount the initial conditions were perturbed was taken to be as large as possible without eliminating possibility of success of a flight to the Moon. The data used was from the early part of a flight, just after injection, when doppler rates would change the most. The mean value was removed from the differenced time series $D(i)$, and the normalized correlation function $\hat{\rho}(\gamma)$ was computed. It was found that, for an assorted collection of launch azimuths and launch days, the correlation function $\hat{\rho}(\gamma)$ fell into the two classifications needed in a test of stationarity: $\hat{\rho}(\gamma) \approx 0$ if $\gamma \neq 0$ and if $\gamma \neq 0$, then $\hat{\rho}(\gamma)$ was approximately the same for the rest of the launch azimuths and launch days. In fact, 341 correlation functions that were in the second classification have the following averages and variances:

$$\rho(1) = 0.936 \qquad \sigma^2 = 0.011$$
$$\rho(2) = 0.911 \qquad \sigma^2 = 0.010$$
$$\rho(3) = 0.868 \qquad \sigma^2 = 0.013$$
$$\rho(4) = 0.822 \qquad \sigma^2 = 0.014$$
$$\rho(5) = 0.771 \qquad \sigma^2 = 0.024$$
$$\rho(6) = 0.714 \qquad \sigma^2 = 0.034$$

This variance would be considered high since a worse case was taken in generating the data, and long periods of time were used, but they lent considerable weight to the hypothesis that the difference time series acted like a stationary time series. A statistical test of stationarity with a known distribution is yet to be developed. The system noise was not considered in the test. The techniques used were so gross that only blunder points would have any effect.

The test to see if the spectral distribution function was absolutely continuous was made on actual tracking data by computing the spectral distribution function and comparing it with an integrated spectral density function (Ref. 6). The main comparison tests were a sign test, and a χ^2 (Ref. 7). Tested in the range between 30 cycles/hr (the Nyquist frequency) and ¼ cycle/hr, the spectral distribution was absolutely continuous. In the range between dc and ¼ cycle/hr, the tests were inconclusive due to problems in techniques. This means that, in batches of tracking data of less than 2 hr in length, it was impossible to detect any pure sine functions.

There is, at present, extensive work being carried out to improve the techniques of computing and testing both the correlation functions and their spectrums. These improved techniques are needed to make further tests to the main assumptions before autoregression is committed for real-time use.

C. *Mariner* C 100-kw Transmitter

1. Klystron Amplifier Subsystem

It has been determined that under certain conditions it will be necessary to have a ground transmitter power of 100-kw continuous wave (CW) in the *Mariner C* operation. At the present time, a complete 100-kw CW transmitting sysem at 2388 Mc is in operation at the Goldstone Venus site and has been in use since mid-January 1963 in planetary radar experiments. To meet the *Mariner C* requirements, it was decided to furnish a 100-kw CW klystron amplifier subsystem in the frequency range of 2100 to 2130 Mc designed to be a direct replacement for the 2388-Mc klystron amplifier subsystem. It was further decided that, in order to increase reliability, a second 100-kw amplifier would be provided in the subsystem with the provisions for rapid transfer from one amplifier to the other.

A functional block diagram of this 100-kw subsystem is shown in Fig. 1. The RF switch will allow either transmitter to be connected to the antenna feed, and either transmitter may be operated into the RF water load. The RF cable from the exciter and those to the RF moni-

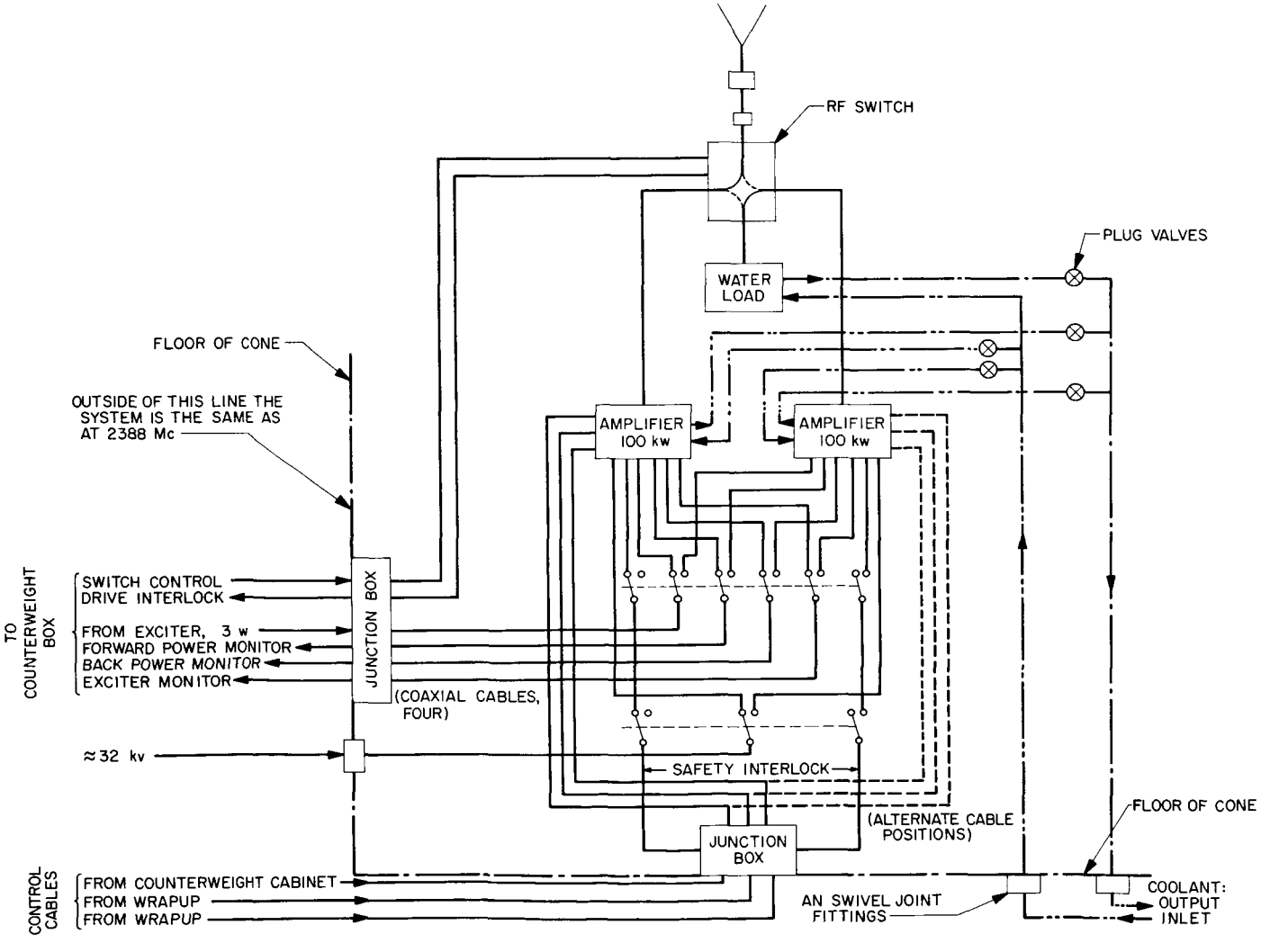

Fig. 1. 100-kw installation for *Mariner C*

tor meters will be transferred from one amplifier to the other by means of switches as will the beam voltage. The three control cables will be manually connected by means of multi-pin connectors to the amplifier in use. Safety interlocks on the high-voltage and coaxial switches and trace wires in the control cables will prevent accidental cross-connecting of the amplifiers. The coolant may be directed to either amplifier or allowed to flow through both amplifiers to prevent freezing and to maintain the nonoperating amplifier in a preheated condition.

The antenna feed cone layout is shown in Fig. 2. This completely assembled cone will be directly replaceable with the 2388-Mc feed cone that is now on the 85-ft Az–El antenna at the Venus site.

The fabrication and assembly of the amplifier subsystem are presently under contract negotiation. The documentation of the complete 100-kw system at the Goldstone Venus site (Ref. 8) has progressed to the point that this 100-kw amplifier subsystem for *Mariner C* will be procured from prints on a fixed price basis. These new amplifiers will incorporate improvements which have been developed as a result of 1-yr operating experience on the original 100-kw, 2388-Mc amplifier.

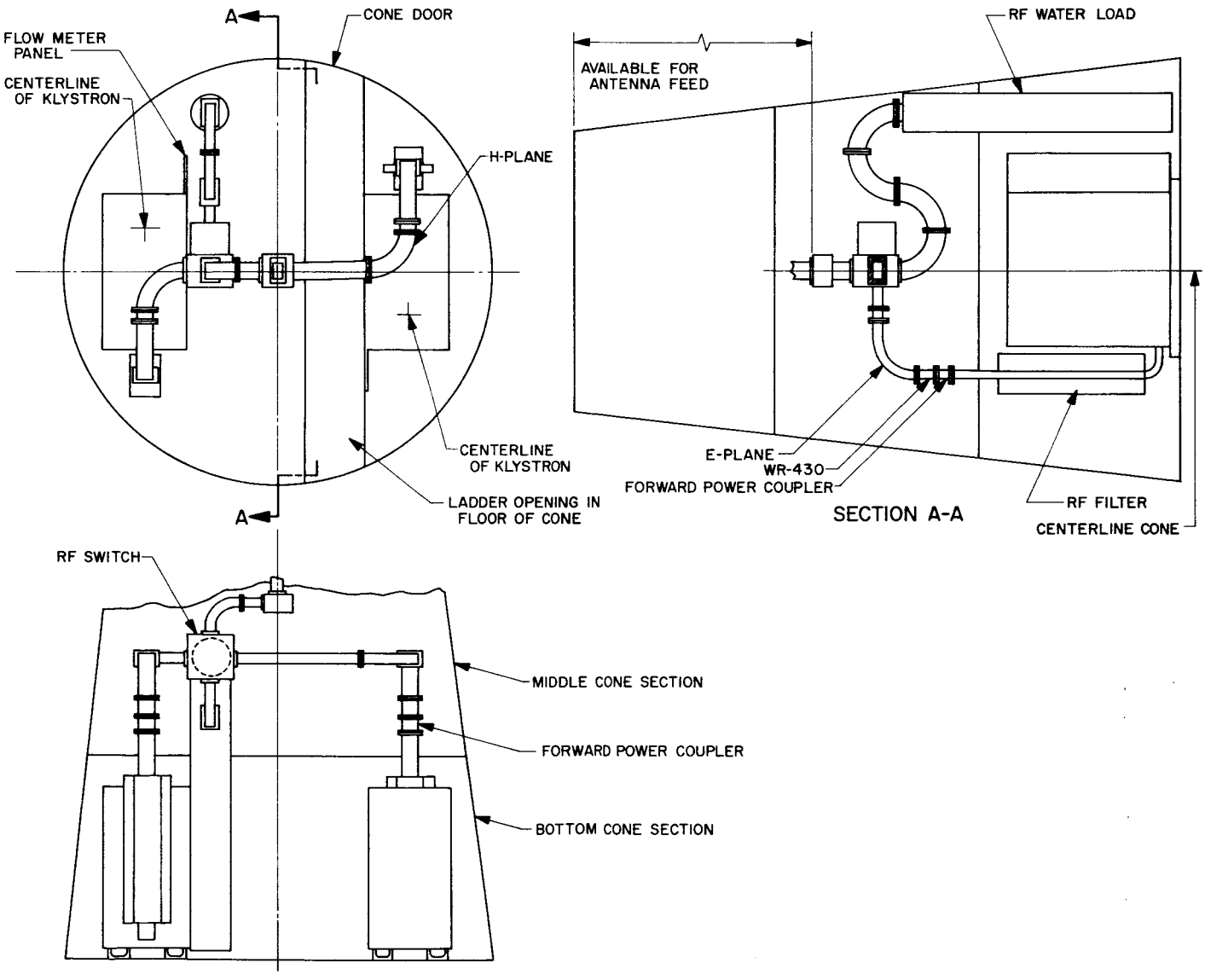

Fig. 2. Cone layout of two 100-kw amplifiers

References

1. "Projects," *Space Programs Summary No. 37-24,* Vol. III, p. 12, November 30, 1963.
2. Wold, H., *A Study in the Analysis of Stationary Time Series,* Uppsala, 2nd Ed., 1954.
3. Hannan, E. J., *Time Series Analysis,* Methuen, London, England, 1960.
4. Parzen, E., *Stochastic Processes,* Holden Day, 1962.
5. Wilkinson, J. H., *Error Analysis of Direct Methods of Matrix Inversions, Journal of the Association of Computing Machinery,* Vol. 8, p. 281, 1961.
6. Parzen, E., *An Approach To Time Series Analysis, Annals of Mathematical Statistics,* 1961.
7. Wilks, S., *Mathematical Statistics,* Wiley & Sons, New York, 1962.
8. "100-kw S-Band Klystron Amplifier," *Space Programs Summary No. 37-23,* Vol. III, p. 40, September 30, 1963.

IV. Research and Development

A. Ground Antennas

1. Boresight Calibrations for DSIF Antennas

a. Summary. Development is proceeding of practical techniques for using radio star sources to boresight the DSIF ground antennas. In Ref. 1, results from the use of a drift curve method for obtaining boresight errors were given. The method used digital recording and digital computer processing of the drift curve data. More recently, boresight measurements on radio sources have been made using different operational techniques. The measurements were made on the 85-ft Az–El antenna at the Venus site. The radio source was continuously tracked using an ephemeris angle drive tape to slave the antenna to the precise computed angular location of the source. If the drive tape did not steer the antenna exactly on the source, angular offsets were inserted until it did. The offsets required determine the boresight error. In Ref. 2, results obtained by using both optical and radio stars were presented. It was found that the elevation angle errors were cyclic with a peak-to-peak amplitude of 0.035 deg. These errors were ascribed to the elevation angle readout system. Recently, the elevation encoder has been replaced and the cyclic error has been eliminated. Results of the radio source and some optical source measurements are reported; on the basis of these data, the antenna was realigned and a few additional verifying tracks were made.

b. Recent work. In Ref. 2, a series of optical and radio frequency star tracks was presented. These star tracks were obtained by plotting azimuth and elevation boresight errors as a function of elevation angle. Figs. 1 and 2 show an optical and RF star track as presented in Ref. 2. A striking feature of these plots is the excellent agreement of the phase and amplitude of the cyclic elevation error as determined for the radio and optical star tracks. This cyclic error was interpreted as an elevation encoder defect.

After an examination of these data, it was decided to replace the elevation angle encoder unit. The original unit was removed and measured on the bench with a divider head. The results are plotted in Fig. 3; the peak-to-peak error is about 0.05 deg. Although the bench data are considerably more noisy than data obtained on the antenna (Figs. 1, 2) a careful comparison of Fig. 3 to these figures shows close agreement in the phase of the elevation error with elevation angle.

A new elevation encoder unit was prepared and installed on the antenna. Figs. 4 and 5 show the elevation error as a function of elevation angle as measured on the

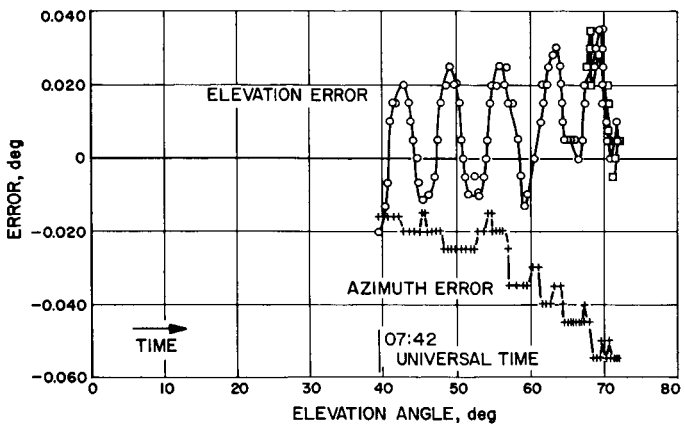

Fig. 1. Optical star track boresight errors for Aldebaran before elevation encoder replacement

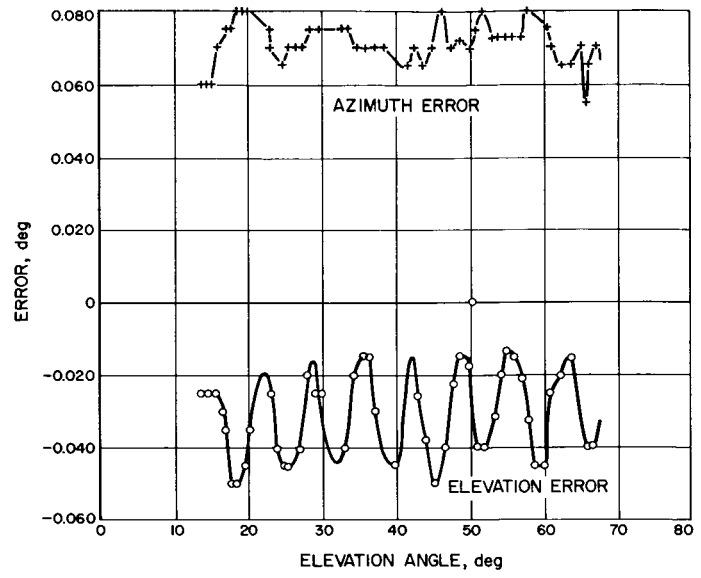

Fig. 2. Radio star track boresight errors for Cassiopeia A before elevation encoder replacement

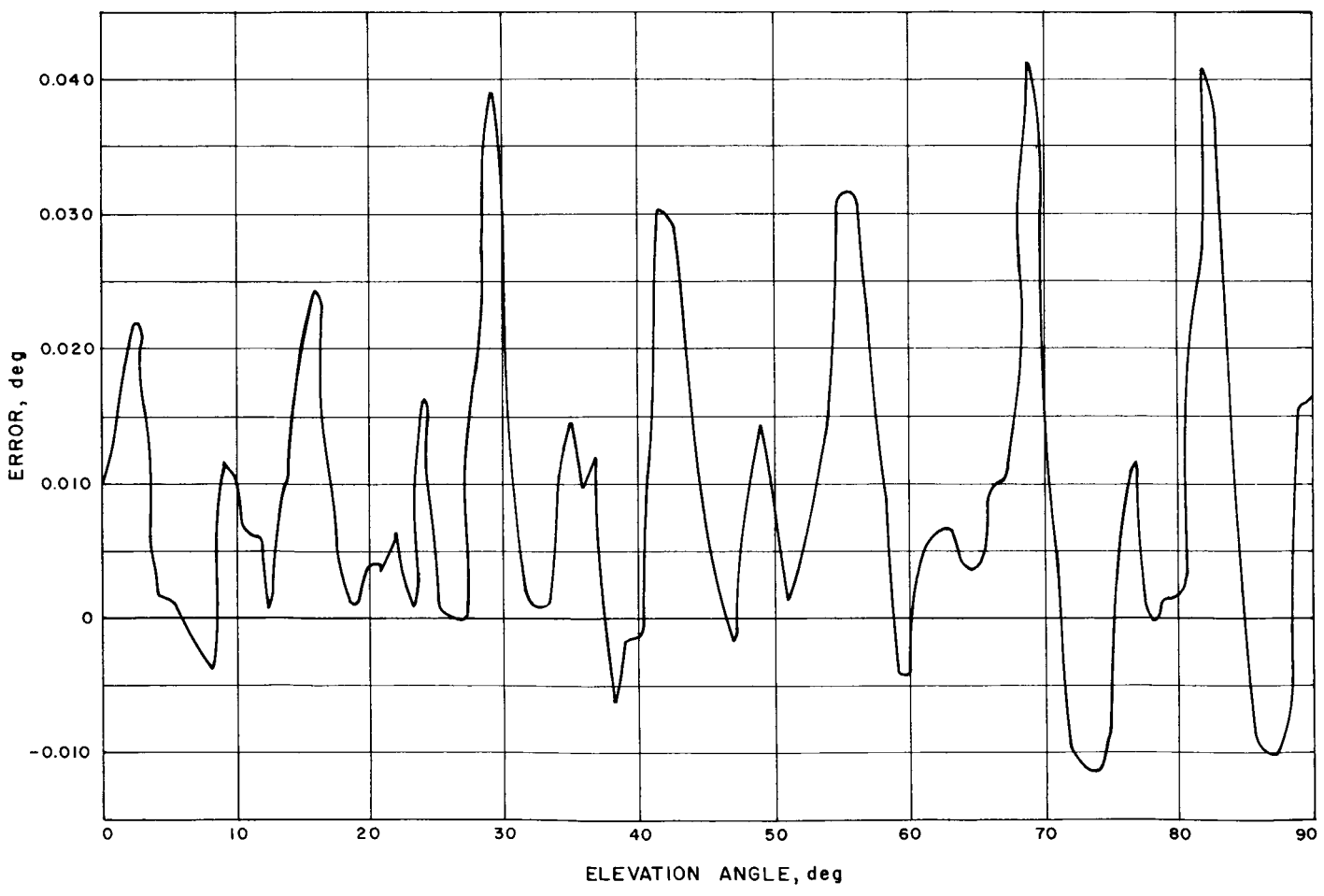

Fig. 3. Original decimal encoder error measured on divider head

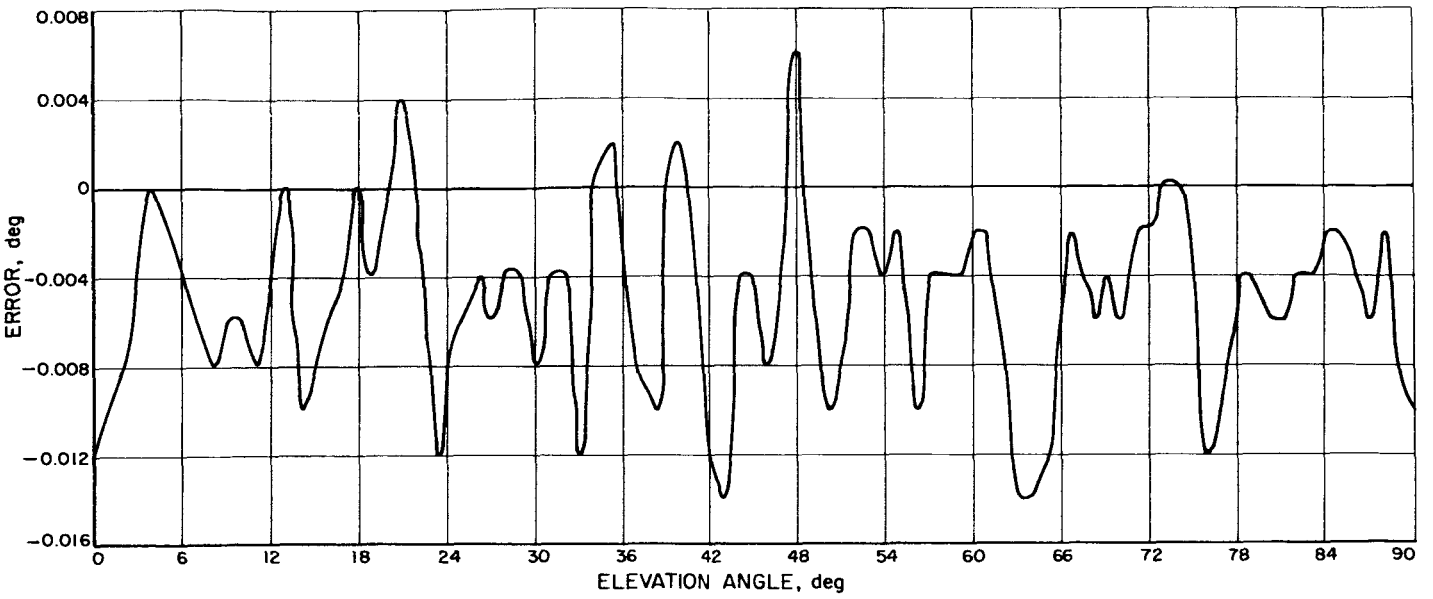

Fig. 4. New binary elevation encoder measured on divider head

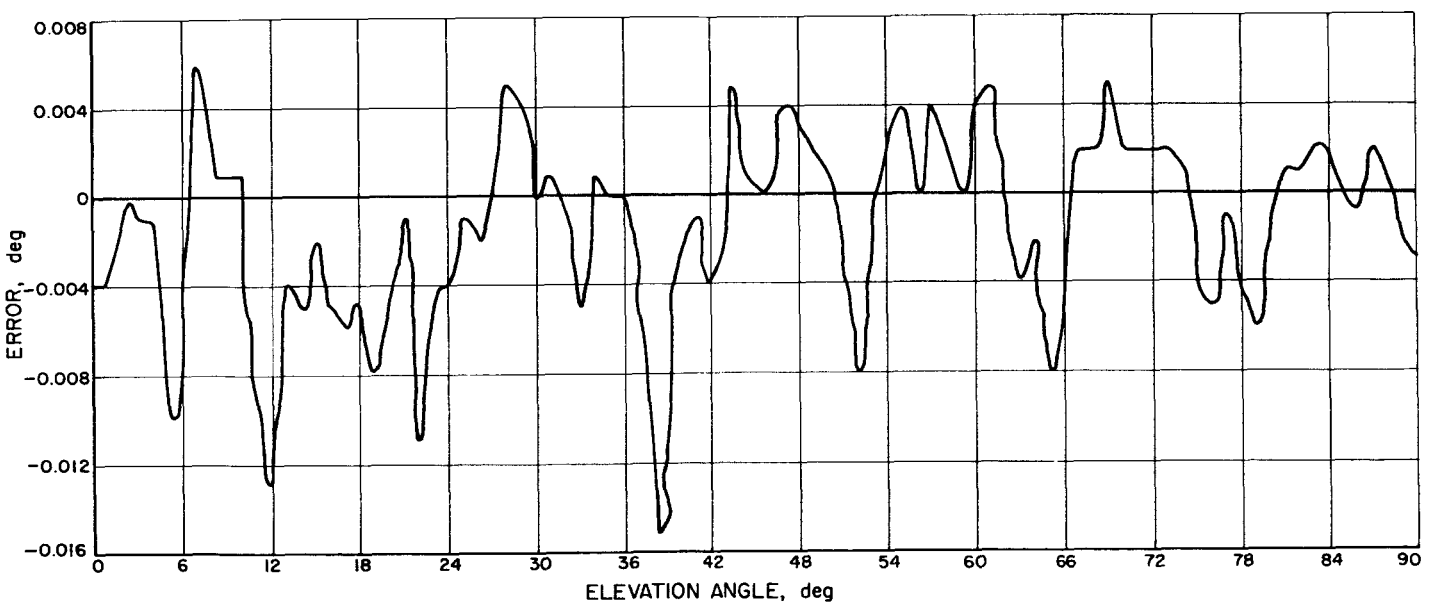

Fig. 5. New decimal elevation encoder measured on divider head

divider head for the new binary and decimal encoders. The peak-to-peak error is 0.02 deg.

After installation of the new encoders, a series of RF and optical star tracks was performed. Figs. 6 and 7 are plots of elevation and azimuth errors as a function of elevation angle. Fig. 7 was obtained from the optical source Aldebaran and Fig. 8 was obtained from the radio source Crab Nebula. The cyclic error in elevation has been removed with the use of the new encoder. The shapes of both radio and optical error curves are quite similar, but the bias offsets are different due principally to an offset in the TV camera reticle. The slightly larger peak-to-peak error in optical boresight, as compared to RF, may be due to a much longer effective time constant of the RF measurements as compared to the optical. After examining many optical and RF star tracks, it was decided to reposition the shaft encoder −0.012 deg in azimuth and +0.005 deg in elevation. Following the encoder adjustments, the TV camera reticle was readjusted

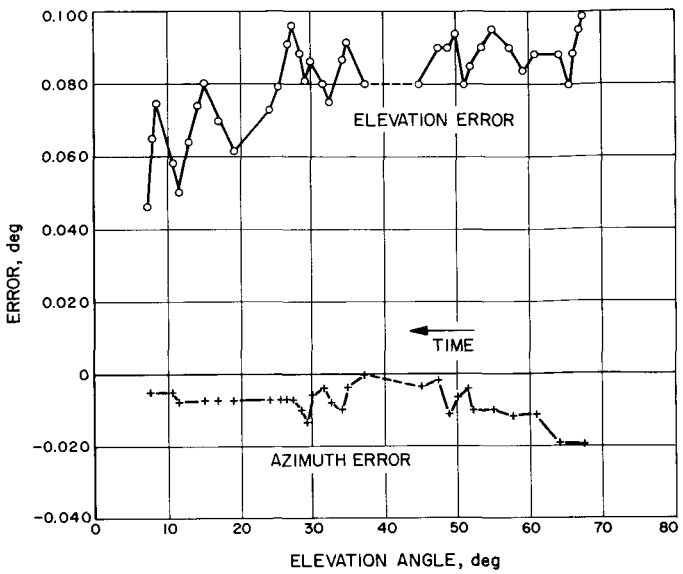

Fig. 6. Optical star track boresight errors for Aldebaran after encoder replacement and before bias reset

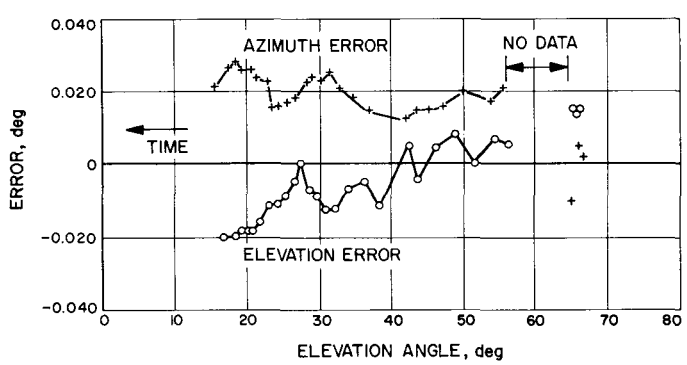

Fig. 7. Radio star track boresight errors for Cassiopeia A after encoder replacement and before bias reset

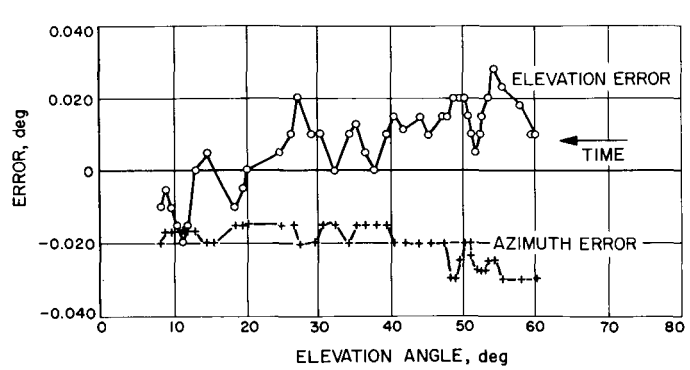

Fig. 8. Optical star track boresight error for Aldebaran after encoder replacement and bias reset

−0.008 deg in azimuth and −0.070 deg in elevation. The corrections were made December 18, 1963 and more star tracks are being conducted. Figs. 8 and 9 are initial data on boresight errors after the corrections from the same sources that were used in Figs. 6 and 7.

2. Antenna Instrumentation

a. Summary. A transportable instrumentation system is being developed for use in research and development testing of the structural and mechanical properties of large ground antennas. It will be used initially on the 30- and 85-ft antennas, and later on the 210-ft-diameter Advanced Antenna System (AAS). In addition to developing the necessary instrumentation for making measurements on the future 210-ft AAS, the data derived is continuously applied to validate the design analysis techniques being employed in the AAS Project. There is a detailed description of the instrumentation system in Ref. 3, and progress reports in Refs. 4 and 5. The system was first used for structural and thermal testing conducted as part of the 85-ft Az–El antenna resurfacing work during July and August 1963. Preliminary results appear in Ref. 6. Additional equipment has been added to the instrumentation system. Further measurements on the 85-ft Az–El antenna are planned.

b. Recent work. Critical antenna time prevented any extensive structural testing of the Az–El antenna after the resurfacing operations in August; this testing is scheduled throughout January 1964. The low-speed data scanning system in the instrumentation system will be used with the addition of a special scanner to monitor the wire span temperatures of the extensometers; this will

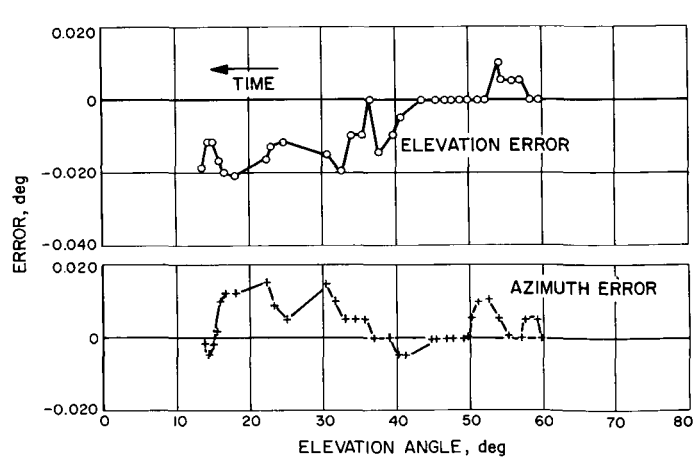

Fig. 9. Radio star track boresight error for Cassiopeia A after encoder replacement and bias reset

provide temperature correction as part of the data scan program information for the data analysis.

A Flexowriter has been added to the system to permit simultaneous automatic on-line printing of the scanned data and punching of the paper tape. Also, using the Flexowriter, hand-logged data and instructions can be coded onto the tape and printed records. In addition, the Flexowriter will permit typing out of data from the punched tape for later verification.

The following series of tests will be conducted on the 85-ft Az–El antenna during the January 1964 series of tests:

(1) Extensometer deflection tests of the reflector structure.

(2) Extensometer deflection tests of the quadripod and subreflector.

(3) Continuous recording tests of key extensometer positions for all reflector elevation angles.

(4) Reflector panel surface accuracy measurements using an automatic surface template sensor arrangement for zenith position.

(5) Reflector panel support point accuracy measurements using all attitude theodolites at various elevation angles.

(6) Vibration measurements to derive additional environmental data for reflector mounted electronic equipment.

3. Radio Frequency Interference Tests

a. Summary. A fluorescent light fixture with radio frequency interference (RFI) shielding has recently become commercially available. S-band RFI tests were conducted at the Venus site to determine the shielding effectiveness and the noise level to be expected. It was found that the shielded fixture provides approximately 15-db decrease in interference when compared to the nonshielded fluorescent light measurements reported in Ref. 7. The shielded light (160-w unit) should not increase the system noise temperature by more than 0.02°K when illuminating an isotropic sidelobe at a distance of 50 ft.

The use of a dc tachometer in place of similar ac devices for rate feedback in the antenna servo systems is being considered. One possible problem is radio noise generation by the dc tachometer. An Inland direct current tachometer No. 8001A was tested. The tachometer noise level was below the threshold; an estimate of the upper limit of interference in an operational situation would be approximately 0.1°K.

b. Recent work. The radio frequency interference level was measured by mounting the test component on the mobile servicer and placing it directly in front of the Cassegranian hyperbolic subreflector of the Venus site 85-ft antenna. Fig. 10 shows the configuration with the dc tachometer being tested. Although the experimental setup is less than perfect, it was the only instrumentation with adequate sensitivity currently available to us. The structure of the servicer boom not only deteriorated the noise temperature from approximately 30 to 80°K, but also increased the system temperature instability to approximately ±5°K. This increase in temperature instability was due to the changes in sidelobe structure produced by the mechanical motion of the servicer boom in the 20-mph winds which occurred during the tests.

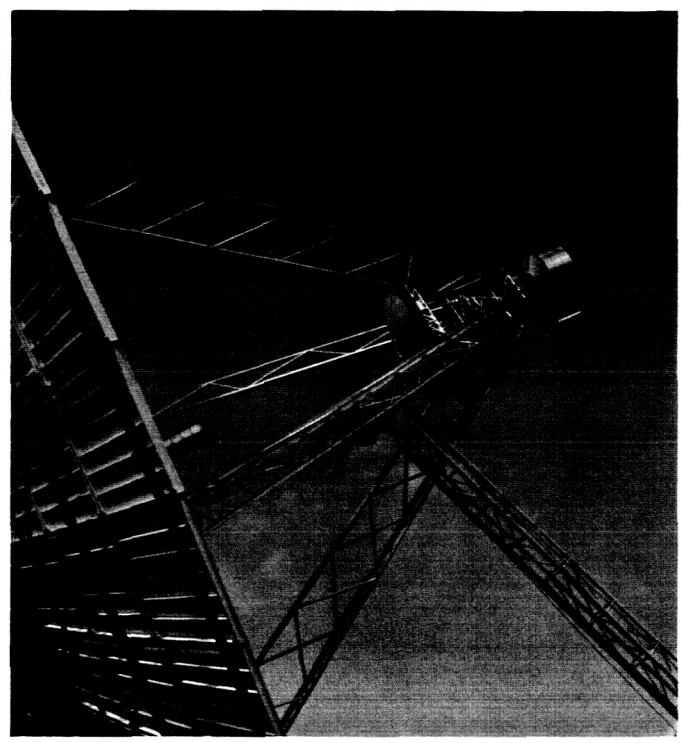

Fig. 10. Measurement of tachometer using Venus site antenna

The 160-w fluorescent light fixture illustrated in Fig. 11 produced a maximum increase in system temperature of 33 ±5°K. This was using a 22-db horn (the Cassegranian feed horn in the 85-ft reflector), at a distance of approximately 16 ft. If one were to assume that all antenna sidelobes that a fluorescent light was likely to illuminate

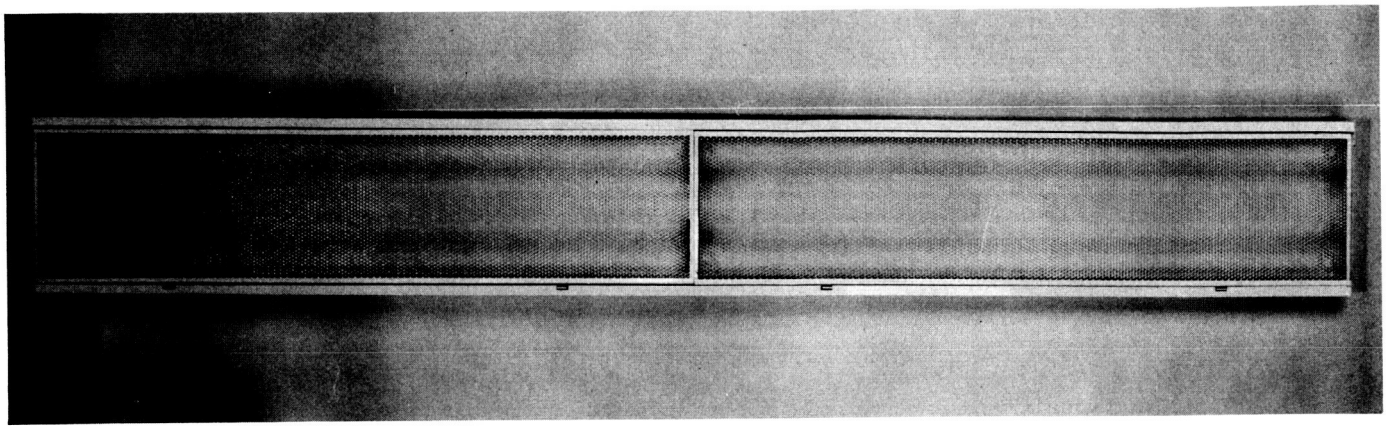

Fig. 11. Shielded fluorescent fixture

would be of isotropic gain or less, then at 16 ft a fluorescent light in the sidelobe would not produce more than 0.2°K increase in antenna temperature. This temperature would fall off with the inverse square of the distance, so that at 50 ft the increase in antenna temperature would be less than 0.02°K.

If one converts to effective radiated power by assuming that the fixture radiated as an isotropic radiator, then at S-band the radiated power would be −152 dbm/cps. If this is compared to the experiment discussed in Ref. 7, the effective radiated power for two 15-w fluorescent tubes was found to be −144 dbm/cps. If it is assumed that the radiated power is proportional to the input power, then we derive an equivalent unshielded level of −137 dbm/cps for a 160-w unshielded lampset, so that the fixture provides approximately 15-db decrease in interference. In recomputing the flux density produced by the fluorescent lamps, Table 1, p. 23 of Ref. 7 was found to be in error. The corrected table is presented as Table 1.

The tests of the dc tachometer were run by driving the tachometer with an ac motor. The largest effect seemed to be the mechanical instability of the mobile servicer. However, there were switching transients apparent, but they seemed to be associated with the motor rather than the tachometer. These transients were less than 15°K. By using the same reasoning as in the case of the fluorescent light, the tachometer should not produce more than 0.1°K increase in the system temperature. The tachometer was tested with an open circuit and a half wave dipole.

The tachometer was then moved from the hyperboloid to the antenna alidade, and changes in the system temperature were looked for; no changes of greater than 0.02°K were caused by turning the motor and tachometer on and off.

Table 1. Results of automotive noise on low-noise radiometric experiments (corrected Table 1 from Ref. 7, p. 23)

Source	Maximum temperature	2.38-Gc flux increase at 50 ft, −dbm/cps/m^2
1954 Jaguar 120	38	178.5
1958 Volvo PR444	7	185.9
1962 International Pickup Truck	6	186.6
1962 Ford Falcon (six cylinder)	6	186.6
1959 Opel	Below threshold	
1956 Ford Station Wagon	10	184.3
1963 Porsche	3	189.6
1959 Renault Dauphine	87	174.9
1960 Rambler Wagon (six cylinder)	4	188.3
1957 MGA	100	174.3
Fluorescent light (two 15-w tubes)		
Horizontal	12	183.5
Vertical	36	178.8

4. 30-ft Antenna Reflector Calculations

a. Deformations of reflector structure from gravity loads.

Résumé. The reflector panels of the Goldstone Venus site 30-ft antenna were set to a paraboloidal shape at zenith look using optical tooling means. The change in shape caused by the directional change of gravity force when the reflector was rotated to horizontal look was then measured. This presented an opportunity to check the measured deformations against the computed deflections

using the STAIR Computer Program. The resulting computed deflections compared within reasonable tolerances with the field data with the exception of one joint; this is being investigated. This work is applicable to validation of the AAS design analysis techniques.

Recent work. At the completion of the 30-ft antenna erection, the manufacturer (Rohr Corporation) set the reflector panels, using optical tooling means, to a paraboloidal shape at the zenith look position. The measurements were repeated at the horizontal look position, and the changes were recorded as deformations of the reflector structure for the 90-deg rotation of the gravity force. The apparent motions at right angles to the optical instrument lines of sight were converted to an equivalent motion parallel to the symmetrical axis of the paraboloid.

The availability of the field deflection measurements made it possible to check the deflections as calculated by the STAIR Structural Computing Program. To do this, the structural data were obtained from the manufacturer and inputted into the 7090 STAIR Program for computing the deflections for all joints of the structure on the reflector assembly side of the elevation bearings. This assembly consisted of the dish structure and the elevation wheel assembly, i.e., the tipping parts.

The STAIR Computing Program was programmed to compute the gravity *off–on* case for both the zenith look and the horizontal look positions. To directly compare the computed deflections to the field readings, the third case which algebraically subtracted the zenith look gravity *off–on* deflections from the horizontal look gravity *off–on* deflections was computed. These third case deflections should correspond to the field deflection numbers where the panels are set at zenith look and the deformations are measured at horizontal look position.

Fig. 12 shows the positions of the joints of the dish structure. The differences between the measured field data and the STAIR computed data are shown in Fig. 13. All deformations are plotted as deviations measured normal to the surface of the best fitted paraboloid.

In order to reduce the field and the computed data to the above described plotted numbers, both deflection data were inputted in the JPL RMS 7090 Computer Program, which computes the normal and path length error of each deflected joint to the best-fitted paraboloid as well as the root-mean-squared (rms) summation of all the path length errors.

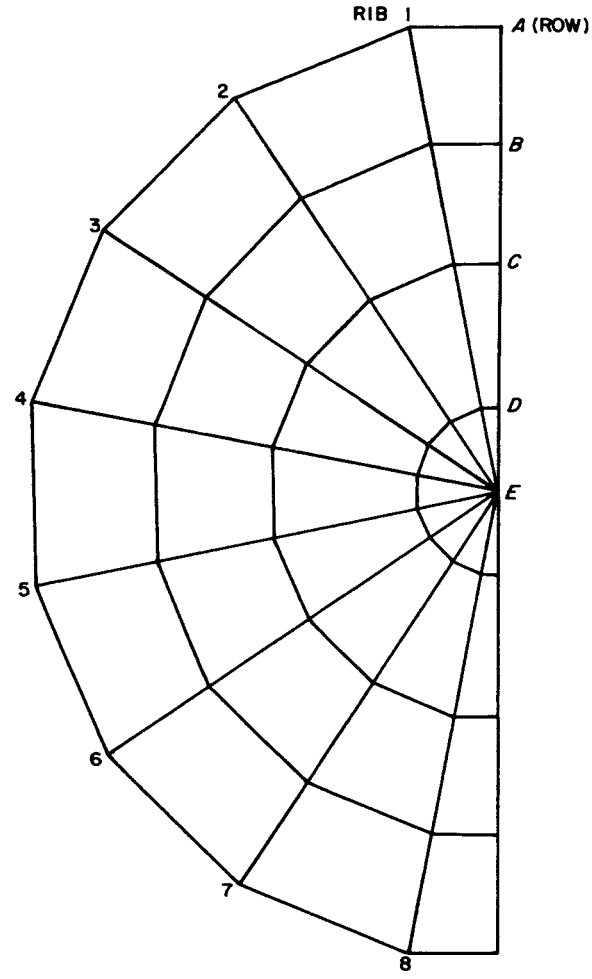

Fig. 12. Joint numbering plan, 30-ft reflector

As Fig. 13 shows, the deflections of the structural joints measured as normal deviations to the best-fitted paraboloid compares within 0.015 in. except for one joint where the difference is about 0.040 in. At the moment, the cause for this larger difference at the particular joint is believed to be that the actual structure is sensitive in the area. The basis for this may be seen in the measured horizontal look deflection pattern of the antenna (Fig. 14); the contour lines are very close together in the region of the joint 4A where the 0.040-in. difference between measured and calculated is observed. Further studies will be made to try to resolve this question. For additional data, the paraboloid was best-fitted to the horizontal look gravity *off–on* case, and the error for this same one joint was 0.012 in. as compared to 0.006-in. error for the largest error of the remainder of the joints. The rms of one-half the path length errors to the best fit paraboloids caused by the deflections compared exactly at 0.012 in. for both the field data and the STAIR computed deflections.

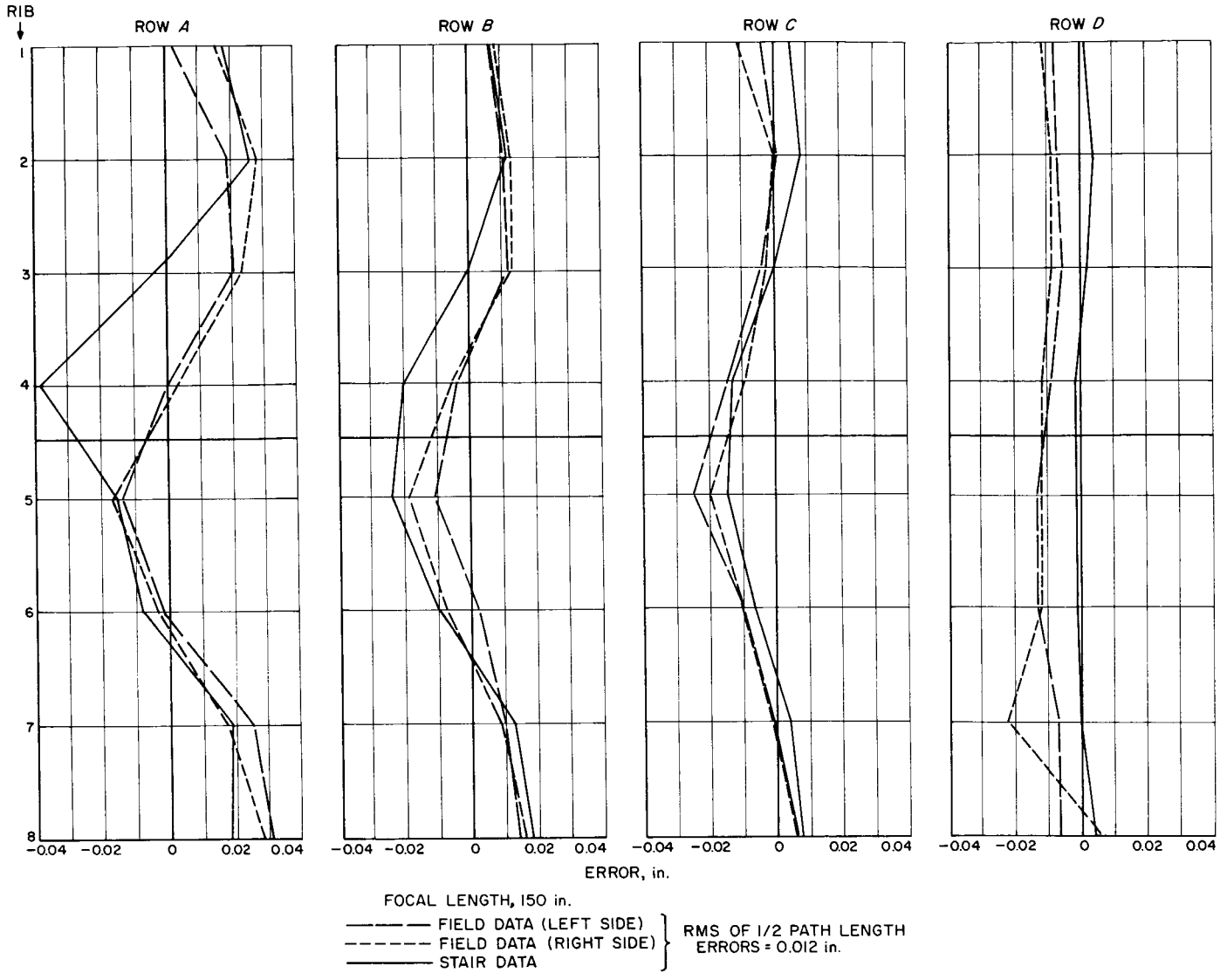

Fig. 13. Calculated and measured errors of 30-ft reflector

5. 85-ft Az–El Antenna, Reflector Resurfacing

a. Summary. In *SPS 37-24,* Vol. III, it was noted that the text for Fig. 3 in *SPS 37-23,* Vol. III, p. 7, was incorrect. The text discussed briefly work on resurfacing the reflector of the 85-ft Az–El antenna at the Goldstone Venus site.

The development of the panel mounting assembly for the new reflector surface is described; Fig. 3 of *SPS 37-23* is presented in this volume as Fig. 18.

b. Discussion. The contract for resurfacing the 85-ft Az–El antenna required a new design of the panel mounting clip. Various concepts were presented to JPL during the preliminary design phase. The specification required a design which would:

(1) Provide a panel mounting device whereby the panels would not contribute to the rigidity of the antenna structure.

(2) Minimize the effect of temperature differentials between the reflector surface and the reflector backup structure.

(3) Provide adjustment for panel positioning along the normal to the reflector surface. (The contractor's design provides for plus and minus 0.500 in.)

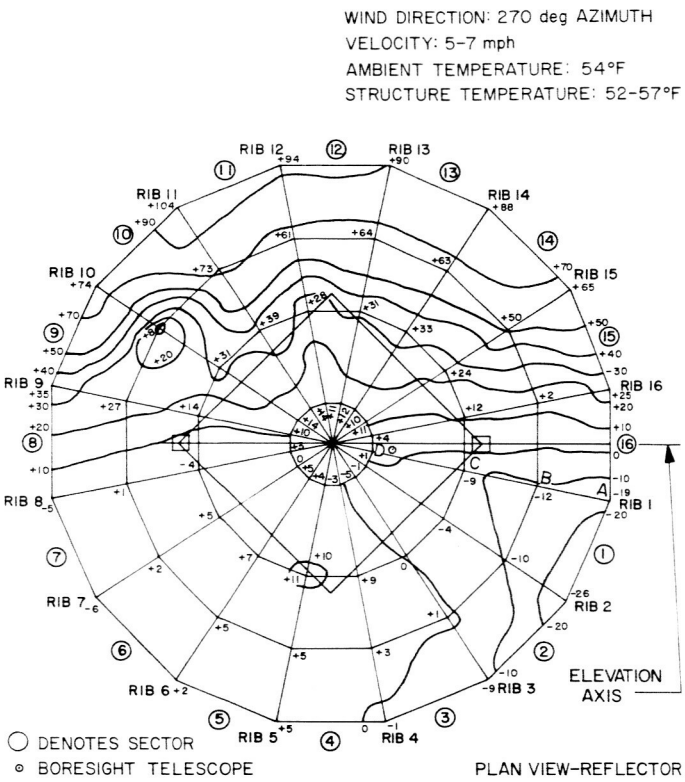

Fig. 14. Contour map of deadload deflections at 5-deg elevation as a change from a perfect paraboloid set at 90-deg elevation

(4) Provide the capability of adjustment from the reflector front surface.

The design accepted by JPL, after extensive experiments and laboratory testing, is shown in Figs. 15, 16, and 17. Various classes of surface treatment for the face of the panel mounting plate were studied. The surface

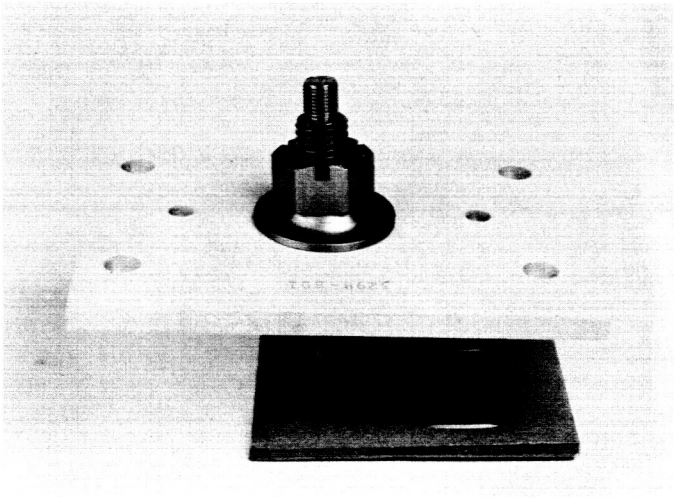

Fig. 16. Panel mounting clip assembly

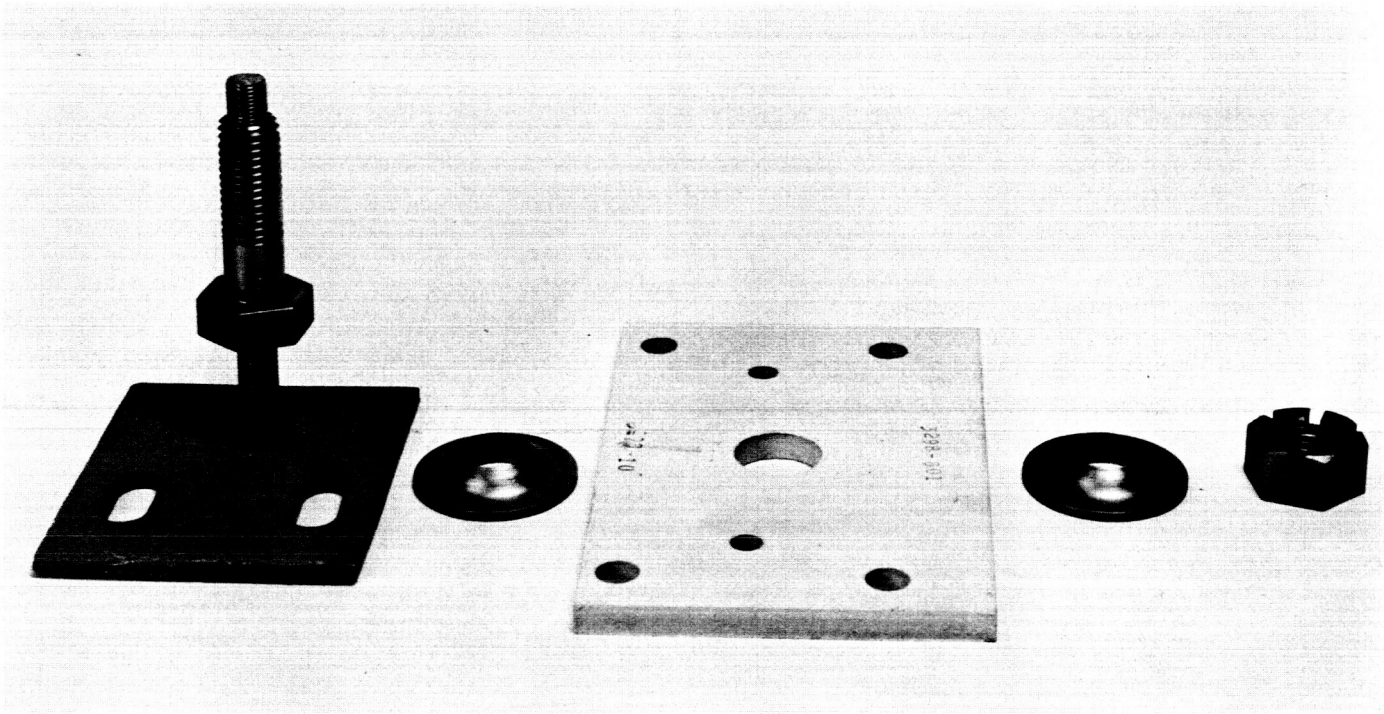

Fig. 15. Panel mounting clip components

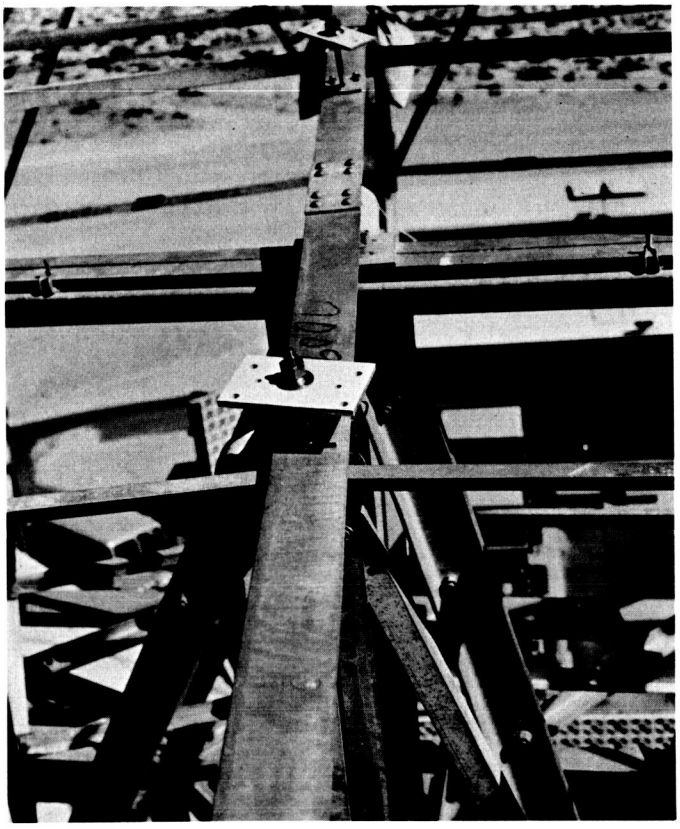

Fig. 17. Panel mounting clip secured to support structure

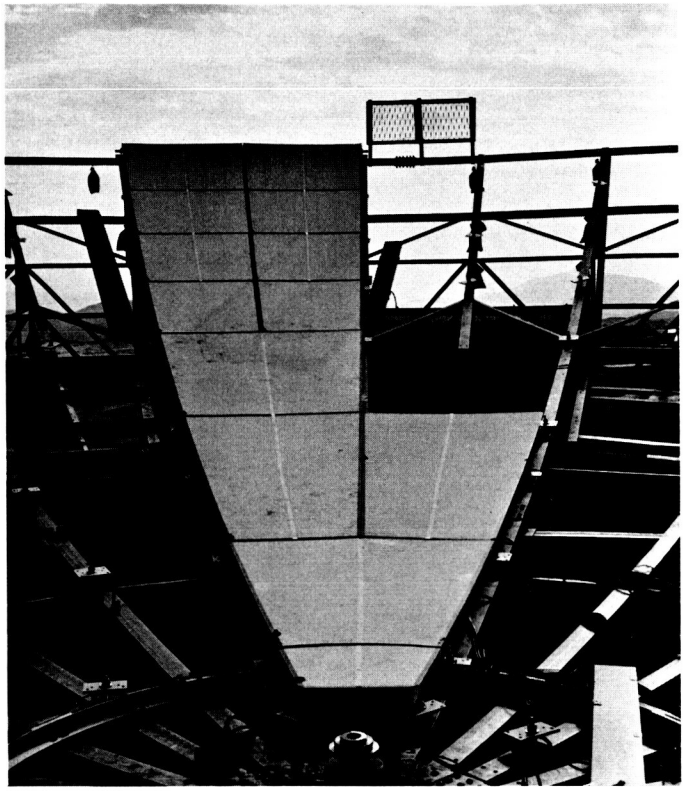

Fig. 18. Panels secured to reflector structure

treatment is to provide an allowable thermal growth differential between the surface panels and the reflector backup structure. A Teflon coating was determined as the best surface treatment to provide this action.

The panel installation, as shown in Fig. 18, is controlled during the assembly to specific torque values at the bolted joints to restrain the panel for location at one corner and to allow thermal differentials to act at three corners. Fig. 18 shows one set of panels secured in place to demonstrate that every joint can be made with proper panel gap and X, Y, and Z coordinates established.

The installation of the new surface has been completed and initial mechanical (acceptance) tests have been made; the resurfaced antenna has been used in the experimental planetary/lunar radar work this Fall, and gain has been measured with the interesting result of approximately 0.4-db gain increase as compared to the old surface (Ref. 6). Additional mechanical measurements on the 85-ft antenna surface and structure are planned. (See Sec. IV-A-2, "Antenna Instrumentation," of this issue.)

B. Planetary Radar Project

1. Water Rotary Joint for Az–El Antenna

a. Summary. A high-capacity rotary joint was developed to carry cooling water for the high-power transmitter across the azimuth axis of the 85-ft Az–El antenna. In Ref. 8, the final installation and testing were discussed. This report covers the joint performance.

b. Discussion. The carbon face seals used in the design of the rotary joint should seat after a period of operation. This length of the seating period is a function of rubbing velocity and temperature fluctuation. Normally carbon face seals are used in water pump applications where the rubbing velocity and duty cycle is high; a few days of operation in a pump application is equivalent to many years of use in the rotary joint. It is expected that the seating period for the rotary joint seals should be many weeks or even months.

Fig. 19 is a graph of the rotary joint leakage rate for the past 3 mo. The leakage rate depends upon the operating conditions of the transmitter and the antenna, which vary from day to day, and are believed to account for the variations from a smooth curve of the leakage rate. The volume of water leaking across the faces appears to be reducing; it is believed that the seals are seating in properly.

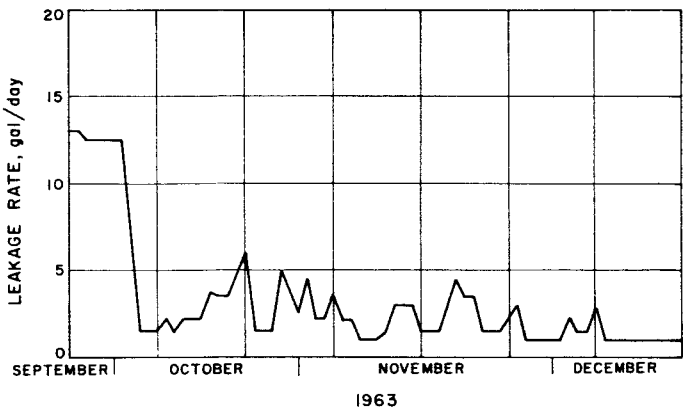

Fig. 19. Rotary joint leakage

2. High-Power 100-kw S-Band Transmitter

a. Introduction. The high-power (100 kw) experimental 2388-Mc transmitter at the Goldstone Tracking Station (GTS) Venus site was described in Ref. 9. It has now been installed for approximately 1 yr and, during this time, the expected number of problems and deficiencies was encountered. Many of these have been corrected, and the transmitter is now operational at a full 100 kw. A continuing program of test and rework is being carried on with the objectives of increasing reliability, simplifying and improving operating controls with an ultimate objective of automatic machine control, developing and testing new techniques, and increasing the output power to the full capability of approximately 500 kw. Three specific areas of this work are reported in this issue.

b. Series limiter. The series limiter is a component of the high-power transmitting system in use at the Venus site, GTS. Its function is to limit the beam current drawn by the klystron RF power amplifier in the event of an internal arc in the amplifier. Microwave power klystrons frequently have internal arcs during initial phases of operation and occasionally thereafter as a result of outgassing. Current-limited arcs are less destructive to the tube.

A water-cooled triode, connected as a diode, with an emission-limited cathode, is used in the series limiter. Emission limiting is accomplished by lowering the filament voltage. The filament supply is a three-phase, 400-cps, Variac-controlled, solid-state rectifier device. The tube filament is rated at 25 v, 650 amp. The maximum plate dissipation of the triode is 150 kw.

The limiter was tested to determine if it would hold the current constant for wide ranges of beam voltage and to ensure that the triode had not become gassy. The filament voltage was adjusted to limit the beam current to 2.1 amp, and the beam voltage was varied from 10 to 40 kv. This beam current was selected so as not to approach the rated plate dissipation of the triode. The results are shown in Fig. 20. No internal arcing occurred, demonstrating that the tube was free from gas.

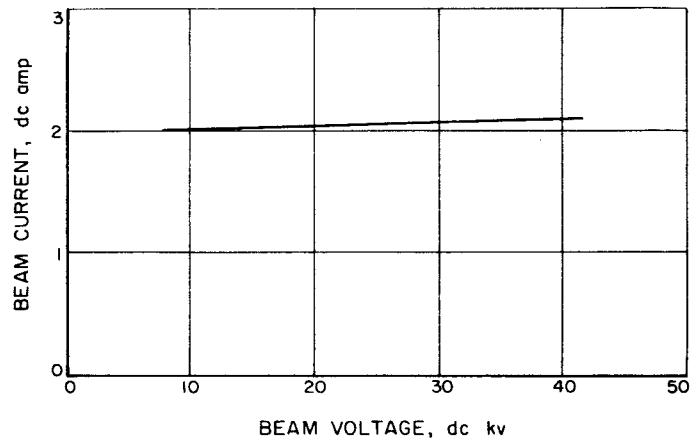

Fig. 20. Series limiter characteristics (approximately 14.7 v on filament)

In a second test, the filament voltage was varied in steps to determine the proper operating point for use with the VA-858 klystron. At 100-kw RF output power, the klystron beam voltage is 31.5 kv and the beam current is 8.2 amp. A 6-kv voltage drop was maintained across the series limiter. Fig. 21 is a plot of the results.

c. Measurement of incidental phase modulation. Incidental phase modulation (IPM), produced by a klystron, traveling wave tube (TWT), or triode microwave amplifier causes spurious components in the output signal. In a klystron, IPM usually results from ripple on the beam, filament, and focus magnet supplies; in a TWT, from ripple on the helix voltage; and in a triode, from plate voltage ripple.

Measurement of IPM is difficult due to the small amount of modulation permitted; for instance, IPM = 1 deg peak-to-peak maximum for the 100-kw, 2.388-Gc

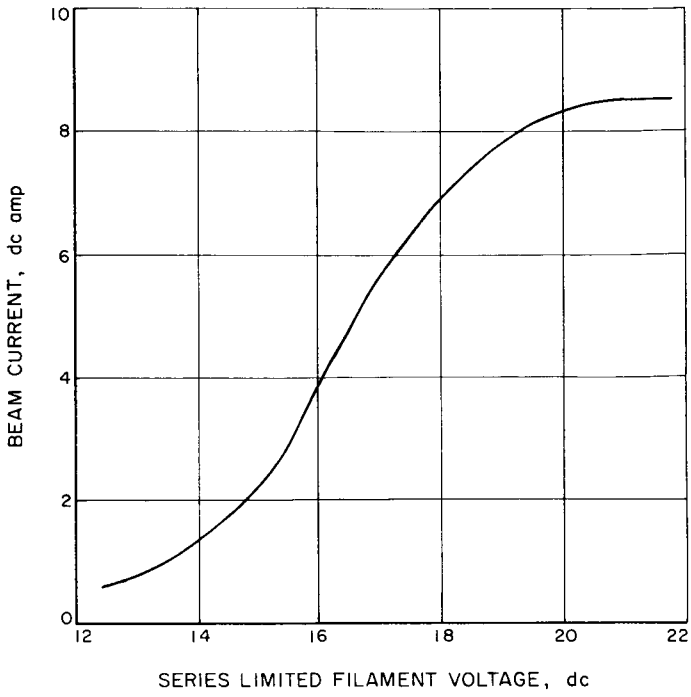

Fig. 21. Limiting characteristics, series limiter with plate–cathode voltage constant at 6 kv

klystron amplifier. With the best available voltage controlled oscillators used in a phase-locked receiver, where $2\beta_{L_0} = 5$ cps, the total system phase instability with the receiver locked to the transmitter exciter is 2.7 deg rms at a strong signal level. This would mask the IPM produced by the klystron amplifier. A more sensitive circuit for measurement of IPM has been tested and is being packaged in a shielded case for field use. The residual noise instability of this circuit is 0.039 deg peak-to-peak. A functional block diagram of the circuit is shown in Fig. 22. A common local oscillator chain supplies two coaxial balanced mixers. A portion of the input signal to the microwave amplifier under test is coupled into one mixer through a directional coupler. Similarly, a part of the output of the device under test is applied to the other mixer. The two signals are each heterodyned to 30 Mc, amplified, and compared in a phase detector. The phase shifter serves to calibrate the measurement device and to zero out fixed phase shifts in the system. The output of the detector is recorded as shown.

Fig. 23 shows the graphic recordings for several tests. Fig. 23(a) shows the 0.027-deg peak-to-peak residual instability in the measuring system when the signal generator was fed into both mixers simultaneously, through couplers and isolators. Fig. 23(b) shows the results obtained (0.039 deg peak-to-peak) when a TWT under test was fed into both mixers, with the output of the signal attenuated to the same level as Fig. 23(a). Thus, the residual instability is to a small degree a function of the driving source IPM; however, it is not directly proportional, as the TWT IPM is more than 10 times that of the signal generator. Fig. 23(c) shows the IPM of a triode under test, and also includes a calibration curve obtained by manually operating the phase shifter. Fig. 23(d) shows the IPM of the TWT.

d. Klystron filament supply. The system reliability of the high-power transmitter has been degraded as a result of repeated failures in the klystron filament supply. The malfunctions were due to insufficient capacity of the circuit components, such as the solid-state rectifiers, and the voltage breakdown of the filter inductor and power transformer.

Recently, a new rectifier assembly has been designed and built. This unit (Fig. 24) has an adequate full-wave solid-state rectifier, special input surge-protection capacitors, and two shunt diodes for output surge-current protection. These protective diodes prevent current surges from damaging the klystron filament or the rectifier assembly. Since the assembly must operate at voltages up to 55,000 v dc (Fig. 25), the cylindrical brass housing is designed to minimize corona and to protect the internal circuit from arc discharges to ground that might otherwise occur.

The filter choke for the klystron filament supply is a separate unit from the rest of the power supply. In the original design, the mounting structure and core of the choke were at ground potential which required that the winding insulation withstand the full high voltage. In the new design, the choke is enclosed in a corona shield and operated with the core at the high voltage. The winding insulation must now stand only the filament voltage; the high voltage is withstood by the standoff insulators. The resulting unit is much more reliable and, since an inexpensive choke can be used, is less expensive than the original unit (Fig. 26).

3. Mod IV Planetary Radar Receiver—A Note on Reliability

The Mod IV planetary radar receiver (Ref. 10) has been operated for more than 7400 hr since November 1962. During this period, no vacuum tube failures were experienced Some measure of credit for this performance may be attributed to the tube selection and aging program, which was instigated prior to construction of the

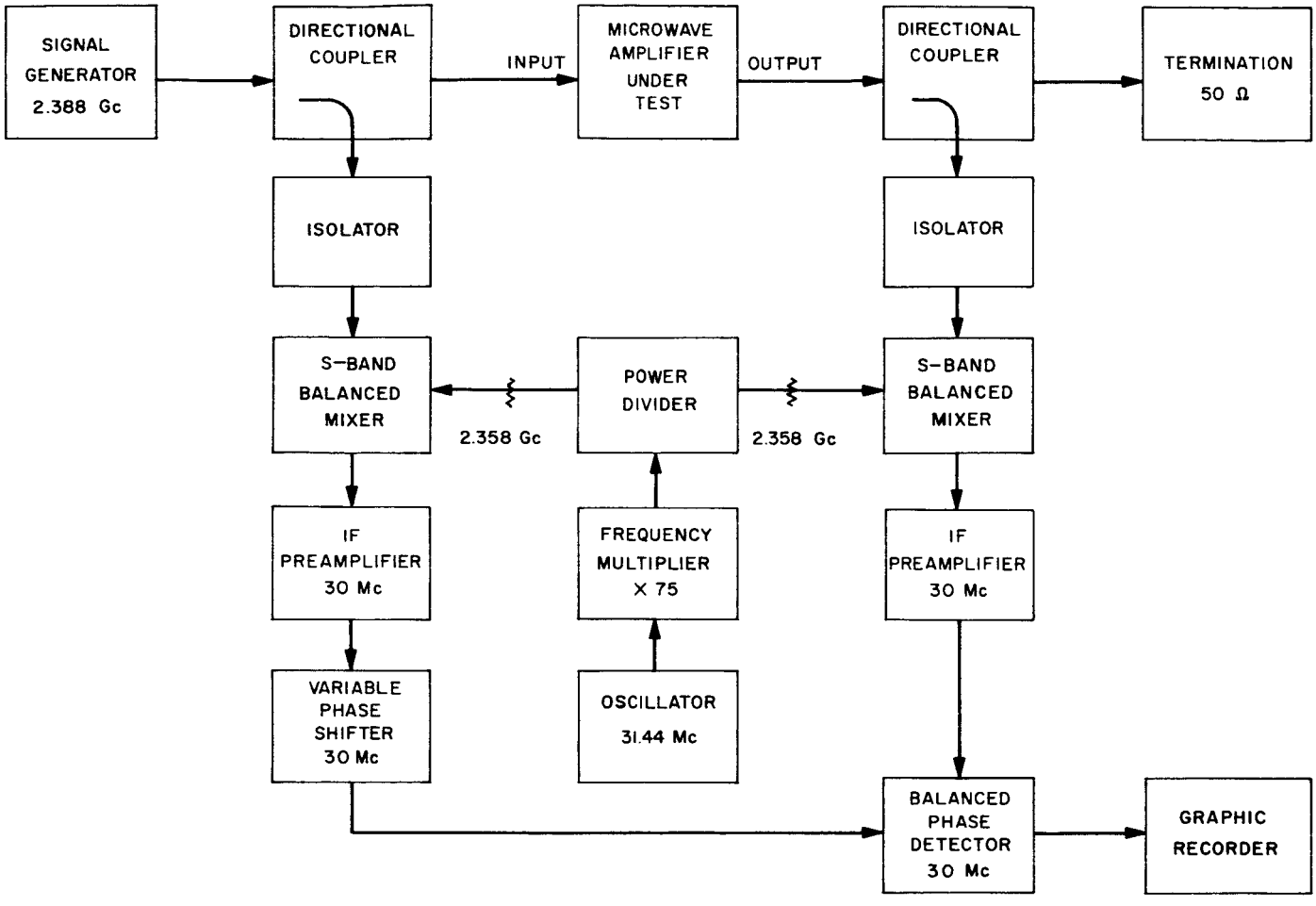

Fig. 22. Functional block diagram incidental phase modulation (IPM) test unit

receiver. Briefly, the program consisted of aging lots of 100 tubes at a time under dynamic conditions, for 100 hr in a "burn-in" rack. Periodically, the tubes were removed from the rack, their characteristics measured on a Weston tube tester, then restored to the rack. Only those tubes with normal transconductance, and which exhibited only slight changes in characteristics during the aging period, were returned. The receiver uses a total of 68 No. 5702 tubes and 17 No. 5639 tubes; only these two types were aged.

In this receiver, the tubes are operated at a plate voltage of 120 v. In previous systems, a plate voltage of 150 v was used, which is only 5 v below the maximum rating of the tubes. It is thought that the lower voltage may increase the reliability and tube life.

The receiver is more stable and drift-free than the previous model. This is partially due to the use of higher stability oscillators and operational amplifiers, and improved filtering and isolation. The only adjustments required after 5 mo of operational use were small corrections in the output frequencies of the free-running third local oscillators of the radiometer channels.

The equipment was installed at the Venus site, Goldstone Tracking Station in June 1963, following an extensive evaluation period at the Laboratory. It has been used almost constantly since August 1963 for planetary and lunar radar studies.

4. Nine-Channel Autocorrelator

A nine-channel autocorrelator is currently being constructed for use with the planetary radar receiver located at the Venus site in Goldstone, California. This instrument is a real-time device for processing the reflected signal from a planetary surface.

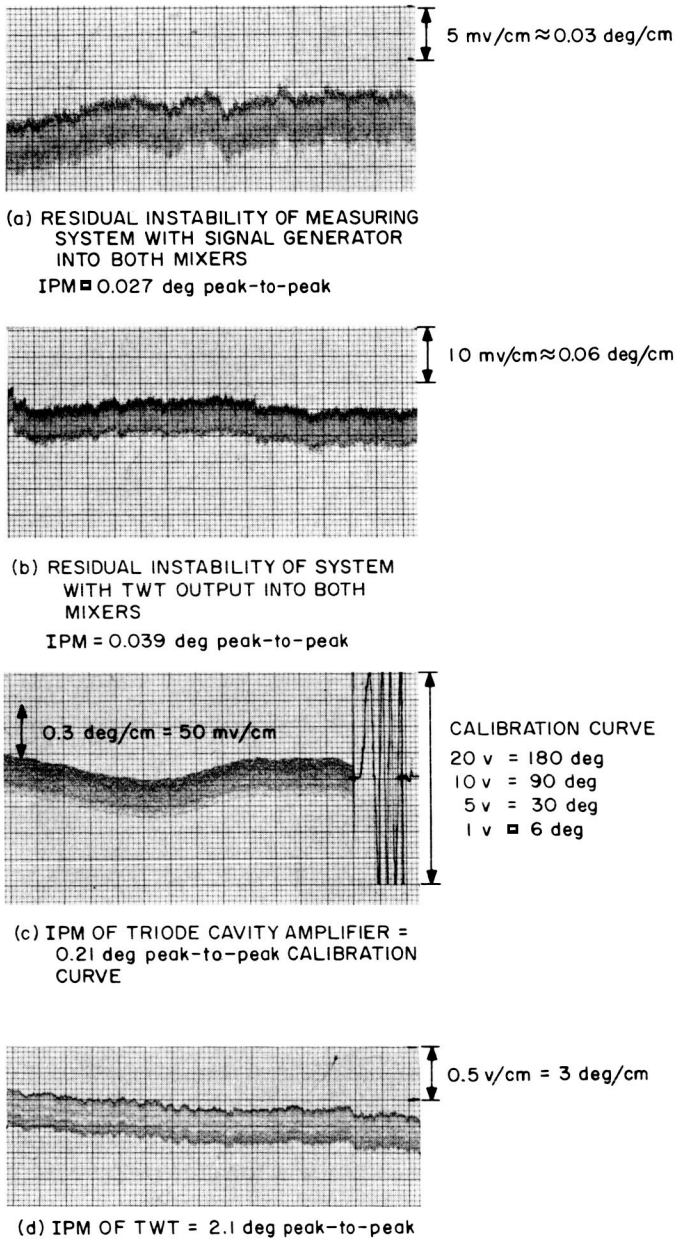

Fig. 23. Test results, incidental phase modulation

a. Function. The received radar signal may be considered to be a summation of individual signal components each reflected from a different geographical zone on the planet. These planetary zones are defined by their relative distance from Earth. Thus, the closest zone is the front cap of the planet; the second zone is an annular ring adjacent to the front cap; the third zone is a concentric annular ring adjacent to the second zone, etc. The mean distance of each zone is a given number of miles farther from Earth than the nearer adjacent zone.

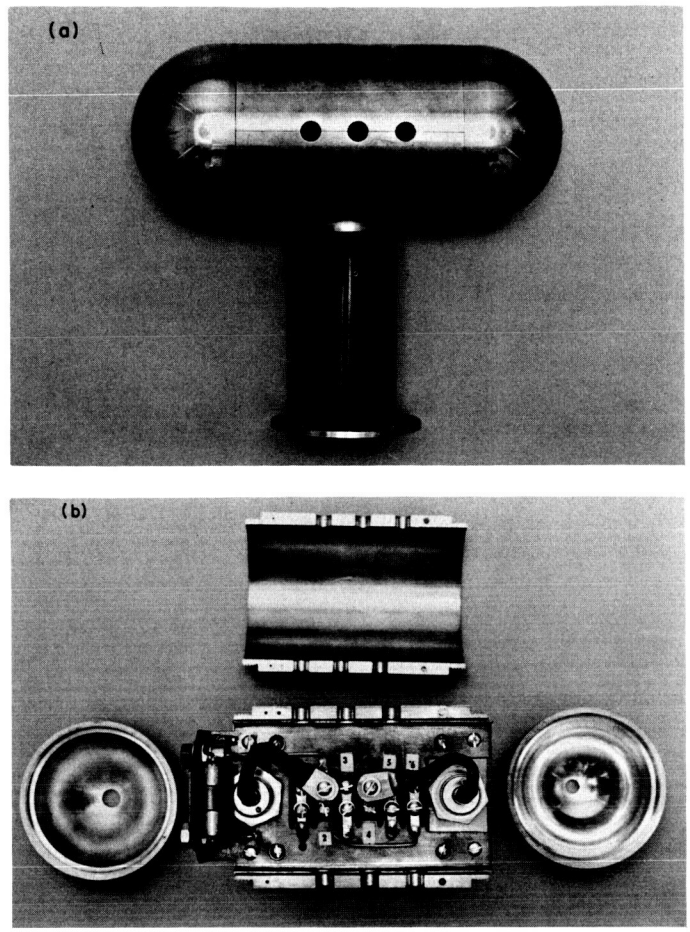

Fig. 24. Klystron filament rectifier assembly: (a) assembled and (b) disassembled in preparation for making external connections

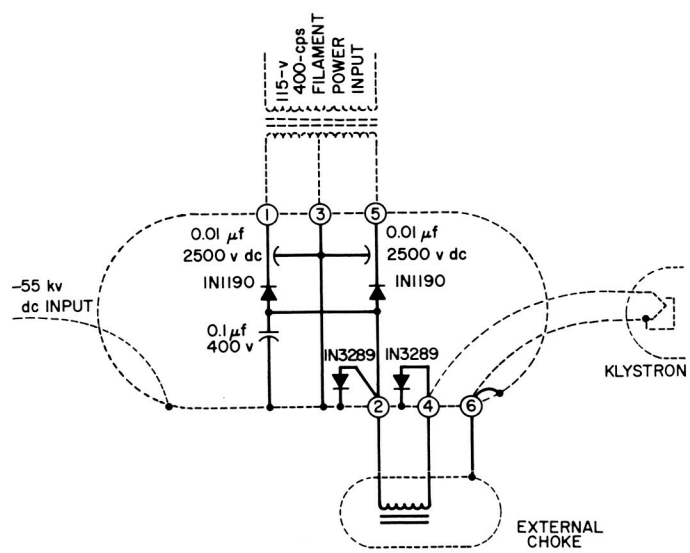

Fig. 25. Filament rectifier assembly and filter choke

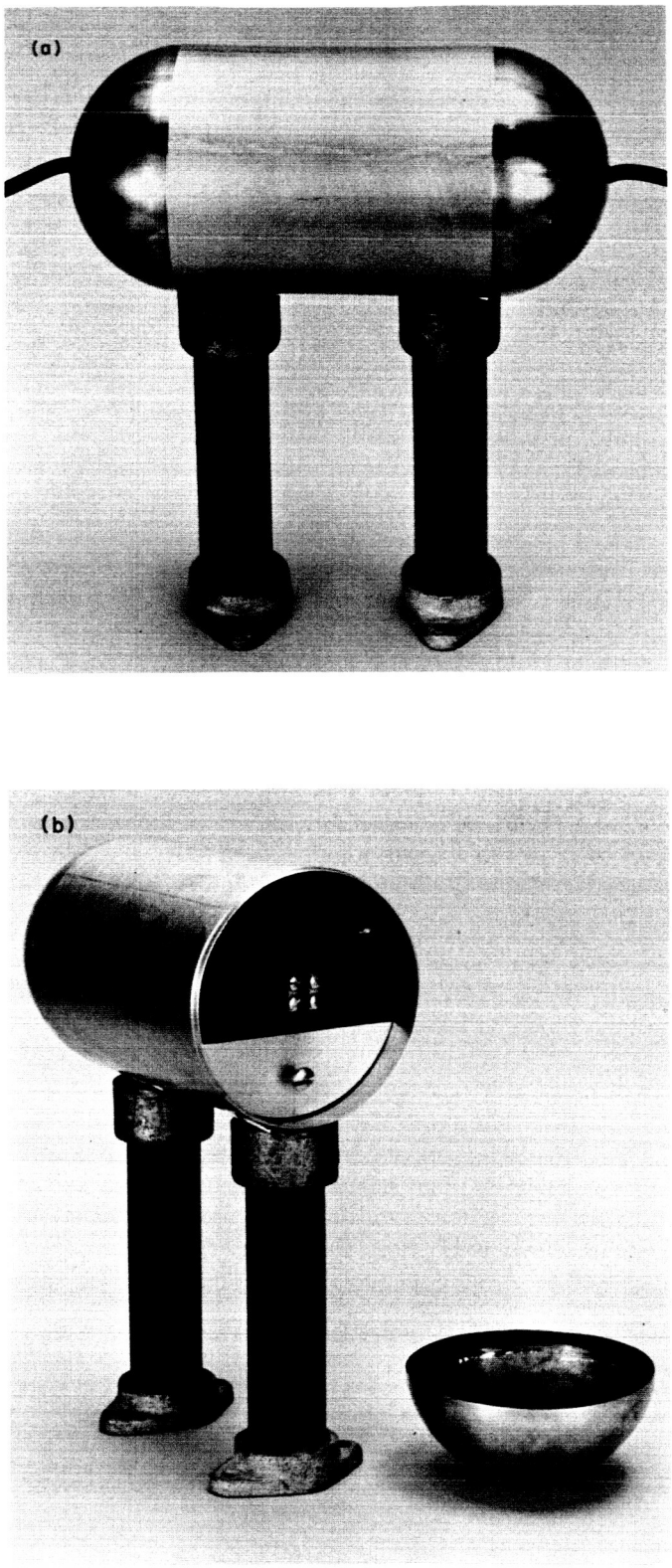

Fig. 26. Filament choke assembly: (a) with cover attached and (b) cover removed showing terminals for external connections

It is the function of the nine-channel autocorrelator to resolve the received signal components from nine adjacent geographical zones and accumulate the autocorrelation function for each signal component in a separate channel. Information from each channel accumulator is fed to an off line, general purpose, stored program digital computer which then computes the power spectrum of the reflected signal from each of the nine planetary geographical zones.

When it is installed, the nine-channel autocorrelator will replace the current method of first recording the total received signal on magnetic tape and then successively replaying the tape for each zone desired. The current method consumes a prohibitive amount of time when long receiving periods and small zone distances are used. Coarser zone distances permit a savings in time by allowing the playback speed to be increased with respect to the record speed.

b. Operation. In order to make the return signal resolvable, the transmitted signal is modulated by a pseudonoise (PN) code. Each reflected signal component is thus modulated by the same PN code, but the phase of the code is proportional to the signal time-of-flight to its geographical zone. Signal components from adjacent zones will have their modulating codes displaced in phase by exactly 1 code bit. Thus, a code bit rate of 1000 bits/sec will define a zone 93 mi in depth. Higher code rates will define narrower zones.

The property of a PN code is such that when the received signal is multiplied by the same PN code, all out-of-phase signal components remain wide-band, where they are suppressed by filtering, and only the in-phase component is demodulated into a narrow-band. Accordingly, each channel in the nine-channel autocorrelator starts by multiplying or demodulating the received signal with a different phase of the PN code. The remainder of the channel is used to compile the autocorrelation function of the separated signal component as is described in Ref. 11.

c. Block diagram. Fig. 27 is a block diagram of the nine-channel autocorrelator. The reflected signal is received and amplified by the main body of the planetary radar receiver, and transformed to an intermediate frequency of 15,625 cps. This IF signal is fed to the demodulators of each of the nine channels. The demodulator is essentially a phase switch which passes the signal either normally or inverted according to whether the demodulating PN code is one or zero. Although the input signal

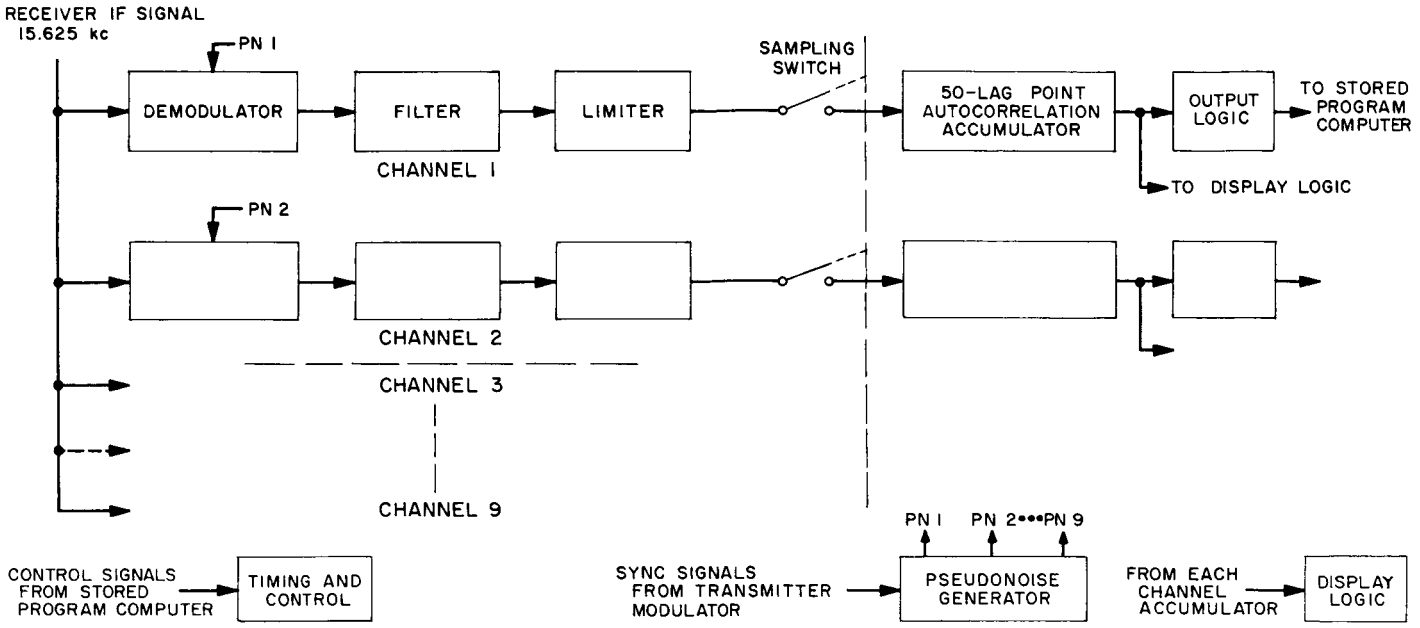

Fig. 27. Nine-channel autocorrelator

to the demodulator is relatively wide-band because of the PN modulation, the output from the selected zone has no PN modulation, and therefore has a relatively narrow bandwidth.

The demodulated zone signal is passed through a narrow band-pass filter to prepare the signal for its subsequent processing. Maximally flat multipole filters are used to prevent altering the shape of the signal spectrum. Matched sets of filters are used with bandwidths ranging from 400 to 25 cps. The filtered signal then goes to the limiter which selects the sign of the signal, thus converting the signal to a two valued quantity.

After the limiting process, the signal is sampled at a frequency whose period is determined by the bandwidth of the filter used, and is manually set by front panel controls. The minimum period is limited by the accumulator access time which is 1020 μsec. At this sampling rate, the maximum permissible signal bandwidth, equal to one-half the sampling frequency, is 490 cps. The sampling period is controllable in steps of 20 μsec to a maximum period of 20,460 μsec.

The accumulator contains a recirculating delay line storage for 50 autocorrelation (lag) points plus the lag point for zero argument. Each lag point occupies 20 bits of binary storage which provides a count capacity of 1.05 million samples. The total line length is thus 51 lags multiplied by 20 bits per lag or 1020 bits. Since the bit rate is 1 Mc, the total recirculation time for the line is 1020 μsec. Fifty lag points allow the derived power spectrum to be resolvable to one-fiftieth of the total system band-pass. Table 2 summarizes the design limits of the equipment.

Information in each accumulator is fed by the output logic to the stored program computer 1 bit at a time. This transfer takes place in response to computer commands, and all nine-channels output simultaneously.

The timing and control block generates the required timing signals for logic operation and also controls the sampling rate. In addition, the block also interprets and executes commands from the stored program digital computer.

Table 2. Summary of design limits of equipment

Characteristics	Maximum sampling rate	Minimum sampling rate
Sampling rate, samples/sec	980	48.8
Sampling period, μsec	1020	20,460
Bandwidth, cps	490	24.4
Resolution, cps	9.8	0.48
Integration time, hr	0.29	5.9

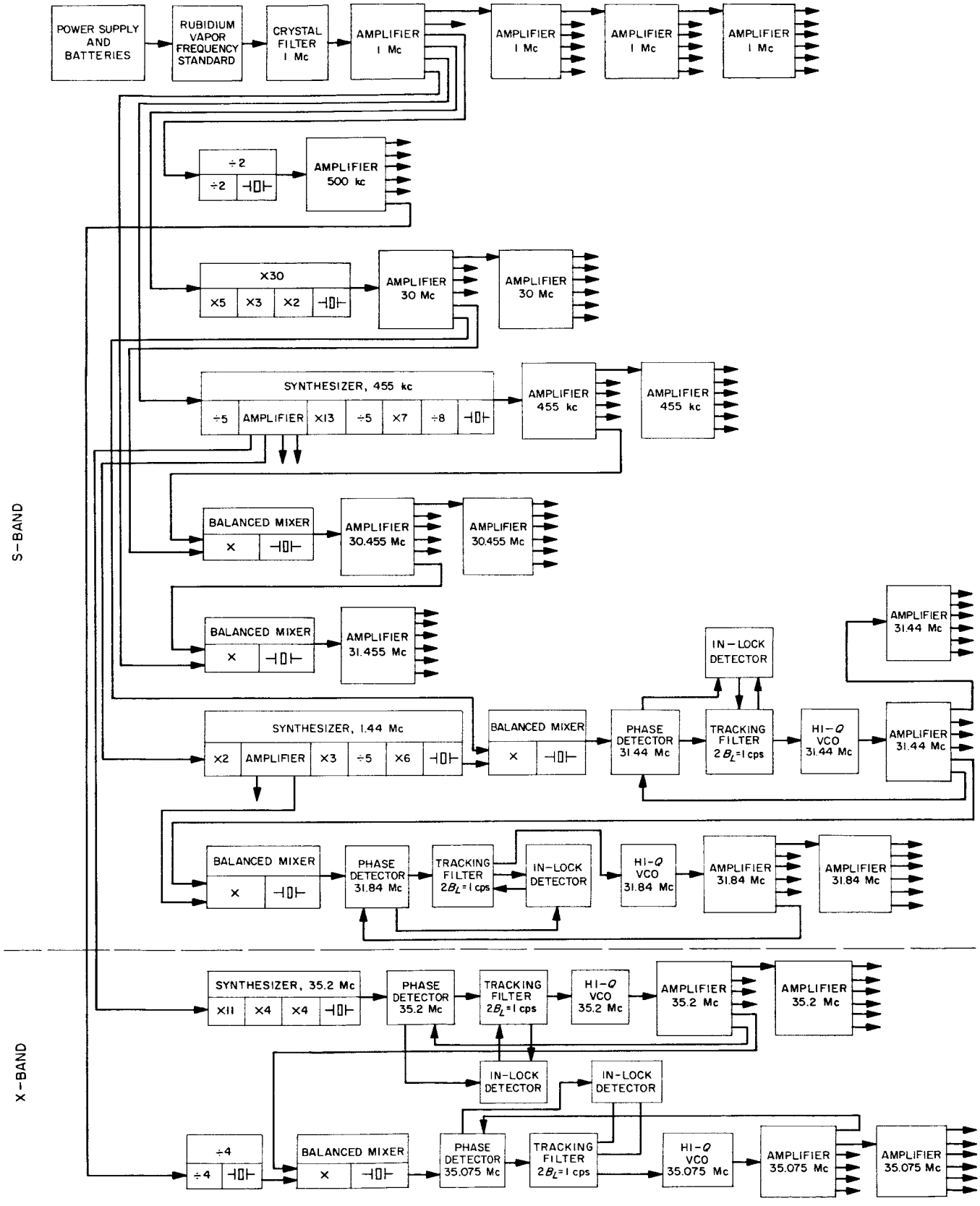

Fig. 28. S- and X-band central frequency synthesizer

The PN generator produces the nine phases of the PN code and also contains logic circuitry to permit synchronization to the PN generator which modulates the transmitted signal.

The display logic provides visual indication of the contents of any lag point in any channel as selected by a front panel control digitswitch.

5. Central Frequency Synthesizer

a. Summary. A central frequency synthesizer is planned for use at the Venus site to supply all the coherent reference frequencies for the present receiver–transmitter system (Mod IV) and the receiver–transmitter system (Mod V) for the 30-ft antenna. Considerable reduction in equipment is possible by consolidating all the equipment. Improvements (such as that all reference frequencies will be coherent) will be made in some cases.

The Mod IV planetary radar receiver contains, as do most other phase-locked receivers used by JPL, all the necessary reference frequency synthesizers or oscillators. In the Mod IV receiver–transmitter system, there are 44 modules used for the generation and distribution of reference frequencies of the required spectral purity, as well as 10 modules for the generation and distribution of third mixer reference frequencies for various experiments.

A new receiver, Mod V, is being designed to be used with the 30-ft antenna at the Venus site. This receiver will be in the same control building as the present receiver, Mod IV, and will require a large percentage of the reference frequencies that are used in the present receiver. Because of a lack of space in the present receiver for additional cables, these frequencies are not available for use in the new receiver.

In order to eliminate duplication of the reference frequency generation equipment, all the synthesis and distribution of reference frequencies for the two receivers is to be consolidated in a separate subsystem—the central frequency synthesizer. This subsystem will supply all the common reference frequencies for the two receivers, Mod IV and Mod V, and their associated transmitters, for operation either at S- or X-band. It will not supply third conversion frequencies for use in the various planetary experiments since the present equipment is adequate in this respect, and these frequencies are not needed except for the individual planetary experiments.

In the process of consolidating the reference frequency generating and distribution equipment, considerable simplification and improvement is possible. For example, the 455-kc reference frequency will be coherently generated from the 1-Mc system standard, using no more modules than the present system uses to generate a noncoherent reference.

A block diagram of the central frequency synthesizer is shown in Fig. 28. The portion shown above the dashed line contains all the necessary frequency synthesis and distribution equipment for two S-band receivers. The additional equipment below the dashed line is necessary for X-band operation. The total number of modules for generation of all the necessary frequencies for S-band operation and distribution of these frequencies to both receivers is 35 as compared to the 44 modules required in the present receiver–transmitter system.

C. Lunar Radar Project

1. A Range-Gated Lunar Radar Experiment

a. Introduction. In Ref. 12, some of the aspects related to the capability and feasibility of a lunar radar experiment to be conducted at the Venus site at Goldstone were introduced. Since the writing of that article, the system, as described, has been put into operation, and recent results indicate a large measure of success. This article describes the system concept in more detail, the programming of the stored program controller, variation and measurement of some system parameters, and calibration of the equipment; some of the data obtained from the lunar range-gated radar is also presented.

b. System concept. As discussed in the cited reference, experiments with a "tunneled" auxiliary antenna mounted at the apex of the 85-ft Venus site antenna indicated that it was possible to modify the monostatic planetary radar system for lunar use. Fig. 29 shows a simplified block diagram of the modified system. Here, the large antenna is used for transmitting and the auxiliary one for receiving, to lower the system noise temperature (using the large antennas as the receiver would allow the Moon to fill the entire beamwidth of the antenna, and thus raise

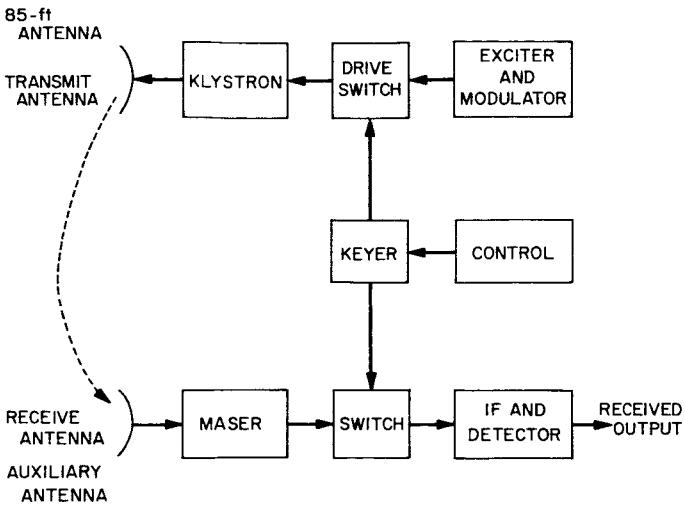

Fig. 29. A two-antenna klystron drive-keyed radar system

the system temperature because of the Moon temperature).

The control turns the drive on to the klystron for part of a round-trip signal-travel time and simultaneously turns the receiver off by turning off the local oscillator (LO). For the next round-trip time the klystron drive is turned off and the LO is turned on (Fig. 30). The system depends on the isolation between the antennas to protect the maser when the transmitter is on and to reduce the noise from the klystron beam to an acceptable level at the receiver input when the receiver is on. It was not possible to switch the klystron beam with present equipment. The performance of the system is, of course, dependent on the isolation between the antennas, i.e., how much noise leaks into the receiver. The performance also depends on the power transmitted since an increase in power transmitted not only yields a corresponding increase in power received, but also causes an increase in beam noise. The optimum transmitter power to be used was discussed in Ref. 13.

A more detailed diagram of the system appears in Fig. 31. During the transmit portion of the cycle, the carrier is balance-modulated by a pseudonoise sequence of length 16,383 (a 14-stage linear shift-register sequence), running at a 1-Mc digit rate. Correlation of the return during the receive portion of the cycle with a fixed delay between transmitter and receiver coders allows only that energy in the return originating within a 150-m increment, or range-gate, about the distance corresponding to the fixed delay to be investigated by the receiver. This way, a lunar target can be very accurately analyzed in depth.

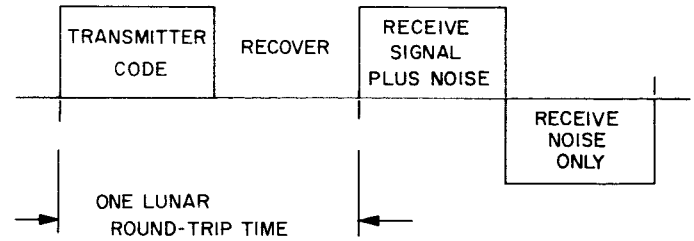

Fig. 30. Transmit–receive duty-cycle for lunar radar

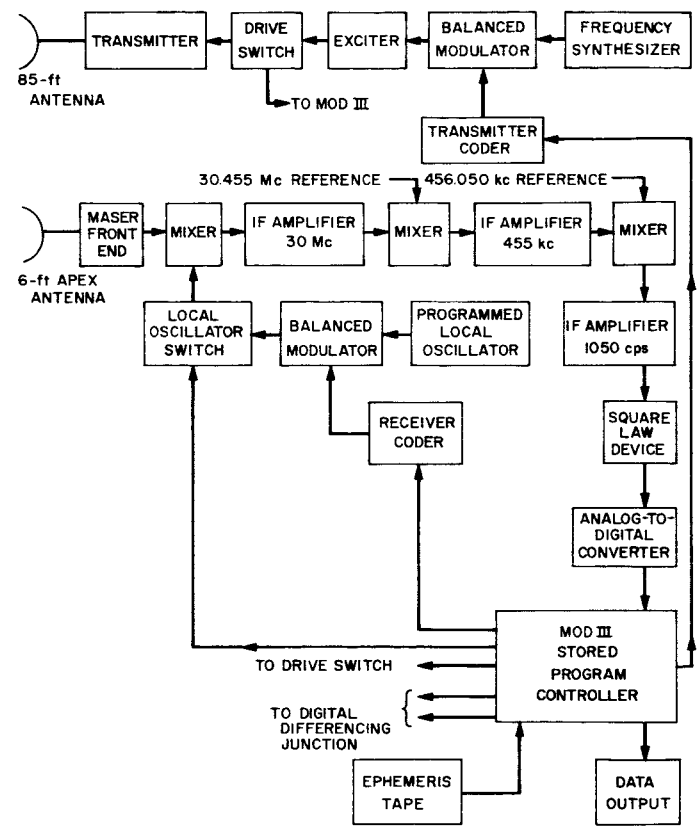

Fig. 31. Two-antenna, klystron drive-keyed, CW-lunar radar

The code period is sufficiently large that the distance corresponding to the code length, i.e.,

$$D = (16{,}383)\,(150)\,\mathrm{m} = 2457.45\,\mathrm{km}$$

is greater than the diameter of the Moon (1738 km). Thus, there is no chance that lunar echoes originating from gates separated by one code-period are received simultaneously.

The multiplication portion of the correlation operation performed by the receiver takes place in the mixer fol-

lowing the preamplifier in the Cassegrain cone on the antenna. The output of this mixer has three components:

(1) A 30-Mc signal proportional in strength to the correlation between the received waveform and the receiver code.

(2) A wide-band signal, corresponding to reflected signals not in the range-gate setting.

(3) Noise.

The first, the 30-Mc component, has in it some component due to carrier leakage—caused by imperfect balanced-modulation. The remainder is the information-bearing portion. It is a 30-Mc signal whose strength is proportional to that part of the transmitted code reflected from points on the Moon inside the range-gate.

The second of these is made negligible by narrow-band filtering in the third IF amplifier.

Amplification and filtering finally yield a voltage to a square-law device whose output is proportional to the received signal power from a particular range-gate, plus the instantaneous noise power. Converted to a digital series, this output is sampled and integrated (summed) by the Mod III stored programmed controller (SPC).

During the final portion of the transmit–receive cycle, there is no signal component in the received waveform, and so the output of the square-law detector is the instantaneous noise power. The Mod III integrates this series and subtracts it from the value obtained the previous quarter cycle, giving an estimate of the received signal level. This information is recorded on both punched paper tape and a printed paper tape readout.

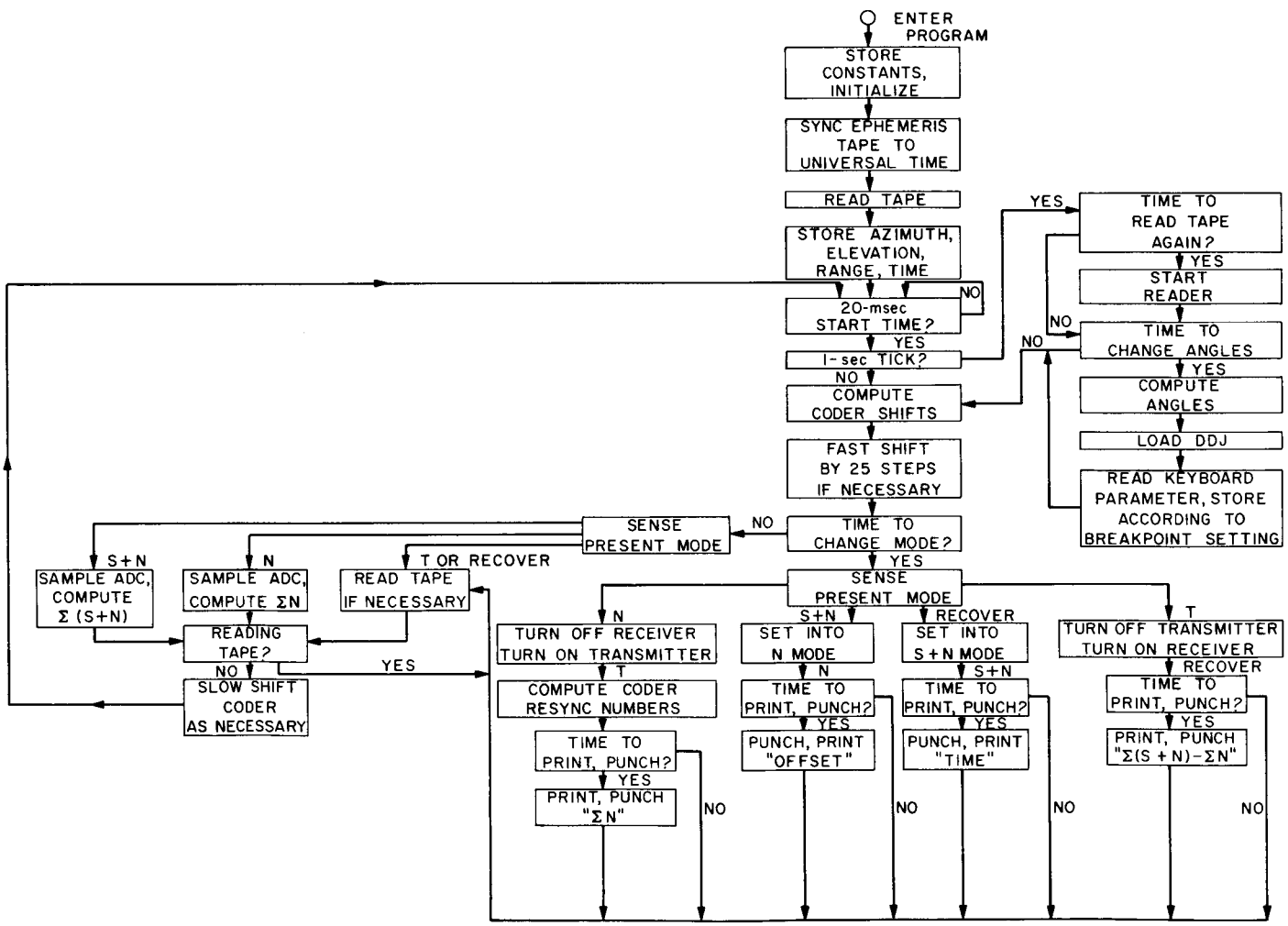

Fig. 32. Functional flow diagram of the Mod III program for the lunar radar

c. Stored program controller. The Mod III SPC which controls the experiment is programmed to read a lunar ephemeris and, based on this data, to provide all the necessary command and control functions for the duration of the experiment. During system calibration, the Mod III is manually operated to test the several operation modes to obtain properly set signals for adjusting the transmitter and receiver modulators, etc.

The experiment, then, is under program control of the Mod III SPC. The ephemeris tape is read every 64 sec, and interpolated antenna angles are supplied at 2-sec intervals to the digital differencing junction (DDJ) in the antenna pointing system. Further, interpolated range data from the tape causes the receiver coder to track ephemeris range to within 150 m (1 μsec). Manual and internally programmed range offsets, as well as automatic programmed range-gate selection functions, are provided by the Mod III also.

A functional flow chart is given in Fig. 32, for the operation mode. It may be noted that the receiver and transmitter coders are resynchronized every transmit period, and the program is arranged to run on a 20-msec major cycle and a 1-sec minor cycle. The major cycle performs the ephemeris range tracking, sampling of the ADC, integrating the data, and output functions in such a way that the machine never waits for the reader, punch, or ADC data. The minor cycle interpolates the pointing angles between points furnished to it every 64 sec by the ephemeris tape.

d. Variation of system parameters. As previously mentioned, the fact that the klystron noise leaks into the receiver during the receive portions of the cycle raises the effective system noise temperature as a function of the isolation between transmitter and receiver antennas.

Experiments recently conducted at the Venus site indicate that this isolation is dependent on the antenna system orientation, principally due to noise transmitted through one of the sidelobes of the transmitting antenna, bouncing off of the nearby terrain into one of the receiver sidelobes. As shown in Figs. 33 and 34, this effect becomes quite serious at elevation angles below 30 to 40 deg.

With the antenna at zenith, the system temperature was measured at several settings of the beam voltage, and thus it was possible to compute and plot (Fig. 35) the curve relating the ratio of the klystron power output (exciter on) to the system noise temperature (exciter off),

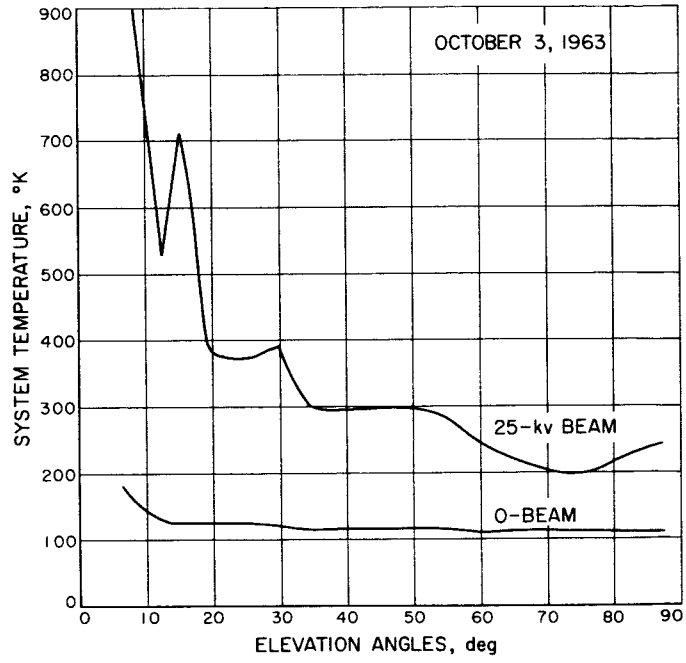

Fig. 33. System temperature versus elevation (azimuth = 260 deg)

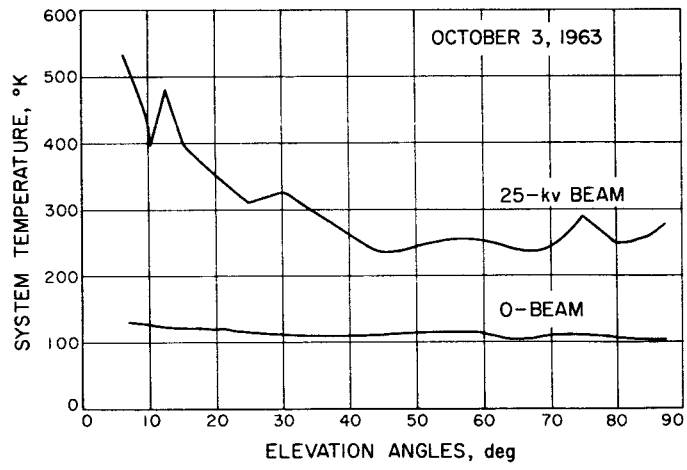

Fig. 34. System temperature versus elevation (azimuth = 180 deg)

as a function of the klystron power output. This parameter, $P_0/Temp$, being proportional to the received signal-to-noise ratio, was found to be maximized (for zenith operation) at about 52-kw transmitted power. According to a curve published in Ref. 13, this indicates that the two antennas have about 99- to 104-db isolation at zenith (which decreases drastically below about 45-deg elevation, according to Figs. 33 and 34). At 75-deg elevation, the optimum power was found to be about 42 kw

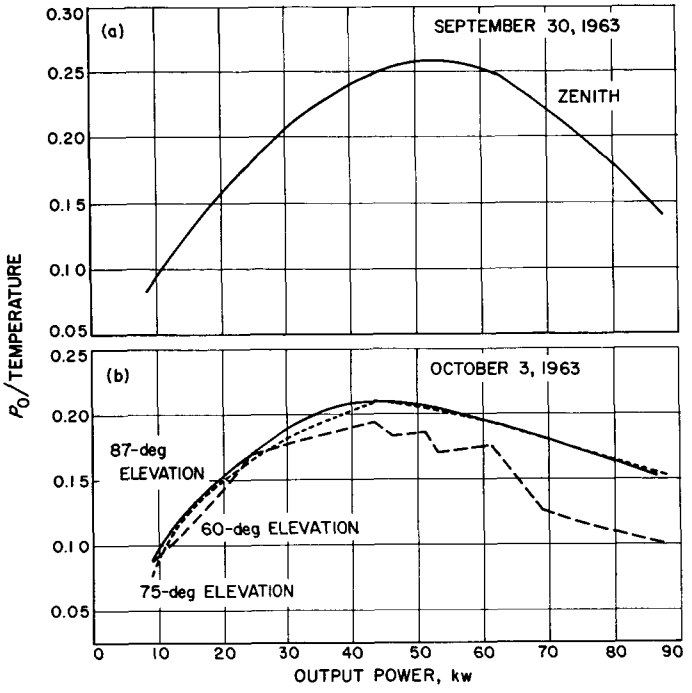

Figure 35. Output power versus P_0/Temperature

(Fig. 35) which corresponds to about 97- to 101-db isolation. The degradation in optimal performance is less than a db loss in SNR; but if a fixed transmitter power of 52 kw is assumed, then a degradation greater than 1.5 db arises at a 75-deg elevation angle. At lower elevation angles, this becomes even more serious.

e. Calibration. The return signal is demodulated inside the receiver cone by a signal from the LO balanced modulated by the receiver coder. Similarly, the transmitter is modulated in the cone by a signal from the RF exciter balanced-modulated by the transmitter code. The fact that these operations take place in the Cassegrain cone means that all delays and instabilities occurring in the receiver (or transmitter) proper do not affect range readings. Both transmitter and receiver signal lines run from the control building to the antenna and are subject to the same environment, and thus fluctuate, if at all, together. Thus, almost a minimum calibration delay exists between the two coders at "zero" range. With both transmitter (at very low power output) and receiver on, the leakage from transmitter into the receiver (a "zero" range configuration) was sufficient to indicate less than 1-μsec system delay—giving the system an inherent accuracy, without calibration, of better than 150 m.

With the antenna pointing at the collimation tower, it was possible to tune the modulators for maximum carrier suppression which, with the present equipment, ran 47 to 65 db.

It was also possible to range-gate the vicinity of the collimation tower, and thus to measure the time delay between the antenna and collimation tower (Fig. 36). The antenna-to-collimation tower distance has been surveyed, but the distance has not been referred to any particular point on the antenna, and thus provides only an estimate of the correct range.

The cross-correlation function is of a known triangular shape. With a system delay of τ sec, this appears as in Fig. 37, when a target lies in the beam. With readings

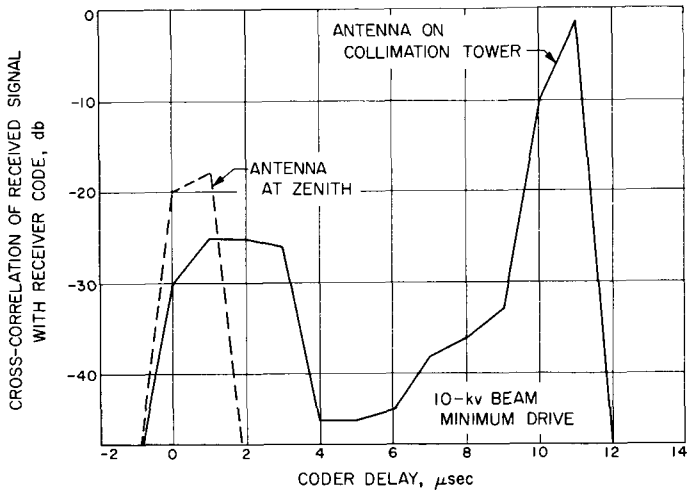

Fig. 36. Measured range-gate calibration data

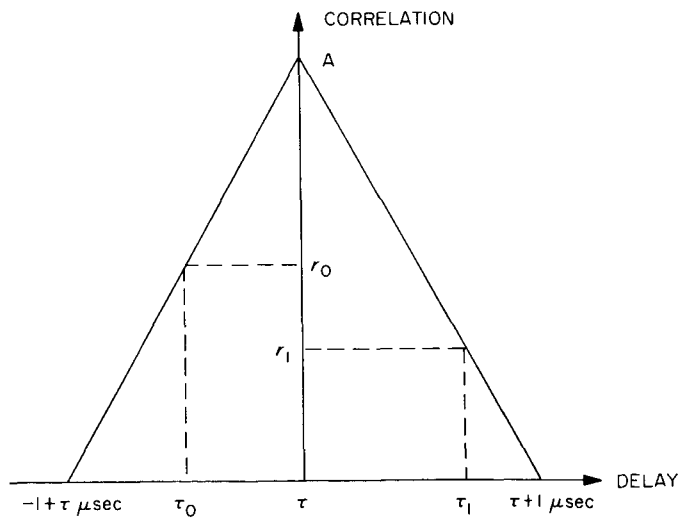

Fig. 37. Cross-correlation of transmitted and received codes at various delays (point-target and system delay of τ sec)

taken at τ_0 and $\tau_1 = \tau_0 + 1$ μsec, the value of τ can be found by interpolation:

$$= \tau_0 + \frac{1}{\frac{r_0}{r_1} + 1}$$

where r_0 and r_1 are defined in Fig. 37.

Using the data plotted in Fig. 36, the "zero"-range system delay is about 0.55 μsec, while the collimation tower range system delay is 10.74 μsec. This should give the dish–target–dish range to the collimation tower (Fig. 38) as 10.19 μsec, or 1528.5 m.

The survey distance to the tower is 1547.5 m between line-of-centers, but as mentioned earlier, this has not been referenced to the dish, as yet. These figures agree within 19 m, however, and this number represents the present calibration uncertainty in the system.

f. Data, and the conduct of the experiment. The system was completed for checkout on November 11, 1963, and preliminary runs indicated several items which needed improvement. The most important of these was lack of carrier suppression in the modulators. On November 12, for example, it was possible to tune the suppression only to about 30 to 35 db. The program was changed so that integration time per gate could be varied as desired. The remainder of the week was involved in system checks, etc. Jupiter and Venus experiments occupied most of the time during which the Moon was visible at Goldstone.

On November 18, 19, and 21, echoes were recorded and that data is presented in Figs. 39, 40, and 41. The abscissa in these represents microseconds of offset delay from the Goldstone working ephemeris value of Earth–Moon distance. Note that the point marked *F* on each chart, corresponding to the estimated distance to the front face of the Moon is 84, 80, and 82 μsec, respectively. These times corresponded to inaccuracies of about 12 km in the working ephemeris.

Since the present state of lunar orbit theory is much more accurate than these figures indicated, the program which generated the working ephemerides was carefully checked and errors were removed. Corrected ephemerides will be available for future experiments, probably to begin in February 1964.

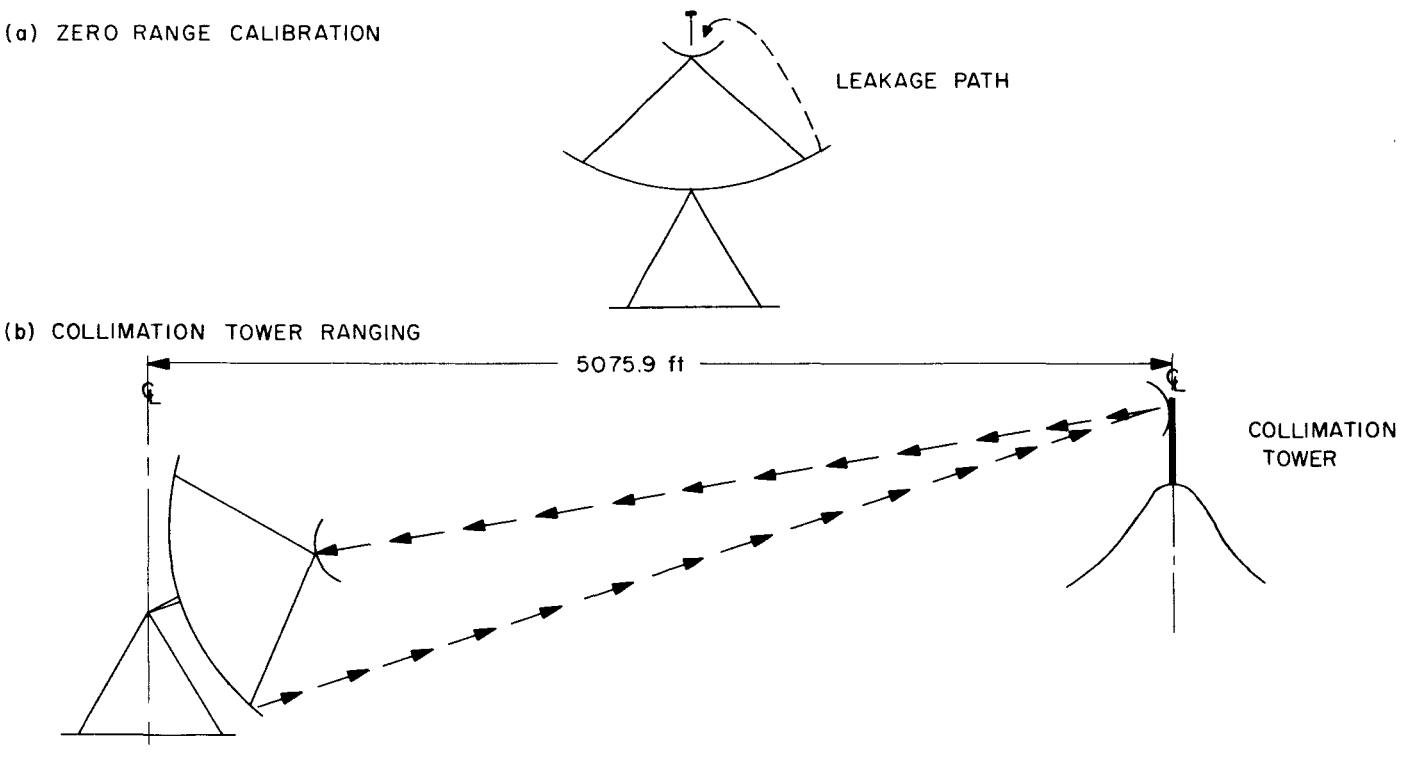

Fig. 38. Calibration of lunar radar system

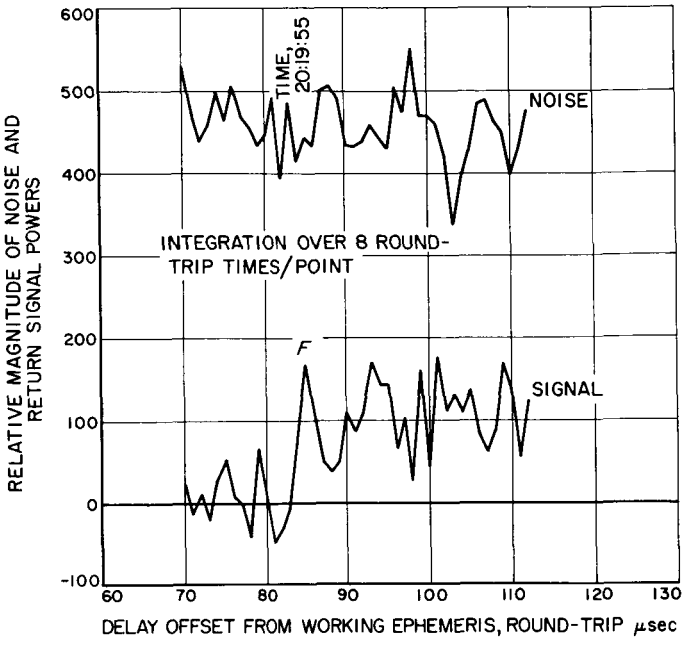

Fig. 39. Lunar radar data for November 18, 1963

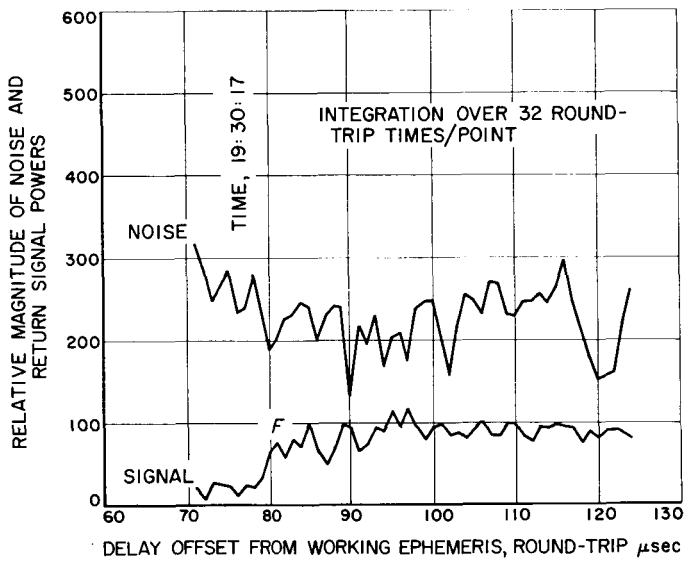

Fig. 40. Lunar radar data for November 19, 1963

Reduction of these data to give specific characteristics about the lunar surface is presently being performed, but extensive results are as yet premature. The next article, however, discusses some of these data in more detail.

2. *Lunar Radar Range Measurements*

This article is concerned with a description of the astronomical aspects involved with the interpretation of

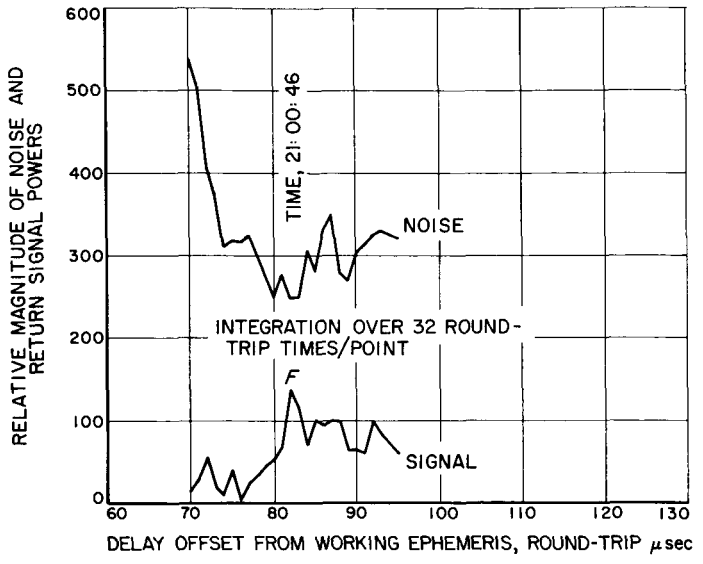

Fig. 41. Lunar radar data for November 21, 1963

Goldstone lunar radar range measurements. Since the intent of this article is descriptive, only very preliminary results are presented, and these only for purposes of illustration.

The radar measurements considered here may be heuristically thought of as consisting of the following: The entire Moon is irradiated with CW radio-frequency energy. Then, by means of coded modulation, the receiver selects only the energy reflected from a specified "range interval" of 300-m depth at a set distance from the radar. The range interval is stepped in 150-m increments (1 μsec) until a returned signal is detected when the interval contains the front edge of the Moon.

Because of the detailed shape of the range interval, the effective width of the range-gate turns out to be about 150 m. Once the front edge of the Moon has been detected, further stepping of the range interval isolates the reflected energy from annuli centered about the sub-radar point on the lunar surface. The instantaneous sub-radar point varies continuously with time due to the librations of the Moon and due to the rotation of the radar about the Earth's axis.

Fig. 42 shows the range zones for the *sub-Earth* point at 0 hr UT on November 19, 1963. The sub-Earth point is the point of the Moon's surface which lies on a straight line connecting the Moon's mass center to the Earth's center. The lunar coordinates of the sub-Earth point are 1.99 deg South and 3.30 deg East in accordance with standard astronomical notation for the Moon. In this

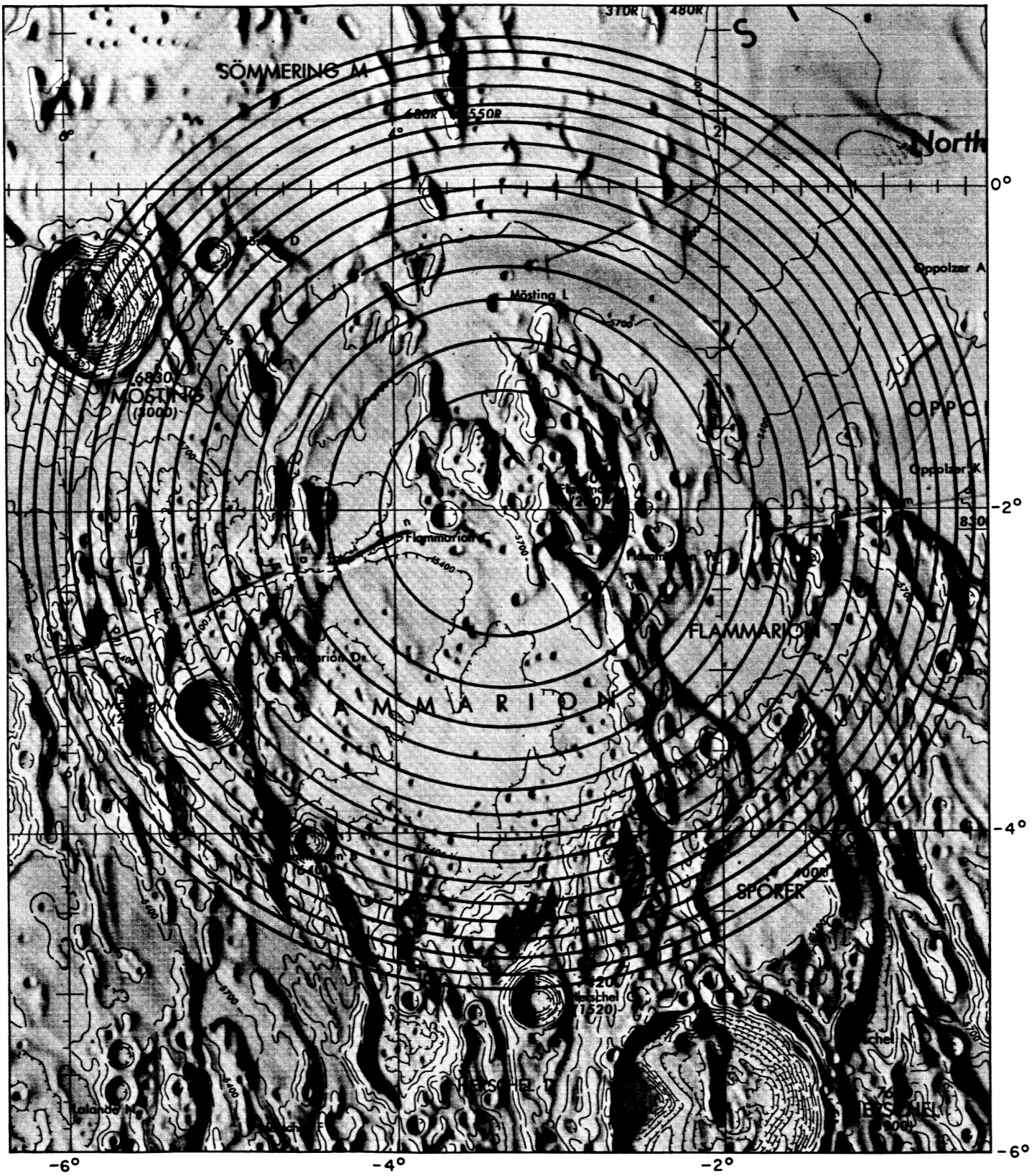

Fig. 42. Lunar topographic map showing range zones

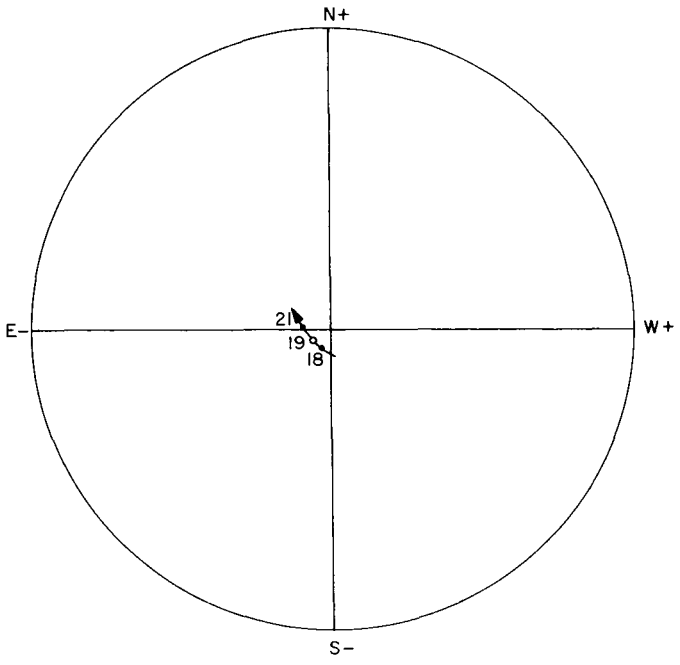

Fig. 43. Scale lunar map showing sub-Earth points for November 18, 19, and 21, 1963

notation, North and West are positive, as shown in Fig. 43. The picture was obtained by centering an overlay of concentric circles on the sub-Earth point. The maps used were Lunar Charts LAC 59 and LAC 77 (published for the United States Air Force and National Aeronautics and Space Administration), which have a scale of 10 km/cm and altitude contours at 300-m intervals.

Since the maps used were mercator projections and the overlay was a plane projection, there will be some error. This error is slight since the map covers a relatively flat area. There are 15 range zones shown on the map, each 150 m deep. The diameter of the first zone is 45.66 km and the outside diameter of the 15th zone is 176.82 km, with a projected width of 3 km. It is a property of a sphere that such zones have equal areas on the sphere and, for the small area in point, the projected areas are almost equal.

It should be noted carefully that the sub-Earth point and not the sub-radar point was used. The sub-radar point is the point on the Moon's surface which lies on a straight line connecting the Moon's center to the radar. The sub-radar point differed from the sub-Earth point by almost 0° 30′, but since the sub-radar point oscillates daily about the path of the sub-Earth point, the sub-Earth point was chosen for illustration.

Fig. 43 shows the size of the first range zone relative to the Moon. The sub-Earth points are shown for November 18, 19, and 21 as they move in a clockwise direction.

The radar measurements for November 18, 19, and 21 were presented in Sec. IV-C-I of this report. The run for November 19 has been given some attention for purposes of illustration (Fig. 40, Sec. IV-C-I). Fig. 40 shows that the first indication of a returned signal occurs at 77 μsec after the position of the lunar front edge was reached. The reference for this front edge was obtained from the working Goldstone lunar ephemeris and the 77-μsec difference represents a bias in this ephemeris.

The working ephemeris was obtained from Brown's Improved Lunar Ephemeris (ILE). Since the geocentric distance of the center of mass of the Moon is expressed as the angle subtended by *an* Earth radius at the center of the Moon in the ILE, a value of the Earth radius must be used to obtain the distance in kilometers (or μsec). The value used in the working ephemeris was the best modern value of 6,378,145 m obtained from terrestrial measurements. The use of this value was incorrect. Brown's lunar theory was constructed using then current values of certain astronomical constants such as the Earth–Moon mass ratio, Earth radius, solar parallax, etc. Consequently, the lunar distance in kilometers can be obtained only by using a pseudo-Earth radius which tends to be consistent with the constants actually utilized in Brown's ILE. If one assumes that the mean lunar distance is given by $\bar{a} = 384{,}000.0$ km, which was obtained by both optical techniques and radar measurements, and the radar value for the solar parallax, one computes the "best" pseudo-Earth radius of 6,378,327 m. The use of any such value is not really ideal since one should regenerate the ILE with each term corrected from the modern constants. However, since there are approximately 2000 such terms in the theory, this procedure would be very laborious. Due to changing the Earth radius from 6,378,145 to 6,378,327, the correction for the lunar radar distance at the epoch of interest for November 19 is 75 μsec. The small disagreement of 1 μsec = 0.15 km in one-way range between the corrected difference and the observation is apparently fortuitous. A surface correction of about 2.5 km (from Fig. 42) should be applied as well as corrections for the nonsphericity of the Moon's figure, and for the difference in the position of the center of mass of the Moon and center of the Moon's figure, each amounting to about 1 km in range.

Furthermore, it is not clear that the point of initial signal rise in Fig. 40 should be selected for analysis. If the lunar surface were a smooth sphere, the response to the radar signal would rise to a maximum value in 1 μsec of range-gate stepping. However, the observations show that the signal rises to a maximum value several microseconds after the first contact. This effect is apparently due to the detail surface contour as a function of height above the mean lunar surface. Thus, the response of the Moon in the range-gate as a function of height above the mean lunar surface is apparently a measure of the quantity of projected area to the radar line of sight in the range zone. The detailed shape of the signal-rise curve is consequently a measure of the probability distribution of this area as a function of height. For purposes of illustration, one can consider an overly simplified model of the lunar surface consisting of conical mountains of equal height. In such a circumstance, it can be easily shown that the measured response would be a linear ramp in time (range), the slope of which depends on the slope of the conical structures in a simple way. Thus, it appears that a study of the observed response curves may be a powerful means of studying the lunar topography over regions of 45-km sizes.

The improvement of the lunar ephemeris for purposes of calculating significant astronomical constants from radar observations has been undertaken as a major research effort. The progress of this work will be reported in subsequent *SPS*'s.

D. Ranging and Tracking System Development

1. Monostatic Radar Operating Parameters

a. Résumé. Preliminary test results of the anti-sideband system now under development, coupled with the effects of target dynamics discussed in Ref. 14, have pointed up several areas of compromise in the selection of receiver loop bandwidth, keying rate, and predetection bandwidth. Inherent in the problem are the uncertainties of prediction of range and range rate at the time of satellite acquisition. A largely qualitative description of the anti-sideband system and its performance is followed by a discussion of over-all system trade-offs.

b. Anti-sideband system. A synchronous sideband detector capable of detecting and rejecting spurious receiver lock to keying sidebands down to receiver threshold has been assembled with evaluation underway at the present time (Fig. 44). In the figure, the cross-hatched blocks represent a conventional receiver. The principal of operation may be stated as follows: The received signal possesses a spectrum corresponding to 100% amplitude modulation of the carrier by a square wave as a result of the keying. If this signal is detected in a phase-locked loop and then multiplied (i.e., the dynamic phase error) by a local model of the keying square wave delayed 90 deg, the resulting output, filtered over a period greater than the keying interval, is zero for carrier lock, but nonzero for lock to any significant (odd-order) sideband. This system has been previously reported in Ref. 15, p. 81.

Also reported in Ref. 15, p. 76, is essentially the same system with two significant differences:

(1) The sequence of performing RF detection and multiplication by the keying reference is reversed.

(2) Once detected, a sideband lock is rejected by means of a cancelling voltage rather than by shorting the loop as implied in the first reference.

The first feature has been incorporated because of hardware design considerations while being functionally equivalent. While the second feature may theoretically offer some advantage in acquisition program, the ability to achieve cancellation in practice is contingent upon maintaining identical performance in the hardware of the main loop and the cancelling loop. In Fig. 44, the dotted blocks indicate additional functions required for lock cancellation as distinguished from loop shorting as performed by the balance of the diagram. Preliminary tests have revealed that, for matched phase detectors and a summing junction designed into the input of the loop filter, the effective loop gain (and hence bandwidth) was substantially reduced by the cancelling voltage; but under static tuning conditions, the lock could not be consistently broken by optimization of reference phasing. As predicted, however, for a fixed polarity, the cancelling voltage aided rather than opposed the main loop on alternate sidebands, thus doubling the loop gain and increasing the loop bandwidth. It would appear that the cancelling method of breaking lock will be dependent upon acquisition sweep rate for the practical case of nonidentical voltages.

On the other hand, the shorting method has performed effectively with this detector as well as in connection

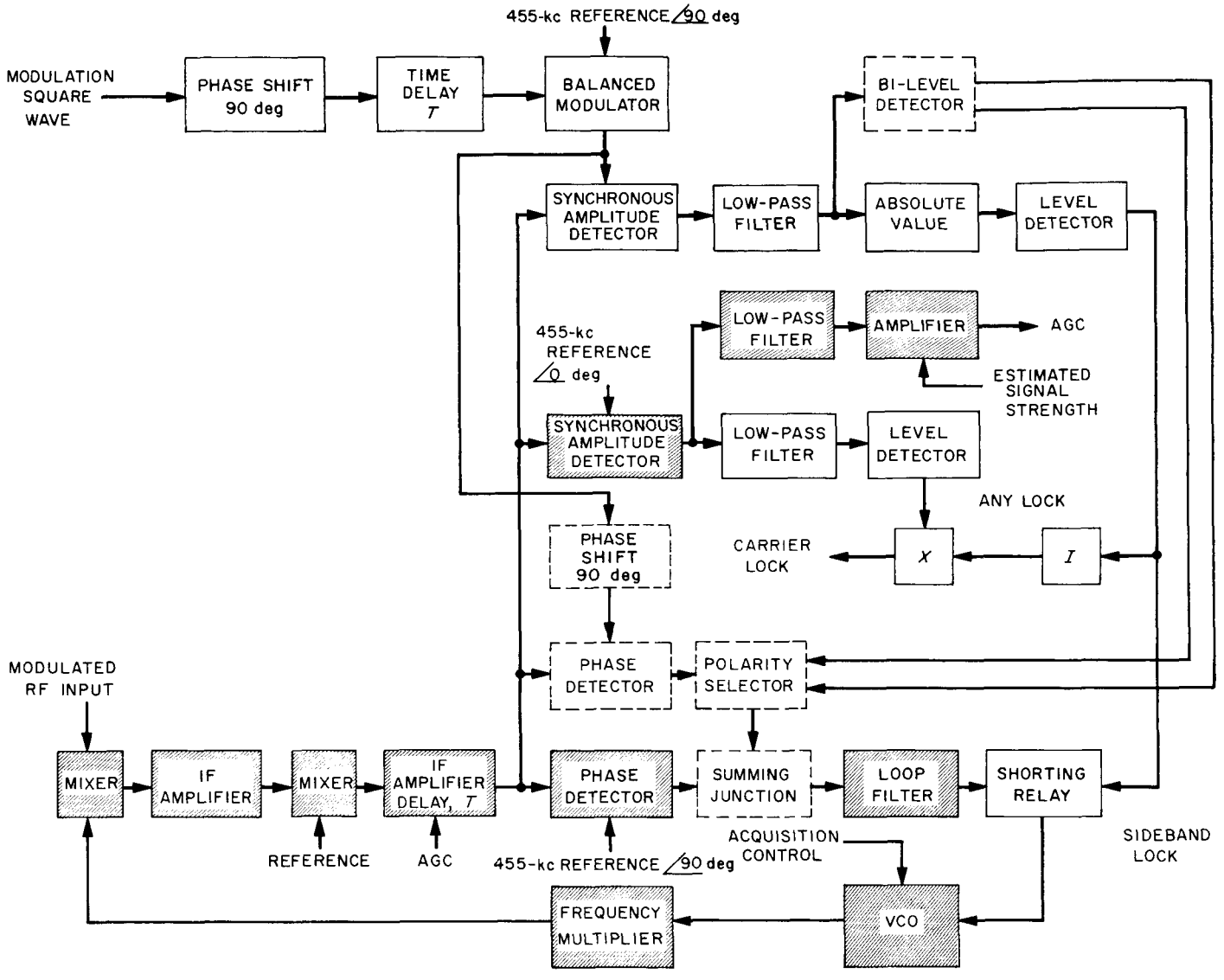

Fig. 44. Anti-sideband system

with a "strong signal sideband discriminator" (Ref. 16, p. 38).

To date, evaluation of the detector proper has indicated generally satisfactory performance with the following conclusions:

(1) Nonideal even-order sidebands arise due to time asymmetry in the IF signal. The performance of the sideband detector is erratic for even-order sideband locks. Analysis confirms nominally zero output for multiples of four. Three most probable sources of asymmetry in an operational system appear to be: error in range prediction at time of acquisition, transmitter rise time, and IF bandwidth characteristics.

(2) Detection of the sideband lock voltage by means of a synchronous amplitude detector yields the desired nominally constant amplitude independent of odd sideband number provided that the overload dynamic range of the receiver is not exceeded.

(3) Receiver overload is reached sooner as a function of sideband number for keying rates less than 10 times the loop bandwidth (β_L). This is a consequence of partial tracking of the modulation with a resulting reduction of sideband amplitude within the loop.

(4) The predetection bandwidth preceding the sideband detector limits the extent of mistuning over which detection is achieved. Assuming that knowledge of the received signal strength could be used to perform amplitude discrimination for sidebands outside this passband, a meaningful choice of bandwidth would be that which just encompasses all sidebands for which receiver overload is not exceeded (2). Assuming linearity to the 15th sideband (27.5 db),

$$BW_{IF} \geqq 2Nf_k = 30f_k$$

where f_k is the keying frequency. For keying rates presently under consideration (Ref. 14), a predetection bandwidth of the order of 10 kc would be required. For reliable sideband detection then, the frequency uncertainty or search range must be kept to within

$$\pm \frac{5000}{2400 \times 10^6} \doteq 2 \text{ ppm}$$

or, 2 ppm/50 ppm = ±4% doppler prediction for minimum altitude satellites.

Typical of data obtained to date is Fig. 45. For this keying rate and predetection bandwidth, the performance is evidently limited by the overload dynamic range. Of interest is the behavior of the "odd" even and "even" even order sidebands. However, within the nominally satisfactory range of operation, the odd side-band output voltages vary in amplitude approximately 7 db. Although the cause has not been completely identified, it is estimated that a tolerance of 3 db could be met with reasonable care with respect to such factors as IF passband ripple and phase response, gain tracking of separate detectors, and optimum phasing procedures. Possibly involved here also is the selection of optimum digital time delay in the keying reference as a function of IF time delay.

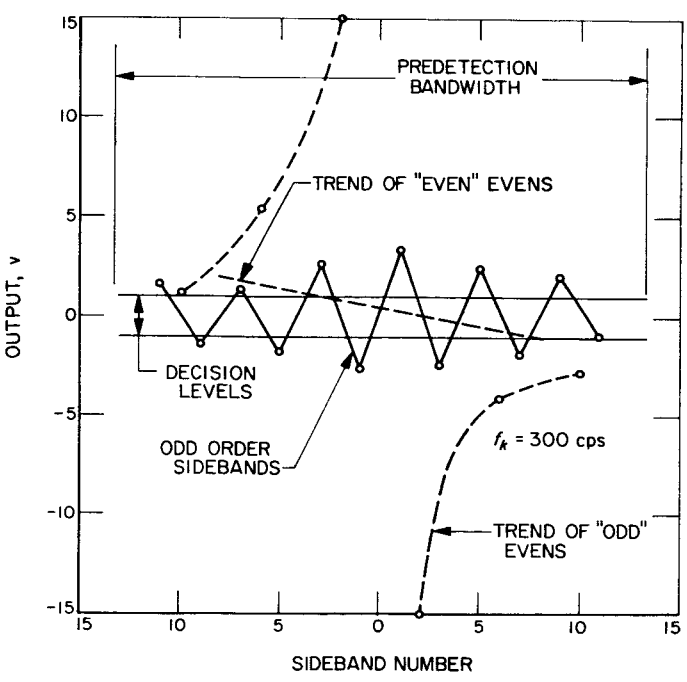

Fig. 45. Sideband detector performance

c. Discussion of system parameters. Although an anti-sideband system with immunity to incidental even order sidebands is conceptually feasible, hardware implementation and complexity do not as yet appear practical. However, it appears feasible, through control of even order sideband amplitude, to obtain effective immunity with the present system as discussed below.

In order to specify control of even order amplitude, consider the following relationship, valid near symmetry:

$$\frac{A_4}{A_0} = \frac{1 - T_1/T_2}{1 + T_1/T_2}$$

where A_4/A_0 is the fourth order amplitude relative to the carrier, T_1 is the *on* time of the signal, and T_2 is the *off* time.

Tentatively assuming a ratio of 1:100 (40 db) in sideband level, $T_1/T_2 = 0.5\%$. This leads to the requirement of range estimation for keying purposes at acquisition to within ±1%. Similarly, for maximum keying rates (assume 1000 cps), the total effective asymmetrical rise-time of the system must be no greater than 5 μsec. In order to meet this over-all requirement, it is estimated that a specification of 1-μsec rise-time per contributing subsystem is necessary. Probably the most critical and difficult to achieve is the klystron beam keyer.

Receiver overload linearity is typically specified as exceeding the predetection-to-loop-bandwidth ratio of nominally 20 db. Design changes have extended this range to near 30 db with the expectation of exceeding this figure in the final hardware. Taken together with 40-db even order sidebands, it is anticipated that signal strength prediction within 10 db will at least inhibit false indication of carrier lock if not actually prevent spurious side-band locks at extreme operating conditions such as experienced outside the predetection bandwidth.

Consideration of predetection bandwidth involves items (3) and (4) above. First, consider the effect of strong

signal bandwidth widening with consequent partial tracking of low keying frequencies leading to degradation of over-all system performance.

Let B = sinusoidal low-pass bandwidth of loop

$$B \propto \frac{\alpha}{\alpha_0} \beta_{L_0},$$

where α is the limiter suppression factor (taken as unity for strong signals), α_0 is the threshold value, and β_{L_0} is the threshold noise bandwidth. Similarly,

$$\dot{f}_{max} \propto \frac{\alpha}{\alpha_0} \beta_{L_0}^2,$$

where $\dot{f}_{max}$ is the maximum doppler rate that can be reliably tracked. Assuming that the system design is rate limited, then, combining,

$$B \propto \sqrt{\frac{\alpha}{\alpha_0}} \dot{f}_{max}$$

and

$$\beta_{L_0} \propto \sqrt{\frac{\alpha_0}{\alpha}} \sqrt{\dot{f}_{max}}$$

It follows then: *For a given strong signal transient performance, the strong signal sinusoidal response may be minimized by maximizing* α_0 *or* $2\beta_{L_0}/BW_{IF}$ *at the cost of threshold sensitivity.*

The choice of keying rates is limited at the low end by this partial tracking and at the high end by such factors as rise time, symmetry, and keyer control complexity. Additionally, for the latter reason, it is desirable to maintain a *band* of keying rates whose upper and lower limits are in the ratio of at least 2 or 3. Taking all the foregoing into account, it is imperative to minimize the sinusoidal bandwidth, B. Since this leads to a diametrically opposite requirement from (4), a dual IF channel approach is presently under evaluation.

To summarize, the following parameters are presently under consideration:

Maximum doppler rate (Echo), 450 cps/sec
Minimum threshold bandwidth ($2\beta_{L_0}$), 40 cps
Nominal threshold bandwith ($2\beta_{L_0}$),[a] 20 cps
Loop predetection bandwidth, 500 or 2000 cps
Sideband predetection bandwidth, 8000 to 16,000 cps
Maximum keying rate, 600 to 900 cps
Minimum keying rate, 300 cps
Loop response to 300 cps at strong signal, 16 or 22[a] db

[a]Accepting an RF cone of silence, as yet unevaluated.

2. Monostatic Satellite and Lunar Radar (MSSLR) Transmitter

a. Introduction. A 10-kw S-band transmitter operating at 2.388 Gc will be used for the initial installation in the 30-ft antenna at the Venus site, Goldstone. The transmitter system is being built at JPL using the klystron and some other components from the Echo and planetary radar transmitter (Ref. 17). The principal difference in the functional block diagram (Fig. 46) is the addition of a klystron beam modulator. The transmitter, as used on those experiments, was found to have many shortcomings that reduced its reliability. It is being modified in design to make it more reliable and to provide better operator convenience.

b. Discussion. The principal modications to the transmitter are to protect the klystron from certain damages. They are as follows:

(1) *Directional couplers.* Directional couplers are used to measure the forward and backpower of the RF output cavity of a klystron. The backpower coupler is especially important in that it is used to detect both excessive transient VSWR due to waveguide arcs and high VSWR due to klystron output load mismatch. Either condition may destroy the klystron by breaking the quartz output window.

New forward and backpower directional couplers had directivities of 20 db or less which made an uncertainty of backpower measurement of 100 w at 10-kw output. Such errors are intolerable since the klystron window can withstand only 900 to 1000 w of backpower.

(2) *Arc detector.* A photodiode directed at the klystron window senses waveguide arcs. Associated circuitry is actuated to remove the RF drive to the klystron so the arc is extinguished. RF drive isolation of about 25 db is necessary to extinguish an arc. Fast response times are necessary to prevent damage to the tube. A new arc detector will be provided for the transmitter that will have a response time of 5 μsec or less. The old unit was inadequate since it had a response time of many milliseconds; it removed the RF drive from the klystron by actuating a relay that removed the B+ voltage from the exciter. The new arc detector will remove the RF drive by biasing a coaxial diode switch placed near the RF input to the klystron.

(3) *Power metering.* New Hewlett Packard 431B power meters will be used to measure the RF output, RF backpower, and RF drive power. The old system

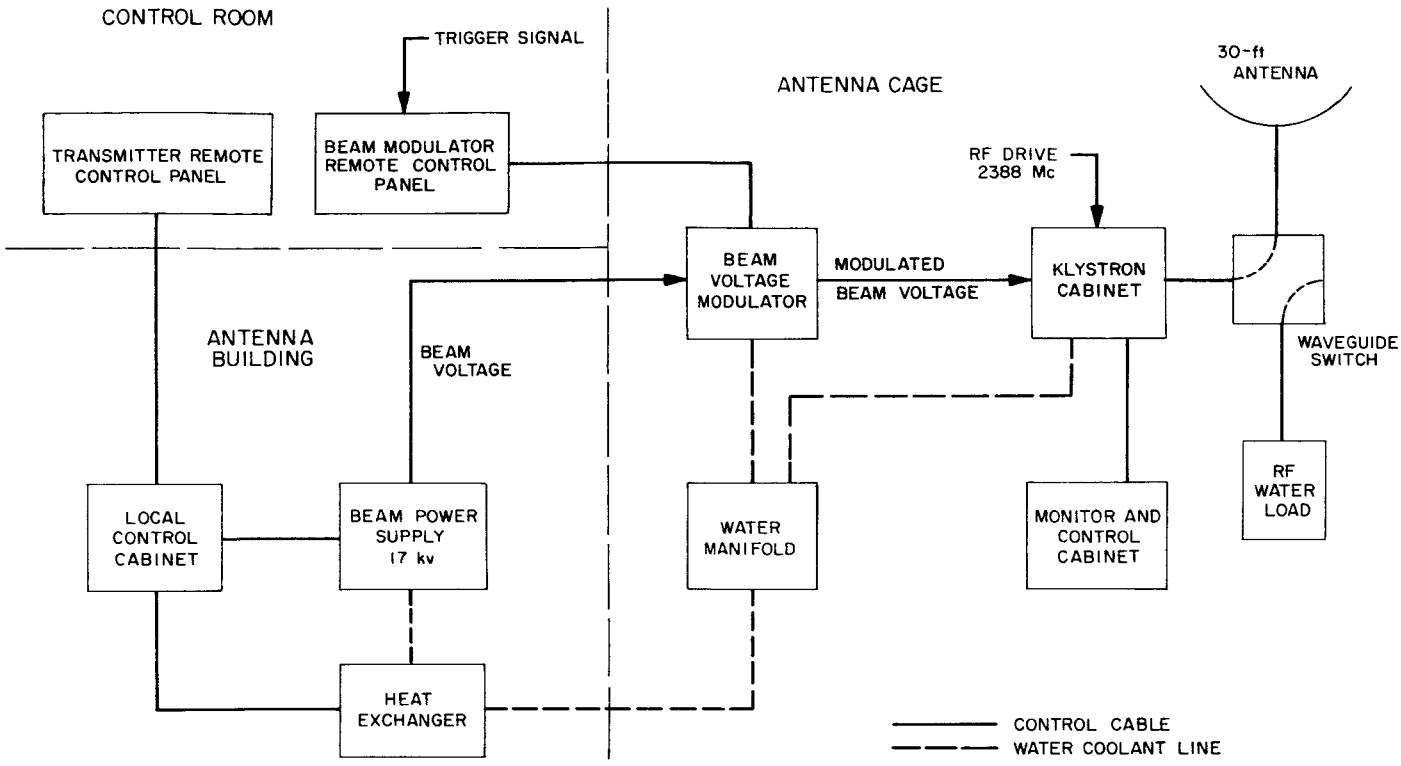

Fig. 46. Functional block diagram, 10-kw, 2.388-Gc transmitter system

used crystal detectors that were both nonlinear and temperature sensitive.

Variable attenuators will be used to set power levels for the power meters. These attenuators are sensitive to temperature changes; they will be housed in a constant temperature oven to minimize any drift due to the widely varying ambient temperature at Goldstone.

(4) *Waveguide switch.* A waveguide switch will be installed to provide rapid switching of the klystron RF output power from the antenna feed to the water load. Prior to this, it was necessary to manually connect the water load to the transmitter by flexible waveguide. Not only was this time consuming, but opening the waveguide introduces the possibility of contamination.

(5) *Water flow gages.* The klystron, klystron magnet, and RF water load are water cooled. This equipment can be damaged by low water flow rates. Water flow meters that incorporate low flow interlocks as well as dials indicating flow rates will be installed in the system. The old system was unsatisfactory in that only low flow interlocks were provided and these were dependent upon the factory setting; actual flow rates were not known. Individual flow valves will also be installed to permit individual flow rate adjustments.

E. S-Band Implementation for DSIF

1. TWM for DSIF

a. Summary. The first two units of the traveling wave maser (TWM) subsystem are nearly complete and will be shipped to Goldstone soon. The closed cycle refrigera-

tors (CCR's) for these TWM's have been received and checked out.

The experimental prototype TWM/CCR system at the Venus site has had one crosshead failure since it was installed.

b. Recent work.

TWM package. Fig. 47(a) shows a side view of the TWM package. The permanent magnet is seen in the bottom compartment, and the klystron pump box is shown in the middle with cover removed. The input and output connections are visible at the top. Fig. 47(b) shows a front view of the TWM/CCR package. The CCR crosshead drive and Dewar are displayed in this view.

Compressor package. The new CCR compressor unit which has been repackaged by the manufacturer (A. D. Little, Inc.) is shown in Fig. 48. The new machine is more compact than the old version, and serviceability is good. A vacuum pump, a liquid nitrogen cooled helium gas purifier, and a CCR control unit are furnished as auxiliary equipment.

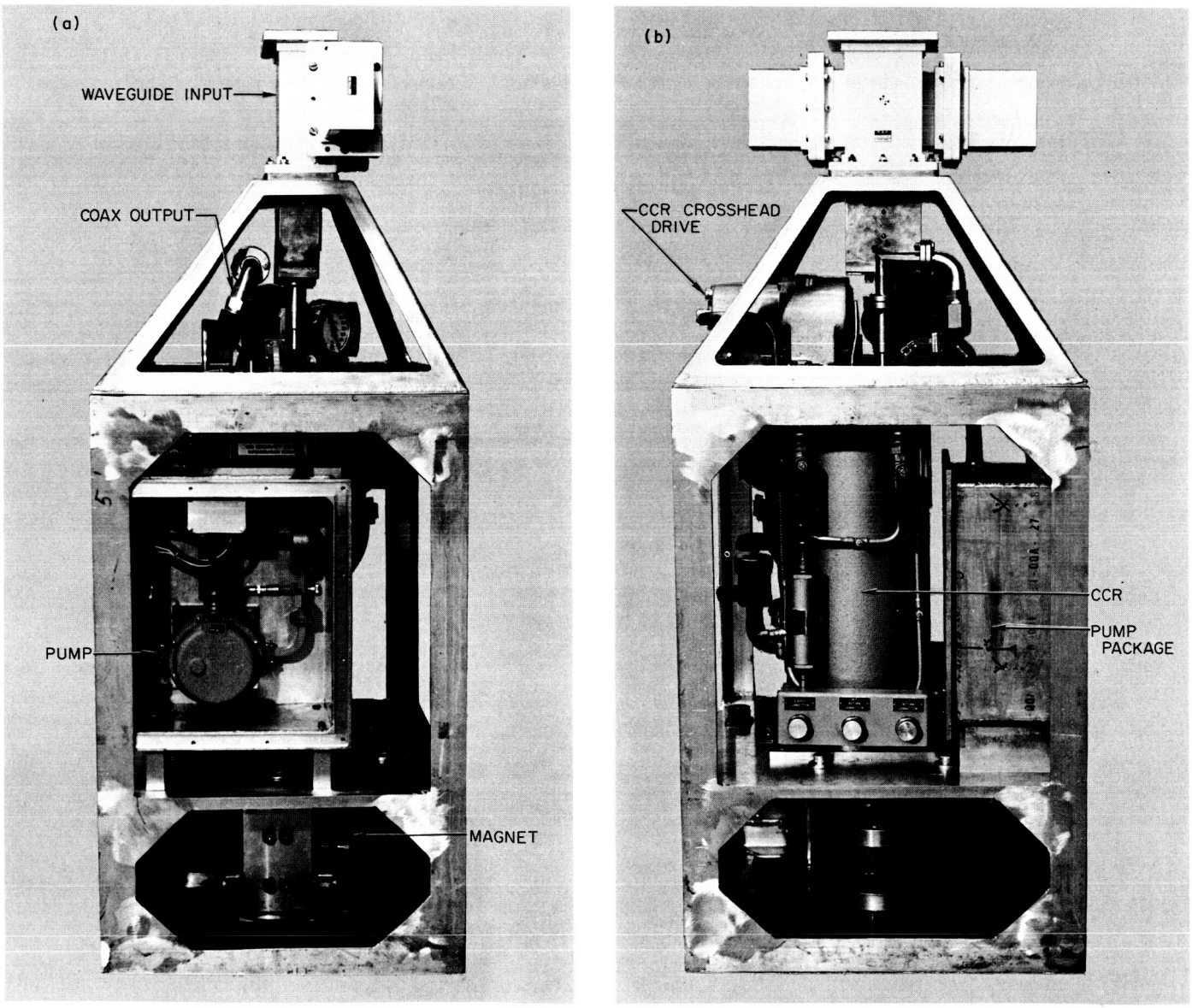

Fig. 47. Traveling wave maser (TWM): (a) side view and (b) front view

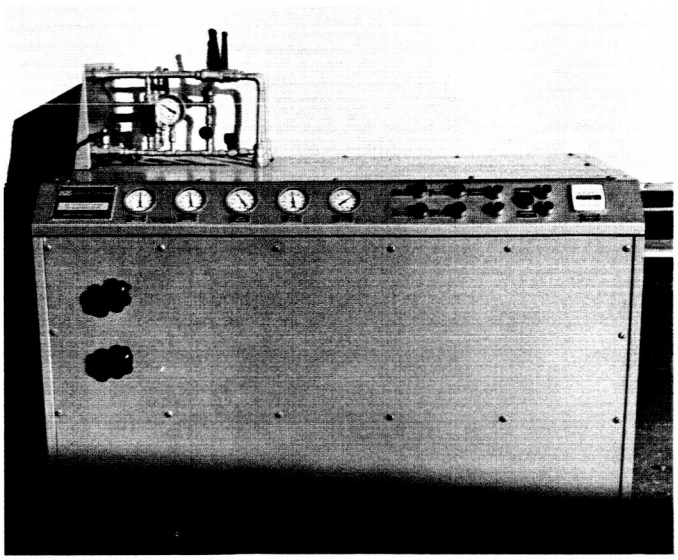

Fig. 48. Front view of compressor

The phase sequence of the 440-v, three-phase supply is immaterial since the compressor can operate in either direction of rotation.

Control and monitoring equipment. Fig. 49(a) shows the front view of the TWM/CCR control and monitoring racks. A solid-state, 50-Mc IF strip and a versatile noise source switching device are to be retrofitted into these racks at a future date. These two items and the monitor receiver are the only remaining components yet to be received.

Fig. 49(b) shows the rear view of the racks. The philosophy on the wiring has been to allow easy maintenance and testing.

Prototype system field testing. Although the operational performance of the experimental prototype TWM/CCR at the Venus site has been fairly good, the recent failure in a new set of gears has caused some concern. These gears failed after 600 hr of operation, less than half of the planned replacement-maintenance period; the (previous) original set was replaced after 5000 hr of duty without failure. The inconsistent performance of these gears has proved to be the weakest point in the CCR. A concerted effort between users and manufacturer is being made to solve this problem.

2. Acquisition Aid for DSIF

a. Summary. An acquisition aid (SAA) is being developed for the DSIF 85-ft antennas at S-band. The basic design has been completed and all major components are on order for the prototype system.

b. Recent work. As described in Ref. 18, an S-band acquisition aid is being developed for the DSIF. This system is basically similar to the existing L-band system (Ref. 19), but with certain changes to improve technical and operational performance. These changes, described previously, basically involve extra angle error receiver channels to improve the tracking presentation to the operator.

The SAA antenna is identical to the SCM feed horn which is the feed for the S-band Cassegrain system, and consists of a multimode, suppressed sidelobe, single horn monopulse unit. A contract has been awarded to the Hughes Aircraft Company, Fullerton, California, for the design, development, and construction of two units together with the antenna mounting and alignment devices. These two SAA antennas, scheduled for delivery in January 1964, will be tested with helicopter flights early in 1964 and, if proven satisfactory, will become the Johannesburg and Woomera DSIF Station operational units.

Design of various items of support equipment is underway. A close-in, erectable collimation tower is being designed to permit rapid multipath-free phasing and collimation of the acquisition system. A standard gain, suppressed sidelobe, circularly polarized horn antenna has been designed for use on these collimation towers. An optical TV package, to be mounted in the antenna structure near the SAA, will provide for remote (control room) alignment and phasing procedures with the erectable collimation tower.

3. DSIF Microwave Switch Control Assembly

a. Summary. During the design of the present DSIF block diagram, it became evident that some means was needed of rapidly and safely controlling the large number of microwave switches. A similar problem had existed in the experimental radar at the Venus site at Goldstone, and had been successfully solved with automatic equipment (Ref. 20). Consequently, an automatic switch control system was designed and is being fabricated for the DSIF S-band implementation project.

b. Recent work. The primary function of the microwave switch control assembly in the DSIF is the alignment and position indication of all waveguide and some

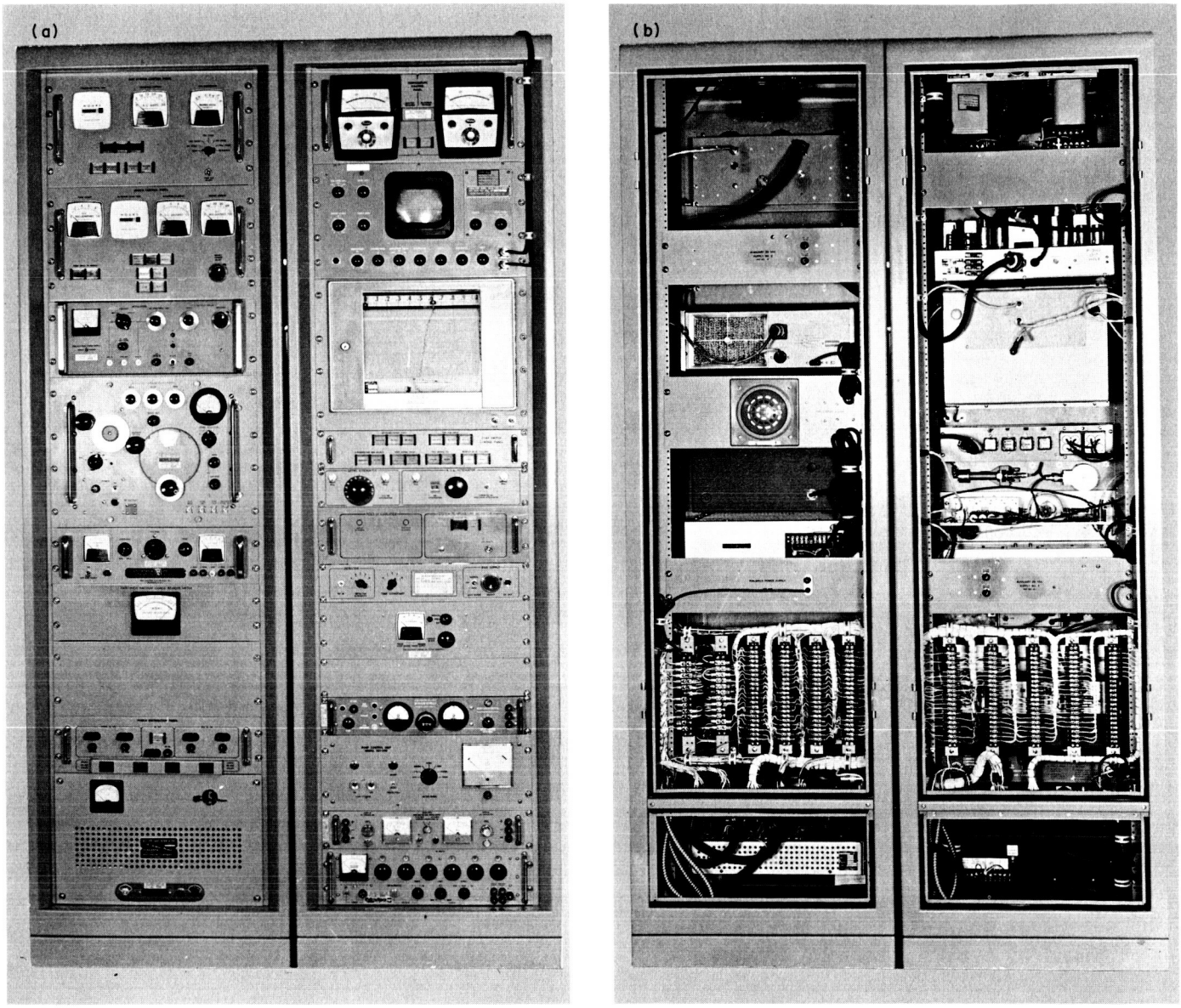

Fig. 49. TWM/CCR control racks: (a) front view and (b) rear view

coaxial switches shown on the DSIF S-band implementation for GSDS 1964. A secondary, but equally important function, is the remote indication, control, and interlock features provided to other interfacing subsystems and assemblies.

The switch control assembly consists physically of one standard DSIF rack of control equipment and one control panel located convenient to the station manager. The switch control assembly functional block diagram is shown in Fig. 50. Following is a brief description and summary of operation.

There are 20 identical units, the individual switch controllers (Fig. 51), which contain the necessary power supply, power line isolation, and command and indicate circuits associated with a given switch in the microwave system. Their individual position can be determined by noting which indication lamp is lit.

Normally these switch controller units are slaved to the switching and interlock logic panel. This unit accepts mode commands from the two control panels (Figs. 52 and 53), and translates them into switch drive commands which it sends to the individual switch controllers.

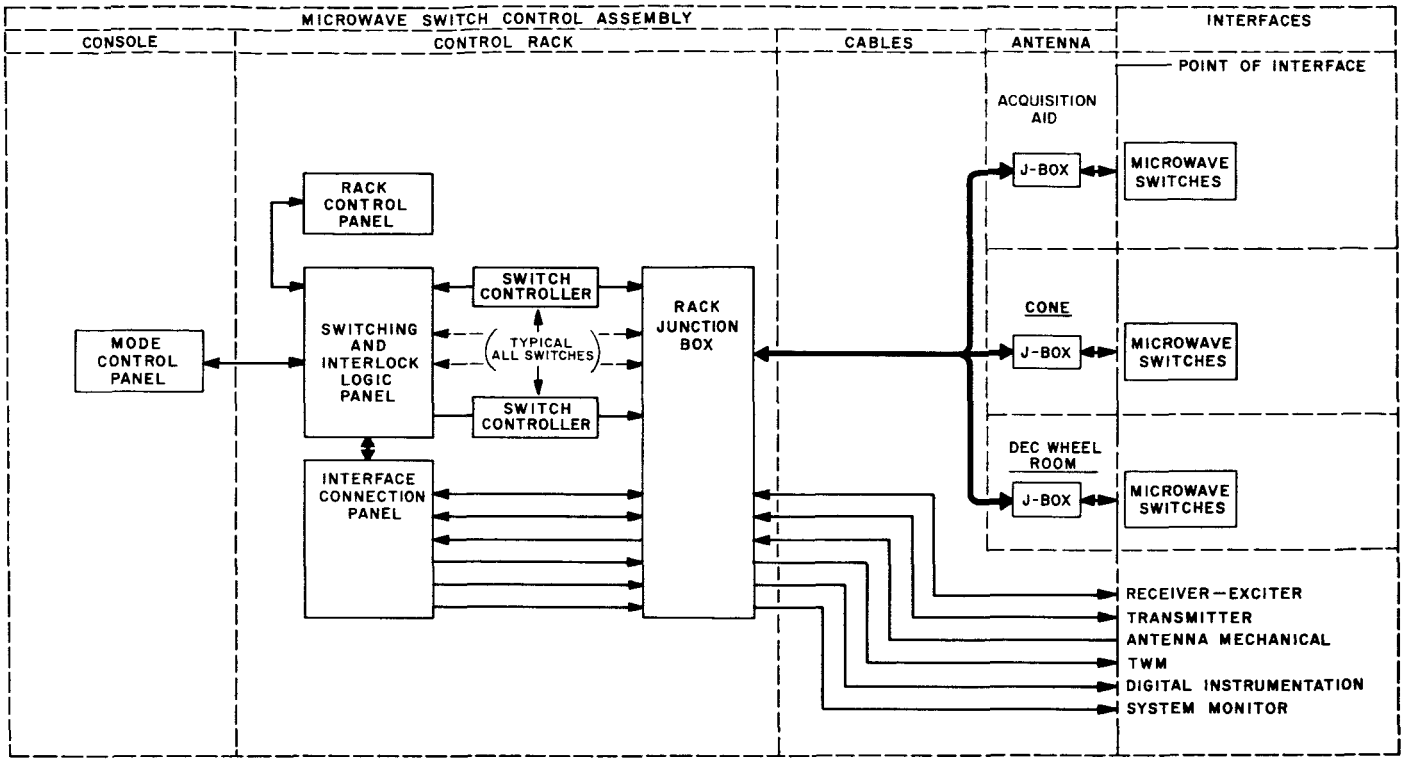

Fig. 50. Functional block diagram

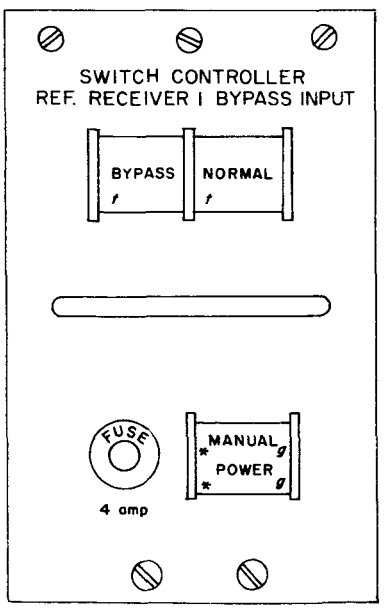

f = INDICATES PUSH BUTTON, INDICATOR UNIT
g = GREEN INDICATOR LAMP AND PUSH BUTTON
* = INDICATOR ONLY

Fig. 51. Typical switch controller

When the switches concerned have executed the command, the individual controllers send position data to the logic panel, which then translates these data into mode indications.

If the particular mode command involves a waveguide switch which could be carrying transmitter power, it would first check for beam and/or exciter condition. If either is on, it will command them off, and wait for indication that they are indeed both off. Only then will it issue the commands to the switch controllers, and will continue to prevent beam or exciter operation until the switching is complete and the correct mode has been set up, at which time it will allow the transmitter functions to turn on again. This type command is not normally given during a tracking mission, but the safety precaution must be included. The logic panel is also completely self-checking insofar as switch positions should agree with mode commands in the logic panel. It also sends switch position data to the interface connection panel. This panel is primarily for isolation between the switch control system and its interfacing subsystems.

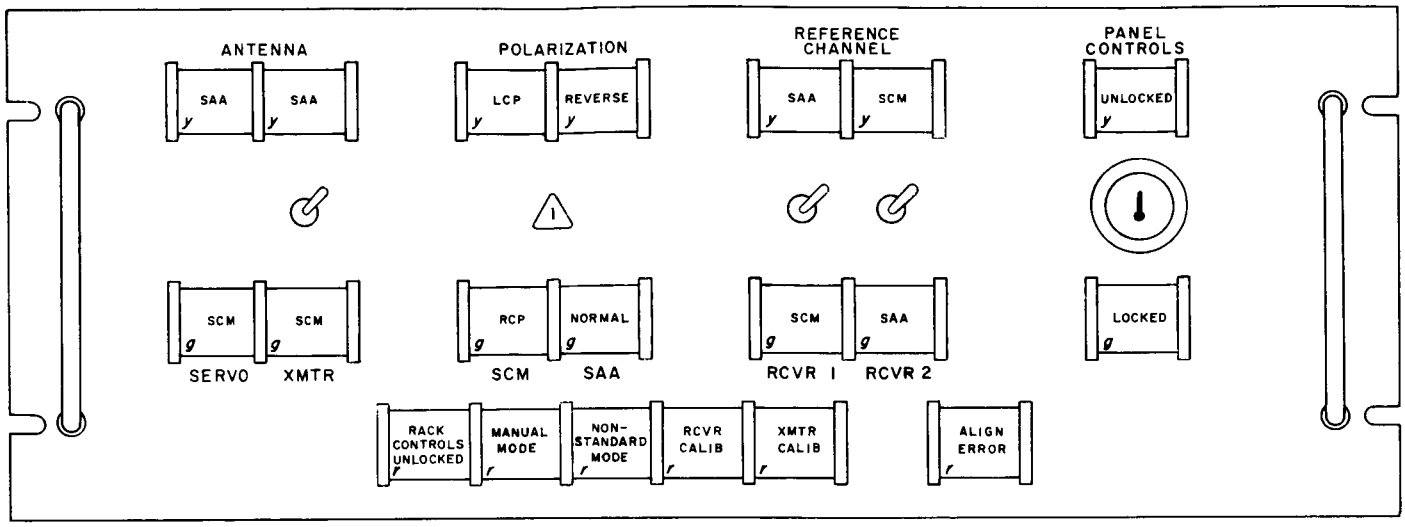

△ SEE TEXT

y = YELLOW INDICATOR LAMP

g = GREEN INDICATOR LAMP

r = RED INDICATOR LAMP

ALL TOGGLE SWITCHES ARE SPRING RETURN TO CENTER *OFF* POSITION

Fig. 52. Mode control panel

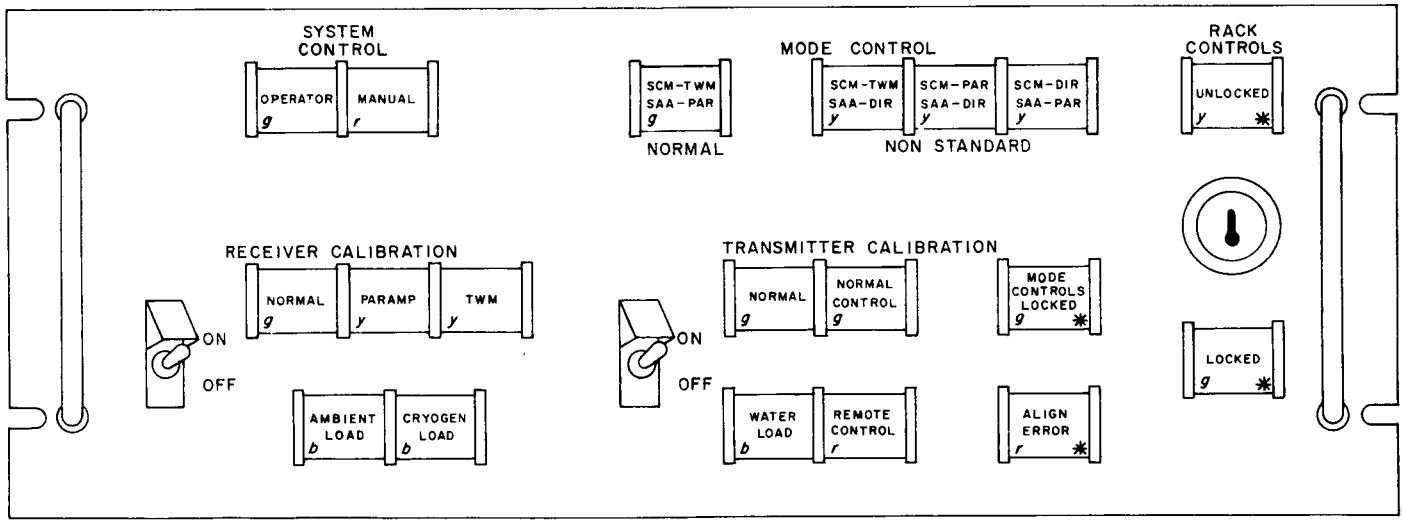

y = YELLOW INDICATOR LAMP AND PUSH BUTTON

g = GREEN INDICATOR LAMP AND PUSH BUTTON

r = RED INDICATOR LAMP AND PUSH BUTTON

b = BLUE INDICATOR LAMP AND PUSH BUTTON

✱ = INDICATOR ONLY

Fig. 53. Rack control panel

There are six interfaces (Fig. 50):

(1) The mission monitor subsystem receives switch position contacts.

(2) The digital instrumentation subsystem receives switch position contacts.

(3) The TWM assembly receives indication of whether the maser is connected to the antenna or one of the reference temperature loads.

(4) The antenna mechanical subsystem supplies indication of which feed is supplying the servo error signals.

(5) The transmitter final amplifier receives beam voltage interlock circuits and remote control and indication of the RF water load waveguide switch and supplies beam voltage on–off indication.

(6) The receiver–exciter subsystem receives exciter interlock circuits, attenuator bypass switch commands, and indications for each receiver as to what its path is through the waveguide to which of the two antenna feeds. The exciter supplies on–off indication.

All rack connections are through the rack junction box, and the antenna cables lead to similar junction boxes in the SAA area, the cone, and the Dec wheel room, where they then break out into individual switch control cables.

There are two control panels in the switch control assembly. The mode control panel (Fig. 52) allows the operator to transfer the transmitter between the SAA (S-band acquisition aid subsystem) and the SCM (S-band Cassegrain microwave subsystem); transfer either receiver reference channel between the SCM and SAA independently; and *at Pioneer only,* the operator can select the polarization of the SCM, i.e., left or right circular, and the polarization of the SAA, as to whether it is normal, i.e., the same as that of the SCM, or reverse, the opposite polarity of the SCM. At all other stations these switches are *not* here, but the operator does have the polarization indication lamps.

The operator accomplishes any of the previous transfers by pressing the spring return toggle switch toward the indicator reflecting his choice. When the indicator comes on, it is his indication that the mode has been completely executed. The key switch allows the operator to lock all controls in any configuration he desires, so that accidental commands by unauthorized persons are eliminated. The indicators in the bottom row tell the operator of some nonstandard condition in the switch control system.

The purpose of the rack control panel (Fig. 53) is for calibration needs of other subsystems; testing and nonstandard mode control.

Various groups of controls allow calibrations of the parametric amplifier or the TWM by connecting them to either of the reference temperature loads, or allow the transmitter output klystron to be connected to the RF water load, either from this panel or, by selecting remote control, from the final amplifier panels. If either of these two calibrate features are in use, the appropriate red light indicates on the mode control panel.

Another set of push buttons defines the nonstandard modes used to bypass low-noise amplifiers or achieve direct waveguide connection to the feeds. Selecting any of these modes lights a red telltale light on the mode control panel.

Additional buttons are used to put the system in manual mode, which allows one to control each switch individually from its own switch controller. The purpose of this mode is for testing an individual switch or possibly such tests as waveguide VSWR or insertion loss measurements of a configuration not obtainable by the various mode commands. When the system is in manual mode, all other mode commands are locked in their existing condition and a red light on the mode control panel notifies the operator.

When the rack control panel is unlocked, a red lamp indicates that to the operator. Locking this panel will leave a nonstandard mode in its existing configuration, but it will return to normal the following: a manual mode command, any receiver calibration command, and if in normal control, return the water load switch to normal. As indicated before, any error or discrepancy between a given mode command and the alignment of the switches concerned shows up by lighting the "alignment error" light on both control panels.

Several criteria were closely followed in designing the circuitry for the switch control assembly. Among the most important is the fail safe nature of the circuits, thereby minimizing the danger to personnel and damage to high-power RF equipment; the self-checking error feature, the modular design allowing modification or change of one part of the system without affecting other parts; and the use of high-quality, long-life components throughout. In general, one particular component part has been used wherever possible throughout the system, thereby significantly reducing the number of spare parts required.

All electrical and mechanical design has been done at JPL utilizing to the fullest extent the experience in circuitry, component part reliability, and system operation gained in constructing and operating the Venus site planetary radar switch control system. Reliability of the DSIF switch control assembly should be equal to, or if possible, better than that of the Venus system. The shortest lived part in each system is guaranteed to have 10^7 operations.

Fabrication of five complete assemblies is being done at the Industrial Products Division of ITT with deliveries scheduled to be commensurate with the Cassegrain cones.

References

1. "Boresight and Gain Calibrations for DSIF Antennas," *Space Programs Summary No. 37-23,* Vol. III, pp. 28–29, September 30, 1963.
2. "Boresight and Gain Calibrations for DSIF Antennas," *Space Programs Summary No. 37-24,* Vol. III, pp. 30–33, November 30, 1963.
3. "Antenna Instrumentation," *Space Programs Summary No. 37-20,* Vol. III, pp. 31–34, March 31, 1963.
4. "Antenna Instrumentation," *Space Programs Summary No. 37-21,* Vol. III, p. 30, May 31, 1963.
5. "Antenna Instrumentation," *Space Programs Summary No. 37-22,* Vol. III, pp. 15–16, July 31, 1963.
6. "Antenna Instrumentation," *Space Programs Summary No. 37-24,* Vol. III, pp. 33, 39–43, November 30, 1963.
7. "Radio Frequency Interference—Automotive Ignition," *Space Programs Summary No. 37-21,* Vol. III, pp. 20–24, May 31, 1963.
8. "Water Rotary Joint for Az–El Antenna," *Space Programs Summary No. 37-24,* Vol. III, pp. 43–44, November 30, 1963.
9. "Mod III Transmitter System, 2388 Mc, 100 kw," *Space Programs Summary No. 37-19,* Vol. III, pp. 23–27, January 31, 1963.
10. "Mod IV Planetary Radar Receiver, 2.388 Gc," *Space Programs Summary No. 37-21,* Vol. III, pp. 49–61, May 31, 1963.
11. "High Speed and High Capacity Autocorrelator," *Space Programs Summary No. 37-14,* Vol. I, pp. 111–116, April 1, 1962.
12. "Relationship to Planetary Radar Project," *Space Programs Summary No. 37-23,* Vol. III, pp. 51–52, September 30, 1963.
13. "Optimum Transmitter Power for Klystron Drive-Keyed Radar," *Space Programs Summary No. 37-23,* Vol. III, pp. 52–55, September 30, 1963.
14. "Monostatic Radar," *Space Programs Summary No. 37-24,* Vol. III, pp. 59–61, November 30, 1963.
15. "Synchronous Sideband Detector," *Space Programs Summary No. 37-21,* Vol. III, pp. 81–83, May 31, 1963.
16. "Strong Signal Sideband Discriminator," *Space Programs Summary No. 37-22,* Vol. III, pp. 38–43, July 31, 1963.
17. "Monostatic Radar," *Space Programs Summary No. 37-19,* Vol. III, pp. 29–32, January 31, 1963.
18. "Acquisition Aid for DSIF," *Space Programs Summary No. 37-24,* Vol. III, pp. 79–81, November 30, 1963.
19. "L-Band Acquisition Aid," *Space Programs Summary No. 37-23,* Vol. III, pp. 8–11, September 30, 1963.
20. "Venus Radar Waveguide Control System," *Space Programs Summary No. 37-18,* Vol. III, pp. 27–30, November 30, 1962.

V. Advanced Antenna System

A. Synopsis

On-site preparations at the Mars site, Goldstone Station, and engineering design for the 210-ft diameter, fully steerable paraboloid continue. The antenna is being designed for operational use at the DSIF Stations at the DSIF S-band frequencies (2.1 to 2.3 Gc).

Preliminary design and engineering analysis for the contractor furnished system, the principal element of the first AAS, is nearing completion at Rohr Corporation, Chula Vista, California. Primary effort of the JPL Project Office has been in assisting the Rohr Corporation effort, resolution of difficult design problems, and supervision of the on-site preparation.

The design progress has been thoroughly reviewed in a series of meetings at the Rohr Corporation and at JPL for the purpose of assuring that the design concept is sound and that the complexities and interrelationships of all phases of the program are sufficiently understood to safely proceed with the first major construction steps—those of placing the concrete for the pedestal foundation and instrument tower. As the result of these reviews, the decision has been made to proceed with the concrete pedestal and instrument tower as scheduled.

The pedestal is to be a reinforced concrete cylinder with a flat slab top which will have a concrete collar in the center. The pedestal will have a ring type footing that will be 11 ft below grade. The weight of the completed pedestal will be approximately 10,000,000 lb. The walls will be 3 ft 6 in. in thickness. Design analysis indicates that pedestal deflections are compatible with the over-all system pointing and dynamic requirements. The pedestal and foundation rotation for a 30-mph wind is 1.5 sec. The maximum soil pressure beneath the foundation, under seismic conditions, is 8070 lb/ft^2. The maximum soil pressure beneath the foundation, under wind conditions, is 6500 lb/ft^2. Comparing this with the JPL design requirement of an allowable 20,000 lb/ft^2 represents a safety factor of 2.5. The shear failure occurs in the soil at the Mars site, Goldstone Station, at 60,000 lb/ft^2; hence, there is a gross soil safety factor of 7.5.

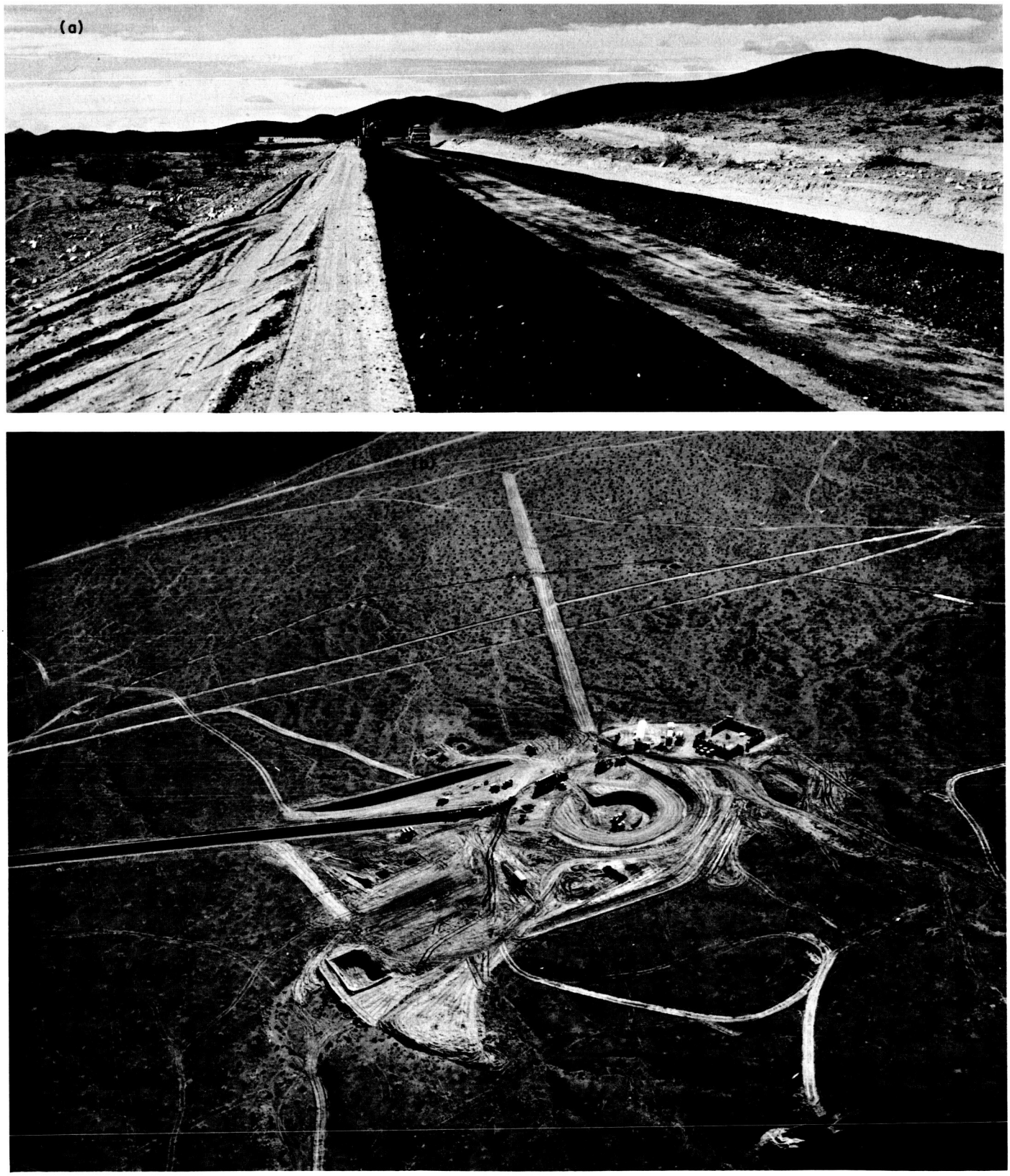

Fig. 1. Mars site: (a) access road under construction and (b) on-site progress as of November 8, 1963

The pedestal reinforcing steel and concrete are designed for maximum moments and shears derived from conservative analysis. This approach, plus the fact that all tensile strength of the concrete has been ignored, lead to a substantial safety margin above and beyond those inherent in normal design codes. The component designs are far enough along to assure that there will be no major design changes in the antenna. The safety factors of the foundation, however, are such that the weight could increase 100% and the foundation would still be adequate.

The instrument tower will be of reinforced concrete and steel and of a height to permit the intersection of the axes of the master equatorial to coincide with the intersection of the axes of the antenna. The purpose of this tower is to serve as the mounting platform for the master equatorial unit which is the primary pointing reference for the antenna system. The tower design consists of a floating silo type foundation, a concrete cylinder to the top of the pedestal, and a steel cylinder and truncated cone to the elevation axis. Design analysis indicates the natural frequency, determined by using Rayleigh's first approximation method, to be 6.61 cps. The rotational motion of the instrument tower about a horizontal axis, due to coupled loads resulting from 45-mph wind gusts on the antenna, has been computed to be 1.9 sec of arc. The weight of the tower will be 1,200,000 lb. The estimated weight of the excavated soil is 1,300,000 lb.

The on-site work at the Mars site, Goldstone Station, is continuing generally on schedule. Figs. 1 through 4 depict the on-site activity progress.

An extension of the present Goldstone road system has been completed to provide access to the Mars site. This extension is almost 5 mi long, is constructed of 4-in. road mix on a select base course, and is 24 ft, 6 in. wide.

Installation of the 315-ft-high guyed derrick is in progress by Rohr Corporation for use in erection and construction of the antenna (Fig. 2). The use of this large derrick facility will enable placement of all components of the antenna except one-half of the outer ribs of the reflector from one location, without movement of the antenna. These outer elements will be placed by rotating the antenna.

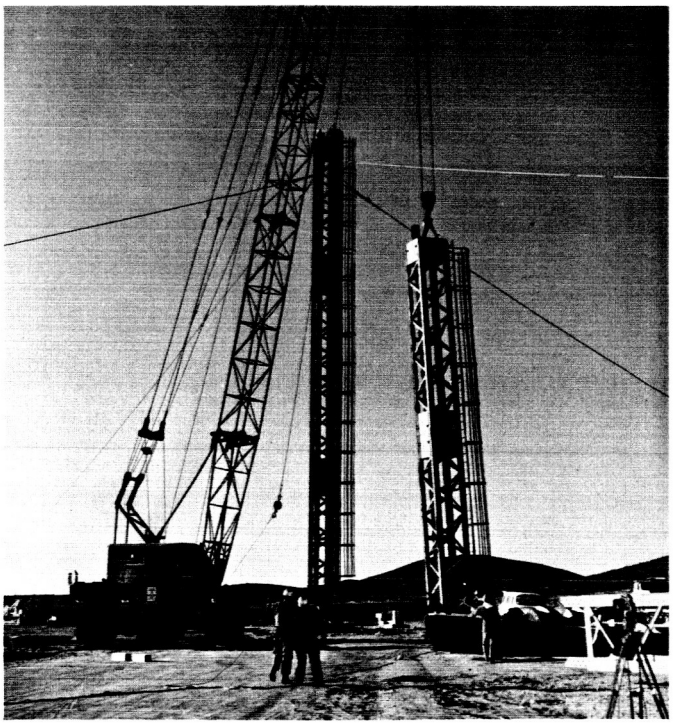

Fig. 2. Installation of the guyed derrick to be used for antenna erection

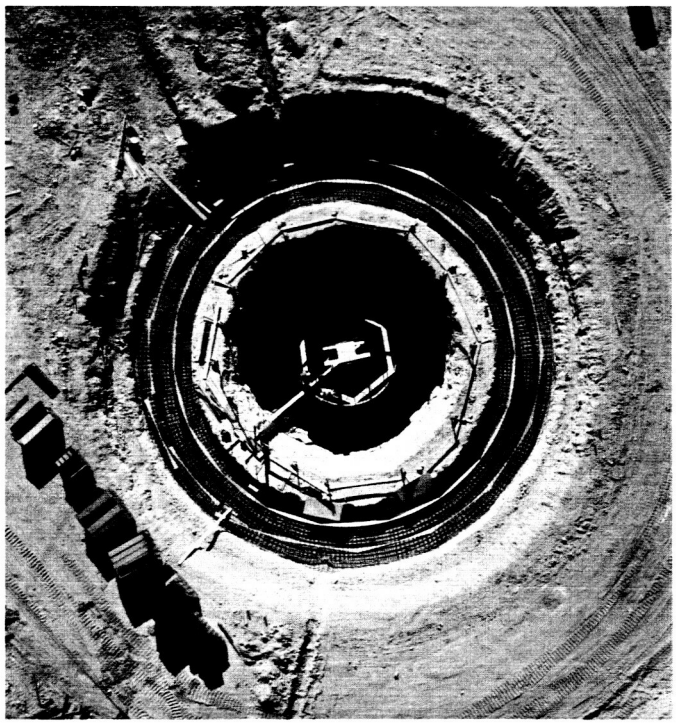

Fig. 3. Pedestal and instrument tower under construction

Fig. 4. Site progress as of December 10, 1963

Excavation for the pedestal and the instrument tower has been completed, and the placement of reinforcing steel, forms, and concrete is in progress (Fig. 3). The depth of the pedestal foundation is 11 ft below the finished grade and its outside diameter is 88 ft, 8 in. The depth of the instrument tower is 35 ft below the finished grade and its outside diameter is 26 ft.

A 12,000-gal underground water storage tank has been emplaced which will be part of the domestic water supply system for the antenna. The water for this tank will be hauled from nearby Fort Irwin and gravity fed into the tank.

The sanitary sewage system for the antenna is being installed. Extra care in installation is being taken so that no moisture from the sanitary sewer system or from any other source will be permitted to enter the soil near the founding system of the antenna.

Related JPL in-house supporting studies are reported in Sec. IV-A-2, 3 of this report.